Detrimental effects of exuberant and restrained immune responses against the central nervous system in the context of multiple sclerosis and glioblastoma multiforme

Dissertation

zur Erlangung des Grades
"Doktor der Naturwissenschaften"
am Fachbereich Biologie
der Johannes Gutenberg-Universität in Mainz

Nicola Hoppmann

geboren am 03.07.1983 in Reinbek

Mainz, 2014

Dekan:

1. Berichterstatterin:

2. Berichterstatterin:

Tag der mündlichen Prüfung: 19.09.2014

Declaration

I, Nicola Hoppmann, hereby declare that I have conducted this present PhD thesis independently under supervision, without inappropriate help by a third person. I have not used other sources or devices than stated and not copied the work of others. All data, tables, figures and text citations which have been reproduced from any other source, including the internet, have been explicitly labeled as such. Moreover, I declare that this is a true copy of my thesis, and that this thesis has not been submitted for a higher degree to any other University or Institution. In carrying out this research, I complied with the rules of standard scientific practice as formulated in the statutes of the Johannes Gutenberg-University Mainz to insure standard scientific practice.''

Mainz, May, 30th, 2014

_____

(Nicola Hoppmann)

Summary

Glioblastoma multiforme (GBM) is the most common and most aggressive astrocytic tumor of the central nervous system (CNS) in adults. The standard treatment consisting of surgery, followed by a combinatorial radio- and chemotherapy, is only palliative and prolongs patient median survival to 12 to 15 months. The tumor subpopulation of stem cell-like glioma-initiating cells (GICs) shows resistance against radiation as well as chemotherapy, and has been suggested to be responsible for relapses of more aggressive tumors after therapy. The efficacy of immunotherapies, which exploit the immune system to specifically recognize and eliminate malignant cells, is limited due to strong immunosuppressive activities of the GICs and the generation of a specialized protective microenvironment. The molecular mechanisms underlying the therapy resistance of GICs are largely unknown.

The first aim of this study was to identify immune evasion mechanisms in GICs triggered by radiation. A model was used in which patient-derived GICs were treated *in vitro* with fractionated ionizing radiation (2.5 Gy in 7 consecutive passages) to select for a more radio-resistant phenotype. In the model cell line 1080, this selection process resulted in increased proliferative but diminished migratory capacities in comparison to untreated control GICs. Furthermore, radio-selected GICs downregulated various proteins involved in antigen processing and presentation, resulting in decreased expression of MHC class I molecules on the cellular surface and diminished recognition potential by cytotoxic CD8+ T cells. Thus, sub-lethal fractionated radiation can promote immune evasion and hamper the success of adjuvant immunotherapy. Among several immune-associated proteins, interferon-induced transmembrane protein 3 (IFITM3) was found to be upregulated in radio-selected GICs. While high expression of IFITM3 was associated with a worse overall survival of GBM patients (TCGA database) and increased proliferation and migration of differentiated glioma cell lines, a strong contribution of IFITM3 to proliferation *in vitro* as well as tumor growth and invasiveness in a xenograft model could not be observed.

Multiple sclerosis (MS) is the most common autoimmune disease of the CNS in young adults of the Western World, which leads to progressive disability in genetically susceptible individuals, possibly triggered by environmental factors. It

is assumed that self-reactive, myelin-specific T helper cell 1 (Th1) and Th17 cells, which have escaped the control mechanisms of the immune system, are critical in the pathogenesis of the human disease and its animal model experimental autoimmune encephalomyelitis (EAE). It was observed that *in vitro* differentiated interleukin 17 (IL-17) producing Th17 cells co-expressed the Th1-phenotypic cytokine Interferon-gamma (IFN-γ) in combination with the two respective lineage-associated transcription factors RORγt and T-bet after re-isolation from the CNS of diseased mice. Pathogenic molecular mechanisms that render a CD4+ T cell encephalitogenic have scarcely been investigated up to date.

In the second part of the thesis, whole transcriptional changes occurring in *in vitro* differentiated Th17 cells in the course of EAE were analyzed. Evaluation of signaling networks revealed an overrepresentation of genes involved in communication between the innate and adaptive immune system and metabolic alterations including cholesterol biosynthesis. The transcription factors *Cebpa*, *Fos*, *Klf4*, *Nfatc1* and *Spi1*, associated with thymocyte development and naïve T cells were upregulated in encephalitogenic CNS-isolated CD4+ T cells, proposing a contribution to T cell plasticity. Correlation of the murine T-cell gene expression dataset to putative MS risk genes, which were selected based on their proximity (± 500 kb; ensembl database, release 75) to the MS risk single nucleotide polymorphisms (SNPs) proposed by the most recent multiple sclerosis GWAS in 2011, revealed that 67.3% of the MS risk genes were differentially expressed in EAE. Expression patterns of *Bach2, Il2ra, Irf8, Mertk, Odf3b, Plek, Rgs1, Slc30a7, and Thada* were confirmed in independent experiments, suggesting a contribution to T cell pathogenicity. Functional analysis of *Nfatc1* revealed that *Nfatc1*-deficient CD4+ T cells were restrained in their ability to induce clinical signs of EAE. *Nfatc1*-deficiency allowed proper T cell activation, but diminished their potential to fully differentiate into Th17 cells and to express high amounts of lineage cytokines. As the inducible *Nfatc1*/αA transcript is distinct from the other family members, it could represent an interesting target for therapeutic intervention in MS.

Zusammenfassung

Glioblastoma multiforme (GBM) ist der häufigste und aggressivste astrozytäre Tumor des Zentralnervensystems (ZNS) bei Erwachsenen. Die Standardtherapie, bestehend aus operativer Entfernung des Tumors mit anschließender Radio- und Chemotherapie wirkt nur palliativ und verlängert das Patientenleben im Durchschnitt um 12 bis 15 Monate. Die Tumor-Subpopulation der stammzellähnlichen Gliom-initiierenden Zellen (englisch: GIC) ist resistent gegenüber Strahlungs- und Chemotherapie, und wird für das Entstehen von aggressiveren Sekundärtumoren nach der Therapie verantwortlich gemacht. Die Wirksamkeit von Immuntherapien, die das Immunsystem ausnutzen, spezifisch maligante Zellen zu erkennen und zu eliminieren, ist begrenzt aufgrund starker immunsuppressiver Aktivitäten der GICs.

Das erste Ziel dieser Studie war die Identifizierung von Mechanismen der Immunevasion bei GICs, die durch Bestrahlung ausgelöst werden. Ein Model wurde genutzt, bei dem GICs aus Biopsien *in vitro* mit fraktionierter ionisierender Strahlung behandelt wurden (2.5 Gy in 7 aufeinanderfolgenden Zellpassagen) um einen strahlungsresistenteren Phänotypen zu selektieren. In der Modell-GIC-Zelllinie 1080 führte dieser Selektionsprozess zu einer erhöhten Zellteilungsrate aber geringerer Migration im Vergleich zu unbehandelten Kontroll-GICs. Des Weiteren haben die strahlungsselektierten GICs verschiedene Proteine, die in der Antigenprozessierung und –präsentation involviert sind, herunter reguliert, was eine reduzierte Anzahl von MHC Klasse I Moleküle auf der Zelloberfläche zur Folge hat. Das zeigt, dass eine sub-letale fraktionierte Bestrahlung eine Immunevasion fördern und somit den Erfolg von kombinierter Immuntherapie hintern kann. Unter den verschiedenen immunassoziierten Proteinen wurde eine erhöhte Expression des Interferon-induzierten Transmembranproteins 3 (IFITM3) in strahlungsselektierten GICs festgestellt. Während eine Assoziation von erhöhter IFITM3 Expression und einem schlechteren Gesamtüberleben festgestellt (TCGA Datenbank), und auch eine erhöhte Proliferations- und Migrationsrate bei differenzierten Gliom-Zelllinien gezeigt wurde, konnte ein signifikanter Beitrag von IFITM3 in der Proliferation von GICs als auch im Tumorwachstum und der Invasivität von GICs in einem Xenograft-Model nicht beobachtet werden.

Multiple Sklerose (MS) ist die häufigste Autoimmunerkrankung des ZNS in jungen Erwachsenen der westlichen Welt, die zur progressiven Behinderung in genetisch empfänglichen Individuen führt, die wahrscheinlich durch Umweltfaktoren ausgelöst wird. Es wird angenommen, dass selbst-reaktive, Myelin-spezifische T Helfer 1 (Th1) Zellen und Th17 Zellen, die den

Kontrollmechanismen des Immunsystems entkommen sind, entscheidend für die Pathogenese der human Erkrankung als auch des Tiermodells der experimentellen autoimmunen Enzephalomyelitis (EAE) sind. Es wurde beschrieben, dass *in vitro* differenzierte Interleukin 17 (IL-17) -produzierende Th17 Zellen, nach Isolierung aus dem ZNS erkrankter Mäuse, zusätzlich das Th1-typische Zytokin Interferon-gamma (IFN-γ) in Kombination mit den entsprechenden Sublinien-assoziierten Transkriptionsfaktoren RORγt und T-bet exprimieren. Pathogene molekulare Mechanismen die der Enzephalitogenität von CD4+ T Zellen unterliegen, sind bis heute nur unzureichend untersucht.

Im zweiten Teil der Arbeit wurden Veränderungen des gesamten Transkriptoms von *in vitro* differenzierten Th17 Zellen im Verlauf einer EAE analysiert. Die Evaluation von Signalnetzwerken ergab eine Überrepräsentation von Genen die in der Kommunikation zwischen dem angeborenen und adaptiven Immunsystem und in metabolischen Veränderungen, u.a. der Cholesterin-Biosynthese mitwirken. Die Transkriptionsfaktoren *Cebpa*, *Fos*, *Klf4*, *Nfatc1* und *Spi1,* die mit der T Zell Entwicklung und naiven T Zellen assoziiert werden, waren in encephalitogenen ZNS-isolierten CD4+ T Zellen erhöht exprimiert, was ihren Beitrag zur T Zell Plastizität suggeriert. Eine Korrelation der murinen T Zell-basierten Transkriptomanalyse mit MS-Suszeptibilitätsgenen, die aufgrund ihrer nahen Lokalisation (± 500 kb, ensembl Datenbank, Veröffentlichung 75) zu den MS-Risiko Nucleotid-Polymorphismen (SNPs), die in der Gesamtgenom-Assoziationsstudie (genome-wide association studies, GWAS) 2011 identifiziert wurden, selektiert wurden, ergab, dass 67.3% der MS Risikogene in der EAE differentiell exprimiert wurden. Die Expressionsmuster von *Bach2*, *Il2ra*, *Irf8*, *Mertk*, *Odf3b*, *Plek*, *Rgs1*, *Slc30a7*, und *Thada* wurden in unabhängigen Experimenten bestätigt, was eine Beteiligung an T Zell Pathogenität suggeriert. Eine erste funktionale Analyse von *Nfatc1* ergab, dass *Nfatc1*-defiziente CD4+ T Zellen keine klinischen Symptome der EAE auslösen können. *Nfatc1*-defiziente T Zellen können zwar aktiviert werden, ihre Differenzierung in Th17 Zellen mit entsprechender Zytokinexpression ist verringert. Da das induzierbare *Nfatc1*/αA Transcript sich von den anderen NFAT-Familienmitgliedern unterscheidet, könnte dieses ein interessantes Target für eine therapeutische Intervention bei MS darstellen.

Table of contents

Figures & Tables

Abbreviations

°C	Degree Centigrade
µg	Microgram
µm	Micrometer
Amp	Ampicillin
APC	Antigen presenting cell
APS	Ammonium persulfate
bFGF	Fibroblast growth factor
BSA	Bovine serum albumin
BTIC	Brain tumor initiating cell
$CaCl_2$	Calcium chloride
CFA	Complete Freund’s adjuvant
CFSE	Carboxyfluorescein succinimidyl ester
cm^2	Square centimeter
CNS	Central nervous system
CO_2	Carbon dioxide
ConA	Concanavalin A
$CuSO_4$	Copper (II) sulfate
DAPI	4',6-Diamidino-2-Phenylindole, Dilactate
ddH_2O	Double-distilled water
DMEM	Dulbecco's modified eagles medium
DNA	Deoxyribonucleic acid
DTT	Dithiothreitol
EAE	Experimental Autoimmune Encephalomyelitis
ECL	Enhanced chemoluminescence substrate
ECM	Extracellular matrix
E.coli	Escherichia coli
EDTA	Ethylene diamide tetraacetate

EdU	5-ethynyl-2´-deoxyuridine
EGF	Epidermal growth factor
ELISpot	Enzyme linked immuno spot
et al.	Et alii
EtOH	Ethanol
FACS	Fluorescence-activated cell sorter
FACS	Fluorescence activated cell sorting
FCS	Fetal calf serum
g	Gram or Gravitational acceleration
GFP	Green fluorescent protein
GM-CSF	Granulocyte monocyte colony stimulating factor
Gy	Gray
h	hour
H_2O	Water
H_2O_2	Hydrogen peroxide
HBSS	Hank's balanced salts solution
HCl	Hydrogen chloride
HLA	Human Leukocyte Antigen
HRP	Horseradish peroxidase
hs	Homo sapiens
IFITM3	Interferon-induced transmembrane protein 3
IL	Interleukin
IR	Irradiated
KCl	Potassium Chloride
kDa	Kilo Dalton
l	Liter
LB-Medium	Lysogeny broth medium
M	Molar
mA	Milliampere

MACS	Magnetic cell sorting
mg	Milligram
$MgCl_2$	Magnesium Chloride
MHC	Major histocompatibility complex
min	Minute
ml	Milliliter
MLTC	Mixed Lymphocyte Tumor Culture
mM	Millimolar
mm	Millimeter
MM	Mouse Medium
Mm	Mus musculus
MOG	Myelin oligodendrocyte glycoprotein
MTT	3-(4,5-Dimethylthiazol-2-yl)-2,5-diphenyltetrazolium bromide
NaCl	Sodium Chloride
$NaHCO_3$	Sodium hydrogen carbonate
ng	Nanogram
NGS	Normal goat serum
nl	Nanoliter
PBMC	Peripheral blood mononuclear cells
PBS	Phosphate-buffered Saline
PFA	Paraformaldehyde
PI	Propidium iodide
PPMS	Primary progressive multiple sclerosis
PTX	Pertussis toxin
qRT-PCR	quantitative Real Time Polymerase Chain Reaction
rh	recombinant human
rm	recombinant murine
rpm	Rounds per minute
RRMS	Relapsing-remitting multiple sclerosis

RT	Room temperature
SA	Streptavidin
SDS	Sodiumdodecylsulfate
SDS-PAGE	Sodiumdodecylsulfate polyacrylamide gel electrophoresis
sec	Second
TBS	Tris-buffered saline
TGF-β	Transforming growth factor beta
Th cell	T helper cell
TNF	Tumor necrosis factor
UV	Ultra violett
V	Volt
WB	Western Blot
WM	Mouse washing medium

1 Introduction

1.1 Glioblastoma multiforme

Glioblastoma multiforme is the most common and most malignant astrocytic intracranial tumor in adults. It is characterized by widespread invasion throughout the brain, resistance to various therapeutic approaches, and destruction of normal brain tissue, ultimately leading to death (2). The World Health Organization (WHO) classified the different astrocytic tumors according to their histopathological characteristics into grade II (diffuse astrocytomas), grade III (anaplastic astrocytomas), and grade IV (glioblastoma) (3). Glioblastoma multiforme (GBM) can develop either de novo (primary glioblastoma) or as the result of the malignant progression from a low-grade glioma (secondary glioblastoma). As reflected in the term “multiforme”, glioblastomas show significant heterogeneity on the cytopathological, transcriptional, and genomic levels (2,4,5). Recent studies have characterized the genomes (6,7) and transcriptomes (8,9) of glioblastomas in more detail providing the basis to further group these tumors according to molecular alterations to adapt treatment plans.

According to the Surveillance, Epidemiology, and End Result Program (SEER) Cancer Statistics Review (CSR) of the National Cancer Institute of the United States, the incidences of brain- and other nervous system cancers were 6.5 cases per 100,000 persons per year (2006 – 2010) and were therefore considered rare diseases. But with 4.3 deaths per 100,000 persons per year, tumors of the central nervous system (CNS) belong to the most fatal diseases (Figure 1). Ionizing radiation (IR) remains the only ascertained factor to increase the risk of developing brain tumors as evaluated by data of atomic bomb survivors (5,10).

Brain tumor patients experience symptoms that consist of seizures, progressive headache, nausea, vomiting, drowsiness, visual abnormalities, motor or sensitive deficits, which mainly reflect the increasing intracranial pressure; and vary depending on the site of tumor and the tumor type. For the diagnosis of a brain tumor, patients are subjected to magnetic resonance imaging (MRI) with and without contrast enhancing gadolinium infusion in combination with histological examination of tumor biopsies or surgical resections (4,5). The standard

treatment for GBM consists of surgery, radiation- and chemotherapy with temozolomide (TMZ), followed by adjuvant chemotherapy, but this regimen is only palliative and prolongs patient median survival to 12 to 15 months (1). The major cause of lethality is the post-treatment recurrence of tumors, which develop from radio- and chemoresistant cells.

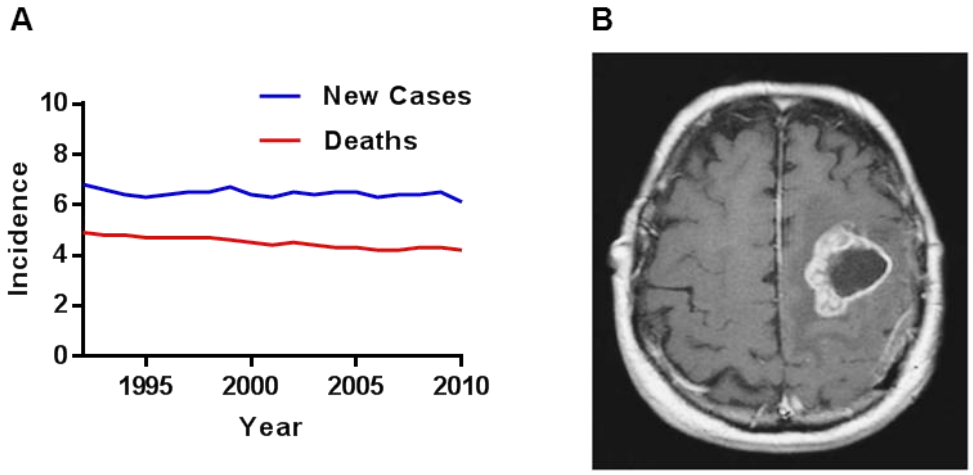

Figure 1: Incidence rate for nervous system cancers and MRI picture of a GBM.
(A) Data on the number of new cases and deaths in the USA for 100,000 persons per year from 1992 – 2010 as published by the NCI is publicly available on the NCI-homepage. Adapted from Howlader et al. 2010 (331). The rate of new cases as well as deaths per year remained stable throughout the last 20 years. (B) MRI picture with gadolinium enhancement of a glioblastoma multiforme in the left frontal lobe. Adapted from DeAngelis, 2001 (5).

1.1.1 Glioma-initiating cells

Cancers arise from a series of mutations that occur in few or even single founder cells. These cells eventually acquire unlimited and uncontrolled proliferation potential (11). After the identification of “cancer stem cells” (CSCs) or “tumor-initiating cells” (TICs) in leukemia (12,13), breast and pancreatic cancers, and melanoma (14–17), the “cancer stem cell” hypothesis of tumor development was postulated. This model assumes that only a rare subset of cells within the tumor has significant proliferation capacity and the ability to generate new tumors, with the remainder of the tumor cells representing differentiating cells (18,19).

In 2004, Singh et al. identified CD133+ tumor-initiating cells in brain tumors (20). These cells maintained the stem cell pool by self-renewal and gave rise to

multiple mature cells *in vitro* and *in vivo* (21,22). The use of the glycoprotein CD133 as a stem cell marker though is controversially discussed as also CD133- populations exhibit tumorigenic potential (23,24). Up to now, a brain tumor stem cell is defined by cancer-initiating capacities upon orthotopic transplantation, extensive proliferative and self-renewal capacities, karyotypic or genetic alterations, and aberrant differentiation potential into multi-lineage cells (18). As such, they share many characteristics of neural stem cells, including self-renewal potential, differentiation capacities into multi-lineage neural tissue cells, and activation of the same intracellular pathways. Therefore, it was proposed that glioma-initiating cells (GICs) could originate from the transformation of multipotent neural stem cells (NSCs) (18,19,25,26). Adult NSCs are found in specialized regions of the brain, the so-called stem cell niches, i.e. the subventricular zone (SVZ) of the cerebral cortex (27) and the subgranular zone (SGZ) of the dentate gyrus (28), in which endothelial cells regulate stem cell self-renewal (29–31). Similarly, also CSCs of other cancers seem to depend on a microenvironmental niche. Calabrese et al. demonstrated that Nestin+/CD133+ brain tumor stem cells rapidly and selectively associate with endothelial cells in co-cultures. Factors secreted by endothelial cells maintained the CSCs in a self-renewing and undifferentiated state (32). GICs also actively shape their surrounding by secretion of vascular endothelial growth factor (VEGF) to sustain vascular development for nutrition supply (33).

1.1.2 Immune suppression and evasion mechanisms by GICs

The CNS has long been regarded as an immune-privileged organ which lacks lymphatic drainage and which is protected from entering of harmful substances and cells by the blood-brain barrier (BBB). Increasing evidence now shows that immune surveillance does take place in the CNS (34,35). Microglia have been identified as CNS-resident macrophage equivalents that belong to the innate immune system and are responsible for immune surveillance in the brain (36).

Glioma cells, i.e. GICs, acquire several strategies to escape the immune responses during transformation, including expression of complement system inhibitors and immunosuppressive cytokines such as interleukin 10 (IL-10), IL-6, TGF-β, and prostaglandin E2 (PGE_2) (37–39). GICs also recruit

microglia/macrophages to the tumor (40) and repolarize them to become immunosuppressive (tumor-associated microglia/macrophages, TAM/MΦ) by expressing soluble colony-stimulating factor 1 (sCSF-1), TGF-β, and growth/differentiation factor 15 (GDF-15/MIC-1) (41–43). These TAM/MΦ can support tumor growth and immune evasion by expression of TGF-β, which can bind to its receptor (TGF-βR2) on GICs, resulting in increased MMP-9 production, breakdown of extracellular matrix (ECM), and a more invasive phenotype (44). The expression of inhibitory cytokines by glioma cells further recruits CD4+CD25+FoxP3+ regulatory T lymphocytes (Treg) to the tumor, which can in turn suppress antigen presenting cell (APC) function and counteract T cell-mediated immune responses (45). GICs also directly inhibit adequate T cell activation by downregulation of essential activation-associated co-stimulatory molecules such as CD80, CD86, CD40, or upregulation of the co-inhibitory molecule B7-H1 (PD1L, CD274) (45,46).

In addition to active immunosuppression, glioma cells also exhibit immune evasion mechanisms by downregulation of major histocompatibility complex (MHC) class I molecules, which was shown to be the case in approximately 50% of glioblastomas (47). Cells with low or absent MHC class I expression are recognized by NK cells via NKG2D-NKG2DL interactions and lysed, but glioma cells also express HLA-E, a non-classical HLA-molecule that inhibits NKG2D-mediated tumor cell lysis (48,49).

Interferons (IFNs) stimulate the cell's immunogenic potential by increasing the quantity of peptides presented by MHC class I proteins to CD8+ cytotoxic T cells (50). They can increase the expression of the transporter associated with antigen processing (TAP) 1 and TAP2 (51,52). This heterodimeric channel transfers peptides generated by the proteasome into the endoplasmic reticulum, where they are loaded onto MHC class I molecules through the interaction of the chaperon calnexin (cln), the thiol oxidoreductase ERp57, calreticulin, and tapasin with the histocompatibility complex (HC) class I heavy chain and β_2-microglobulin (β_2-m). Upon peptide binding to the MHC class I molecule (heavy chain and β_2-m), a conformational change leads to the release of the peptide-MHC class I complex and the transport to the cellular surface (Figure 2) (53).

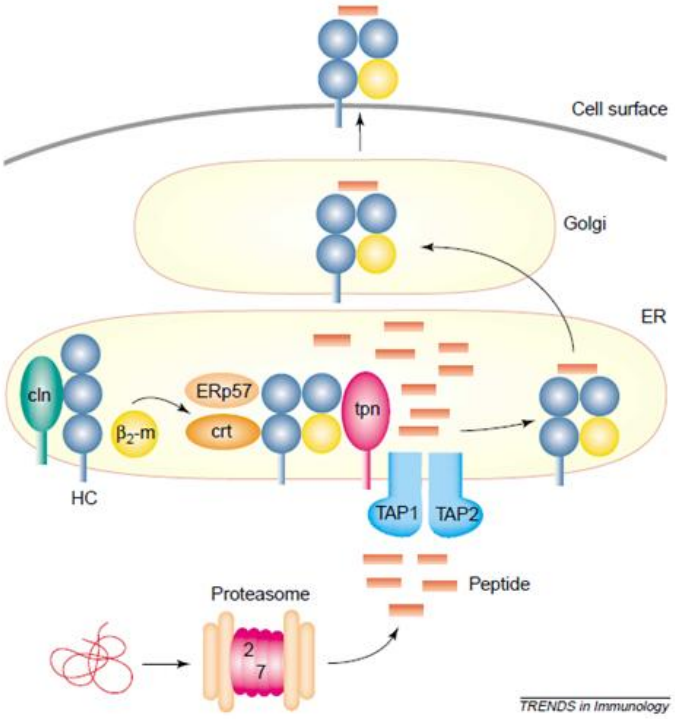

Figure 2: Peptide processing and presentation at the cell surface.
For the presentation of antigens to CD8+ T cells via MHC class I, peptides are degraded in the proteasome and shuttled through TAP1&TAP2 into the ER. The chaperone Calnexin (cln) associates to the histocompatibility complex (HC) class I which is subsequently bound by β2-microglobulin (β2-m) and a complex of thiol oxidoreductase ERp57, chaperone calreticulin, and tapasin for antigen load. The MHC-antigen complex is then transferred to the cellular surface. Adapted from Grandea & Van Kaer. 2001 (53).

1.1.3 The (therapeutic) effects of ionizing radiation

Radiotherapy (RT) belongs to the standard of care in glioblastoma therapy. However, the recurrence of radiation-resistant tumor cells remains a therapeutic challenge. New findings suggest that GICs might be more resistant to radiation and chemotherapy than the tumor bulk. Bao et al. demonstrated in cell culture experiments as well as in a xenograft model that the CD133+ human stem cell population was enriched after radiation compared to the parental population, suggesting that CD133+ cells are more radioresistant than CD133- cells (54). These findings were supported by histological analysis of GBM specimens before and after treatment in which CD133+ cells survived high radiation doses whereas extensive damage to tumor blood vessels was observed (55).

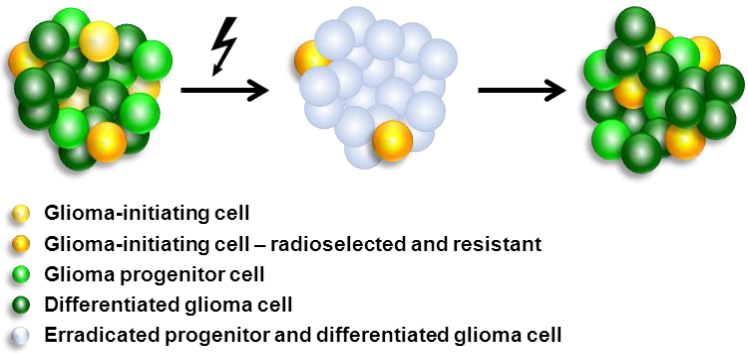

Figure 3: Radiotherapy does not eradicate radioresistant GICs.
Glioma-initiating cells are thought to maintain tumor growth in vivo. Through asymmetric cell division, these cells give rise to glioma progenitor and subsequent differentiated glioma cells that form the tumor bulk. Ionizing radiation can eradicate the progenitor- and differentiated glioma cells. Radioresistant glioma-initiating cells survive and are even selected by this treatment due to enhanced DNA double strand repair mechanisms, leading to subsequent radioresistant tumors. Modified from Hadjipanayis and Van Meir, 2009 (56).

Recent efforts have focused on elucidating resistance mechanisms activated in GICs in response to ionizing radiation (IR). It was proposed that CD133+ cells exhibit their high malignancy and resistance to radiation through preferential activation of the DNA damage response (DDR) machinery, including the DNA repair checkpoint kinases Chk1 and Chk2. The resulting cell cycle arrest led to more efficient DNA repair, reduction of apoptosis, and overall increased survival of CD133+ cells compared to CD133- cells (54). In IR-sensitive cells, radiation induces apoptosis through DNA damage and further triggers apoptotic signaling cascades initiated at the plasma membrane (57,58). Inside the plasma membrane as well as other cellular membranous compartments, lipid rafts represent important signaling platforms. These clusters, also called detergent-resistant membranes (DRMs) are enriched in lipids (cholesterol and sphingolipids) to bring glycosylphosphatidylinositol (GPI)-anchored as well as transmembrane proteins in close proximity for faster signaling (59,60). Upon exposure to gamma (γ-) radiation, the enzyme acid sphingomyelinase (ASMase) is translocated from lysosomes to the outer layer of the cell membrane, which then induces sphingomyelin hydrolysis and ceramide formation. Ceramide clumping with cholesterol enhances clustering of death receptors like Fas, tumor necrosis factor (TNF), CD40, TNF-related apoptosis-inducing ligand (TRAIL) or G protein- coupled receptors, thus inducing apoptosis (58). Defects in this structural

rearrangement were associated with a radio- and apoptosis-resistant phenotype in endothelial cells of tumor vessels (61,62) and human head and neck squamous carcinoma cell (SCC) lines (63).

Radiotherapy of GBM and especially the combination with temozolomide (TMZ) – chemotherapy was proven to cause survival benefits compared to untreated tumors (1). Paradoxically, increasing evidence suggests that IR also selects for resistant tumor cells with a more malignant phenotype (Figure 3) (64). *In vitro* irradiation of sub-lethal doses of 3 Gy, increased migration of glioblastoma cell lines U87MG and LN-18 by enhancing expression of integrin $\alpha_v\beta_3$, MMP-2, MMP-9, and promoted an apoptosis-resistant phenotype by increasing expression of BCL-2 family members. These results suggest that sub-lethal irradiation, which can occur in radiotherapy at the post-operative border of a tumor, promotes invasiveness of GBM cells into the healthy brain tissue and escape lethal radiation doses (65).

1.1.4 Interferon-induced transmembrane proteins

The human 1-8 interferon-inducible gene family has originally been described 30 years ago based on their increased expression after IFN type I and IFN type II treatment (66). This family consists of at least 3 functional genes; interferon-inducible transmembrane protein 1 (IFITM1; aliases 9-27, LEU-13), IFITM2 (alias 1-8D), and IFITM3 (1-8U), which are all linked on an 18 kb fragment of chromosome 11. These genes are highly homologous (67,68) and conserved throughout evolution (69).

IFITM3 was shown to be located at the plasma membrane as well as in exosome-like structures close to the plasma membrane (70). Various topologies have been proposed for IFITM proteins on the basis of flow cytometry and confocal microscopy analysis using N- and C-terminal tag-specific antibodies/probes and the identification of post-translational modifications. The C- and N-termini of IFITM3 were suggested to be located extracellularly or intracellularly or mixed, intermitted by either a transmembrane or an intramembrane domain and a cytosolic domain (Figure 4) (71–74). It was further suggested that IFITM3 topology might be variable, depending on different functions and cell types (74).

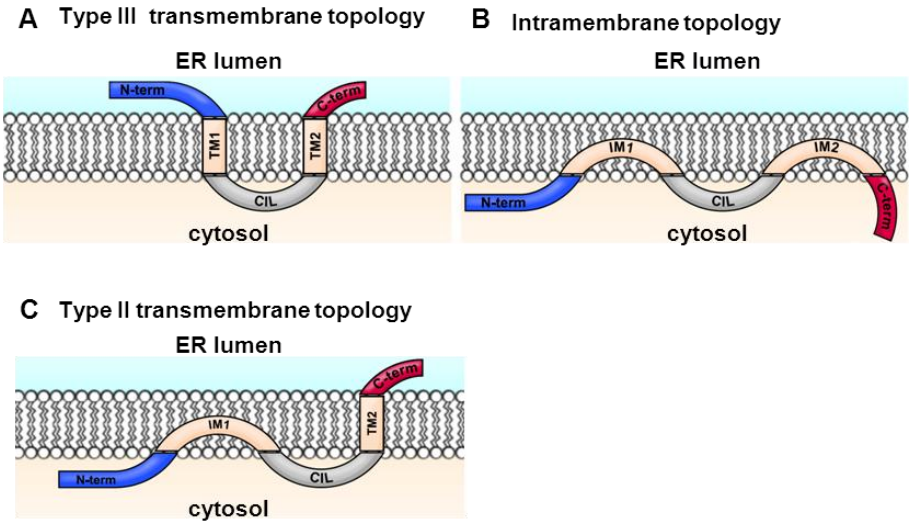

Figure 4: Proposed topologies of IFITM3.
Various topologies were proposed for IFITM proteins. (A) The amino and carboxyl termini lie in the vesicular lumen and extracellularly at the plasma membrane, connected by two transmembrane and one cytoplasmic domain. (B) An alternative model suggests that both amino and carboxyl termini are located intracellularly linked by two intramembrane and an intermediate cytoplasmic domain. (C) The third model predicts that the N-terminus is located in the cytosol and connected to a second cytosolic domain by a intramembrane domain, followed by a transmembrane domain with the C-terminus at the ER lumen. Modified from Bailey et al., 2013 (74).

Up to now, there are only few studies on the function of IFITM proteins and molecular binding partners as well as whole signaling pathways are largely unknown. IFITM1 and IFITM3 exhibit distinct guiding functions in germ cell development (75). They might have roles in controlling lymphocyte differentiation as they form complexes with the tetraspanin CD81 and lineage-specific molecules, such as CD19 and CD21 of B cells as well as CD4 and CD8 of T cells. In B cells, this complex is transferred into lipid rafts, necessary for the co-activation of the B cell receptor (71,76,77). IFITM1, -2, and -3 were associated with antiviral mechanisms as they inhibit an early step in influenza A, dengue and West Nile virus replication (78) by adhesion molecule interaction and disruption of cholesterol homeostasis (79).

IFITM3 was found to be strongly expressed in colon cancer patients and in inflamed colonic mucosa (80), which led to the proposal to use IFITM3 as diagnostic marker in these tumors (81). The homolog IFITM1 was reported to be highly expressed in head and neck squamous cell carcinoma (HNSCC),

especially at the invasive front (82), but less expressed in highly proliferative leukemic B cells and low-grade astrocytomas compared to healthy control cells (83,84). High expression of IFITM3 could also be correlated to poor overall survival of GBM patients, as determined by database analysis based on The Cancer Genome Atlas (TCGA) project, a large-scale collaborative initiative to characterize the genomic changes that occur in cancer (Figure 5).

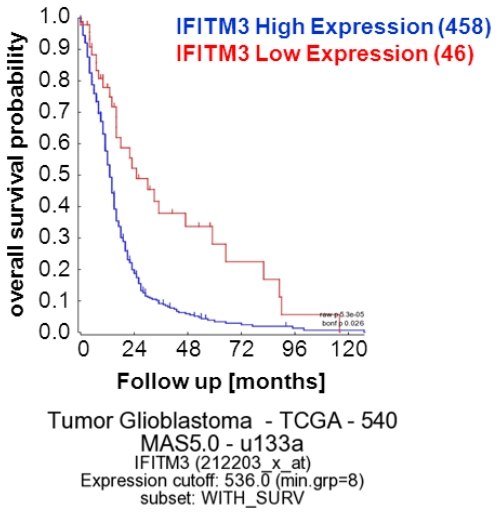

Figure 5: Overall survival probability related to IFITM3 in GBM patients.
The Cancer Genome Atlas (TCGA) is a large-scale initiative to identify genomic changes that occur in cancer by integrating genomic sequencing data with genomic characterization data and making the findings publicly available. Database search for GBM and IFITM3 revealed about 10 times more patients exhibiting high IFITM3 expression compared to low expression. Further, high expression of IFITM3 is correlated with poor prognosis according to TCGA with only 10% surviving more than 24 months after diagnosis.
Source: http://hgserver1.amc.nl/cgi-bin/r2/main.cgi.

The involvement of IFITM proteins in regulating proliferation is controversially discussed. Proliferation of melanoma cells could be inhibited *in vitro* and in a human xenograft model by treatment with high doses of IFN-α, which was associated with increased expression of IFITM1 (85) as well as overexpression of IFITM3 (70). El-Tanani et al. proposed a mechanism in which binding of IFITM3 to the secreted, integrin-binding and phosphorylated acidic glycoprotein osteopontin (OPN) resulted in OPN mRNA-destabilization and reduced protein expression, diminished cell adhesion, cell invasion, colony formation in soft agar, and metastasis in a rat model system (86). On the other hand, knockdown of IFITM3 expression in colon cancer cells by a specific siRNA significantly suppressed the proliferation, colony formation, migration, and invasion *in vitro,* and tumor growth and metastasis in a xenograft model (87). In line with this, knockdown of IFITM1 and IFITM3 reduced proliferation, migration, and invasion, and induced cell-cycle arrest and apoptosis in a glioma cell line *in vitro* (88,89). As the various studies propose tumor promoting and inhibiting functions for

IFITM3, the roles of IFITM3 in various cancers possibly depend on tumor microenvironments.

Recently, IFN-induced genes, including IFITM1, were found to respond robustly with highly increased expression to multiple fractionated radiation in breast, prostate and gliosarcoma cell lines (90). Induction of IFITM1 and IFITM2 expression was also confirmed in p53-deficient leukemic KG1a cells 24 h and 48 h after radiation with 3 Gy (91). Of note, some studies even correlate the increased expression of IFITM1 after IR to a radioresistant phenotype in human fibroblasts and head and neck tumors (92,93)

1.2 Multiple sclerosis

Multiple sclerosis (MS) is the most common chronic inflammatory disease of the CNS in young adults in Europe and North America in which the infiltration of self-reactive lymphocyte leads to neurodegeneration and progressive disability (94).

In 1868, the French neurologist Jean-Martin Charcot was the first to systematically analyzed Multiple Sclerosis and classified it as a distinct neurological disease (95). He recognized the important relationship between clinical observations and pathological findings post-mortem and was the first to diagnose MS on a living patient according to his symptom triad of nystagmus, intention tremor, and scanning speech (96). In his lectures on “Sclérose en plaques disséminée”, he described the pathology of Multiple Sclerosis that included loss of myelin with persistent axons, thickening of small blood vessels, persistence of fatty macrophages around vessels removing myelin residue, and glial scar formation. Charcot further linked the disability of the patients to damage of axons (97). These pathological findings are still valid today.

MS patients may suffer from a variety of clinical symptoms, such as sensory loss, visual problems, muscle weakness and difficulties with coordination and speech (98). Despite intensive research and technical advances to track disease progression, e.g. via magnetic resonance imaging (MRI), the relapse rate of patients with relapsing-remitting MS (RRMS) can only be prolonged but not cured by the use of immunomodulatory drugs such as Interferon-β (IFN-β) or Glatiramer acetate (GA) (99). Therefore, MS patients still have a reduction in life expectancy of 5 – 10 years (100,101).

1.2.1 Epidemiology and etiology

Up to date, the causes of MS are still unclear, but research proposes that diverse environmental factors might trigger the onset of Multiple Sclerosis in patients with complex genetically susceptible background. The gender, age, latitude of residence, genetic aspects, and certain viral infections seem to influence the susceptibility to MS (101). Europe and North America are considered high prevalence regions for MS with 60 - > 100 patients per 100,000 inhabitants (102–104). Females are more susceptible than males with a ratio of 1.6 – 2.0:1 in relapsing-remitting MS (RRMS) but not primary progressive MS (PPMS) (94,101). Evaluation of population, family, and twin studies showed that the prevalence is substantially increased in family members of MS patients. While monozygotic twins have a 20 – 35% risk to develop MS there is already a reduction in risk in first-degree relatives (2 – 5%) to second-degree (1%) compared to an age-adjusted background risk in white northern Europeans of 0.3% (94,105).

The first genetic factor associated with increased risk of multiple sclerosis was the human leukocyte antigen (HLA) locus identified in the 1970s (106,107) and since then the *HLA-DRB1**1501 allele has consistently been reported as the strongest genetic risk variant in the MHC region (108,109). Up to now, large-multicenter genome-wide association studies (GWAS) have identified a total of 110 single nucleotide polymorphisms (SNPs) that contribute to an increasing MS susceptibility risk (108,109).

A variety of environmental triggers were proposed to contribute to development and course of MS (110). Decreased exposure to sunlight and a deficiency in vitamin D was suggested to exacerbate MS as incidence rates increase with distance from the equator and migration from high-risk to low-risk regions in childhood reduces the risk to develop MS (111,112). 100% of MS patients are positive for Eppstein-Barr virus (EBV) antibodies compared to approximately 90% in the general population and latent EBV infections are more often reactivated in MS patients, correlating with relapses (101). Some viral antigens of EBV are highly similar to self-proteins (molecular mimicry) which might lead to cross reactivity with myelin, thus resulting in an autoimmune attack against self-antigens and demyelination (113,114).

There are different forms of MS categorized by clinical description of the disease Figure 6). Relapsing-remitting MS (RRMS) is the most frequent form of MS (85% - 90%) and characterized by discrete clinical relapses followed by complete recovery or residual deficits. Many years after onset, at least half of RRMS patients develop secondary progressive MS (SPMS) with slow but continuously progressive neurological impairments with or without clinical relapses and minor remissions. About 10% - 15% of patients experience a steady progression of deterioration without improvements or clear relapse episodes, termed primary progressive MS (PPMS). Progressive-relapsing multiple sclerosis (PRMS) is a rare form of the disease (5%) with continuous progression and few intermitted relapses. The symptoms of a relapse can develop over hours to days and persist for weeks until recovery. It is not clear which factors are responsible for the different courses (101,115,116).

Classification	Type of incidence at presentation	Schematic typical of clinical course
Relapsing remitting multiple sclerosis (RRMS)	~85%	
Secondary progressive multiple sclerosis (SPMS)	~50% of patients with RRMS will progress to this subform	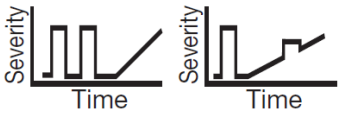
Primary progressive multiple sclerosis (PPMS)	~10%	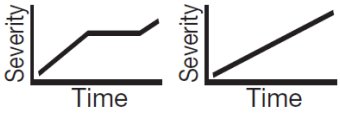
Progressive relapsing multiple sclerosis (PRMS)	~5%	

Figure 6: Classification, incidence and schematic representation of clinical course of MS.
Most patients experience a RRMS with distinct relapses after which symptoms are often fully restored. At least 50% of these patients progress to SPMS with continuous disability. 10 – 15% of MS patients display a PPMS without clear relapses but direct continuous disability, whereas a minor patient group progresses continuously with additional more severe relapses without improvements. Adapted from Thomson et al., 2006 (115).

1.2.2 Pathogenesis

Many findings suggest that the combination of genetic susceptibility and environmental factors results in a misguided immune system activation against self-antigens. The disseminated lesions found in the white and grey matter of the CNS of MS patients are histologically characterized by demyelination, gliosis, and axonal damage next to infiltration of T and B cells, activated microglia and macrophages, suggesting a role for these inflammatory cells in the disease process (117–120). As human brain tissue from MS patients as well as healthy control persons is limited, most knowledge on the underlying pathogenic molecular mechanisms of MS was gathered from its animal model experimental autoimmune encephalomyelitis (EAE).

A general consensus is that multiple sclerosis starts with the formation of acute inflammatory lesions, the breakdown of the blood-brain barrier (BBB) and activation of CNS-resident microglia (121,122) (Figure 7). Activated microglia upregulate their MHC and co-stimulatory molecules for their function as antigen-presenting cells (APCs) (123) and start to release pro-inflammatory cytokines and chemokines for the recruitment of monocytes, lymphocytes and dendritic cells into the lesion (124–126). Peripherally activated T cells can transmigrate into the CNS perivascular niche (127,128), where they are reactivated by microglia and differentiate into mature encephalitogenic T helper cells (Th1 and Th17) in a pro-inflammatory microenvironment (129,130). CD4+ T cells further recruit macrophages, which release additional pro-inflammatory cytokines and neurotoxic molecules such as nitric oxide (NO), interleukin 1 (IL-1), IL-6, tumor necrosis factor alpha (TNF-α), and matrix metalloproteinases, that contribute also to direct axonal damage (131,132).

Additionally to CD4+ T cells, CD8+ T cells were found to be present in MS lesions in the edge as well as the perivascular regions. The exact role and significance of CD8+ T cells is still highly debated as both a tissue damaging (cytotoxic CD8+ T cells) and CD4+ T cell suppressor function (regulatory CD8+ T cells) were described (133,134). Lesions are further infiltrated by regulatory T cells (Treg; CD4+CD25+FoxP3+). These cells are generally responsible to control and dampen inflammatory responses, but seem to be inhibited in their function to restrain Th17 effector function by expression of IL-6 (135).

Recent studies showed strong presence of immunoglobulin-containing cells in the plaques and the cerebrospinal fluid (CSF) of MS patients (136), resulting in the development of B cell specific pharmaceuticals with unexpected outcome. Clinical trials with Atacicept, a human recombinant fusion protein targeting B cell survival factors, were suspended after observation of increased inflammation in MS patients (137). Also, the reduction of acute lesions of MS patients after treatment with the B cell specific monoclonal antibody rituximab (138,139), was rather associated with a reduction in CSF T cells (140).

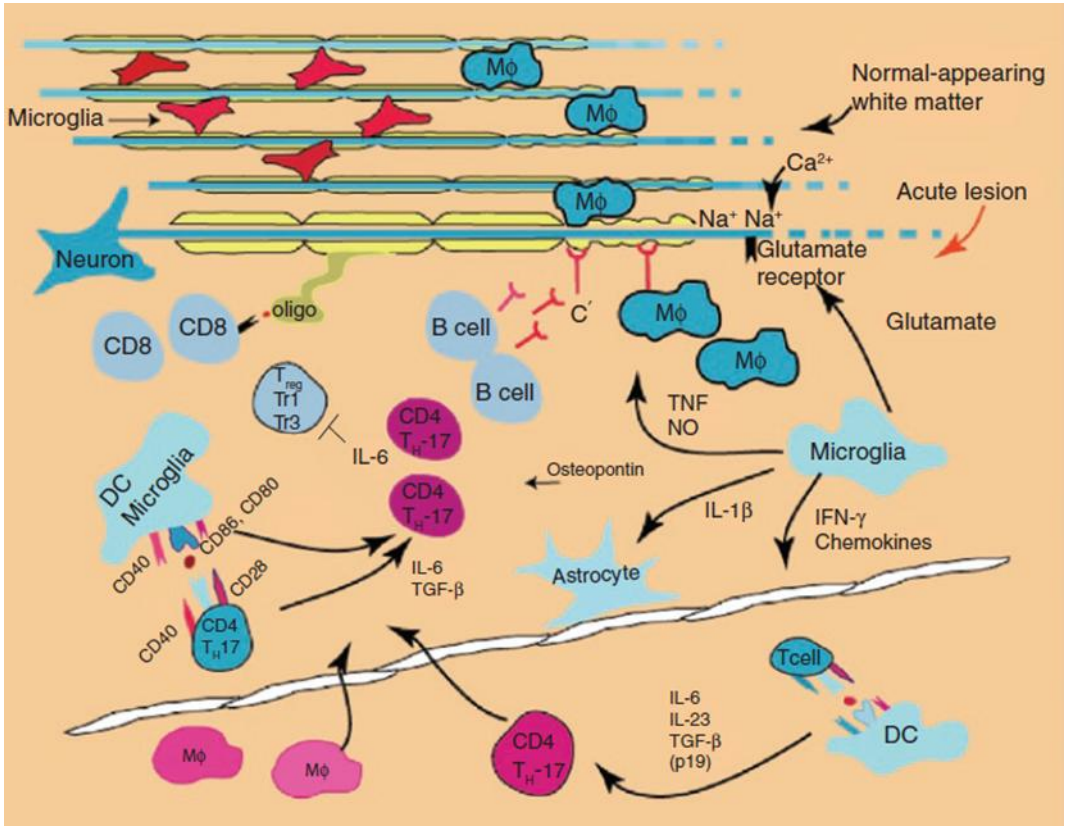

Figure 7: Pathogenic mechanisms that lead to CNS damage in EAE/MS.
Upon blood-brain barrier disturbance and activation of microglia, macrophages and T/B cells are recruited by a chemokine gradient into the CNS where encephalitogenic CD4+ Th1 and Th17 cells are reactivated by microglia/dendritic cells. The pro-inflammatory microenvironment together with release of neurotoxic nitric oxide and glutamate results in the destruction of the myelin sheath and axons. Adapted from McFarland et al., 2007 (122).

1.2.3 The animal model experimental autoimmune encephalomyelitis (EAE)

The animal model of MS, experimental autoimmune encephalomyelitis (EAE) was initially introduced in 1933 by Rivers et al., who immunized monkeys with rabbit brain emulsion to induce disseminated lesions (141) while today mouse models are most common (142). Several key features of MS, such as paralysis, weight loss, demyelination, and inflammation, observed in human patients, are recapitulated during EAE in mice (143,144). Nevertheless, none of the animal models established so far can reflect the full spectrum of MS symptoms and its various forms (145).

EAE is induced in mice actively by immunization with protein or peptide, or passively by adoptive transfer of encephalitogenic T cells (Figure 8). In active immunization protocols, the immunogen, which is derived from myelin basic protein (MBP), proteolipid protein (PLP), or myelin oligodendrocyte glycoprotein (MOG) (146–149), is subcutaneously injected in combination with complete Freund's adjuvant (CFA). CFA contains mineral oil and inactivated mycobacteria which are recognized by pattern recognition receptors such as Toll-like receptors (TLR) and compose a strong inflammatory stimulus. The disease can be enhanced by opening of the BBB through intraperitoneal injection of pertussis toxin (PT) (145,150,151). The immunization results in priming of auto-reactive inflammatory T helper cells (mainly Th1 and Th17 subtypes) in the secondary lymphoid organs that can subsequently infiltrate into the CNS for onset of clinical signs (152).

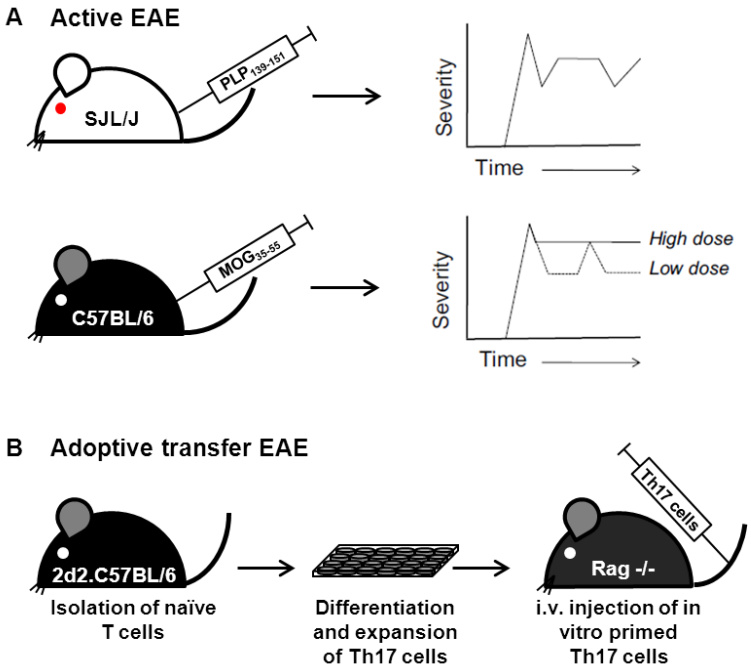

Figure 8: Schematic representation of active and adoptive transfer EAE models.
(A) EAE-susceptible mice are subcutaneously immunized with according myelin peptides. While SJL/J mice, immunized with the peptide $PLP_{139-151}$ exhibit a relapsing-remitting EAE, the course of MOG_{35-55}-induced EAE in C57BL/6 is monophasic but can be modulated by low peptide dose. (B) To study different effector cells, the adoptive transfer EAE model can be used. Naïve T cells can be isolated from transgenic donor mice with MOG-specific T cell receptors, differentiated and expanded in vitro to e.g. Th17 cells and transferred into immunodeficient recipient mice. Modified from Rangachari & Kuchroo, 2013 (145).

Another way of inducing EAE in mice is activation of myelin-specific T cells by active immunization of donor mice followed by isolation of peripheral lymphoid cells and their expansion and restimulation in culture. These T cells can subsequently be injected intravenously into naïve immunodeficient recipient mice (e.g. $Rag1^{-/-}$ mice) where they induce EAE symptoms (145). This “passive” or “adoptive transfer” model was further developed after the establishment of clonal T cell receptor transgenic mice. Naïve myelin-specific T cells can be isolated from the spleen of transgenic mice and directly be differentiated in culture before being transferred into recipient mice without prior *in situ* priming (Figure 8).

Depending on the mouse strain, different forms of EAE can be provoked. Immunization of SJL mice with the peptide $PLP_{139-151}$ induces a relapsing-remitting disease course (148), while disease induced by MOG_{35-55} peptide in

C57BL/6 mice tends to be of a chronic nature, which seems to depend on the peptide dosage (129,150,153). In the classic EAE model, animals develop an ascending paralysis, starting in the tail (score 1), and progressing to the hind limbs (score 2/3) as well as the forelimbs, leading to quadriplegia (score 4) and death (score 5) (142). These patterns of clinical disease manifestation are the consequence of preferential attack of the spinal cord.

The usage of the different EAE protocols in combination with gene knockout strains or different culture conditions are powerful tools to dissect the influence of a gene or drug as well as distinct effector functions of T cells in the onset and course of the disease (145,154).

1.2.4 CD4+ T lymphocytes and their role in MS and EAE

CD4+ T lymphocytes together with CD8+ T lymphocytes build the majority of the T cell compartment of the adaptive immune system. T cell precursors mature in the thymus to naïve CD4+ and CD8+ single positive T cells (155) and move to the secondary peripheral lymphoid organs (spleen and lymph nodes) where they screen their environment for the specific recognition of antigens that are presented by antigen presenting cells (APC) via MHC class II (CD4+ T cells) or MHC class I (CD8+ T cells) together with co-stimulatory molecules (156). After being activated, CD4+ T cells can differentiate into distinct effector subtypes, depending on the cytokine microenvironment, APCs and co-stimulatory molecules (Figure 9).

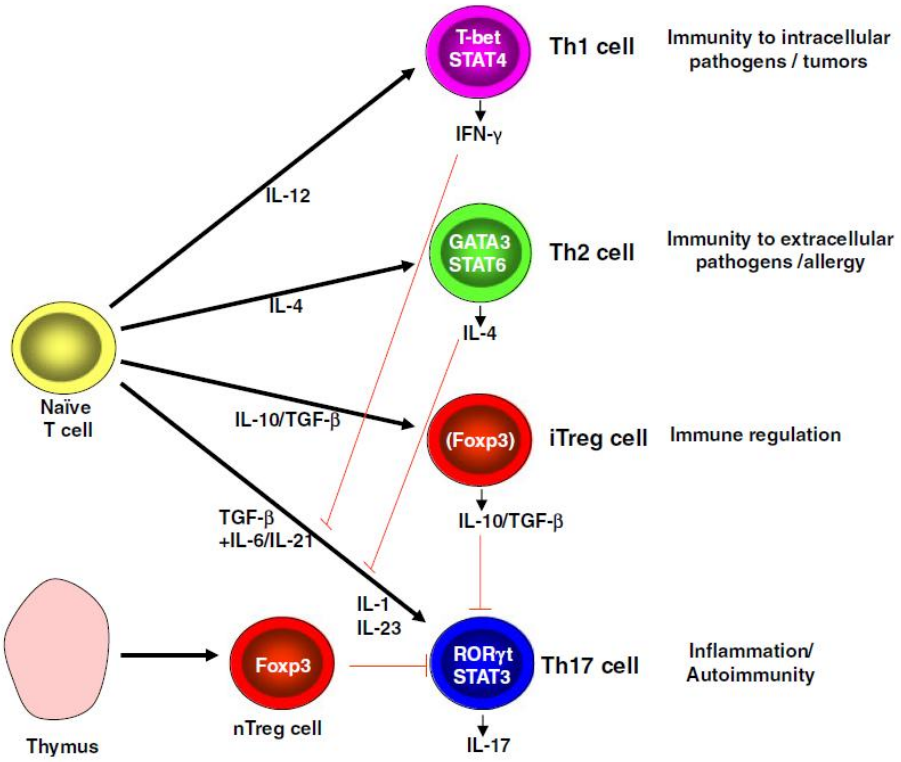

Figure 9: Differentiation of CD4+ T cells.
Depending on the cytokine microenvironment, naïve CD4+ T cells can differentiate into various T helper cell subsets. These can be distinguished by master transcription factors and specific cytokine profiles. Throughout the differentiation phase, the T cell subsets also inhibit cytokine expression that would lead to other lineages. Adapted from Mills, 2008 (157).

Classically, there were only two pro-inflammatory T helper (Th) cell subsets known: Th1 cells, which express the master transcription factor T-bet and the lineage cytokine Interferon gamma (IFN-γ), control intracellular pathogens, whereas Th2 cells, which express GATA3 and IL-4, are responsible for limiting extracellular pathogens (158–162). Throughout the last years, additional T cell subtypes have been identified. Regulatory T cells (Tregs) counteract inflammatory responses and are characterized by expression of the transcription factor forkhead box P3 (FoxP3) and surface molecule CD25. Th17 cells generally protect against bacteria and fungi (163,164). These cells express the master transcription factor retinoic acid receptor related orphan receptor (ROR)γt and contribute to different autoimmune diseases by expression of pro-inflammatory cytokines such as IL-17, IL-9 IL-21, IL-22, GM-CSF, and TNF-α (165–170) (Figure 9). Recently, also Th9 and Th22 cells were described as distinct CD4+ T

cell lineages. Together CD4+ T cells regulate immune response through the secretion of their individual cytokines by which the attract and activate cells of the innate and adaptive immune system to the inflammation site (171).

1.2.4.1 Th1 and Th17 T cells

Until recently, IFN-γ-expressing Th1 cells were regarded as the main effector T cells responsible for the autoimmune inflammation. This conclusion was based on the observation that these cells were frequently found in the CNS of EAE-diseased mice (172) as well as in brain lesions and CSF of MS patients (173,174). This hypothesis was further strengthened as mice, lacking IL-12p40 or IL-12 receptor, which are essential for Th1 differentiation, are resistant to EAE induction (175–177). Nevertheless, IFN-γ-knockout mice that lack Th1 cells are still susceptible to EAE (178). These contradictory results could be explained by the finding that IL-23 and not IL-12 was essential for the development of EAE (177,179). These heterodimeric cytokines share the p40 chain in combination with either p19 or p35 for IL-23 and IL-12 respectively. IL-23 is necessary for the expansion of IL-17-secreting CD4+ T cells (180). Th17 cells became the new focus of MS research as the knockdown of RORγt abolished EAE symptoms (181) similar to therapeutic neutralization of IL-17 with IL-17 receptor-Fc-protein or IL-17 antibodies (182,183). The contribution of IL-17 to the development of EAE though is still controversial: IL-17$^{-/-}$ mice displayed delayed EAE onset, reduced maximum severity scores, and early recovery. In these mice, an increase in IFN-γ-expressing cells was detected, but suggested to be less responsible for the severity of EAE due to diminished clinical scores (184). Th17 cells are nevertheless regarded as key pathogenic players. The expression of IL-17 and IL-22 was shown to lead to the disruption of the BBB, allowing Th17 cells to efficiently penetrate into the brain (185).

IL-23 was shown to be required during the induction but not the effector phase of EAE, as IL-23/p19-knockout mice are completely resistant to EAE induction by immunization with MOG_{35-55}, whereas wild-type recipients develop a mild disease upon adoptive transfer of cells from MOG-immunized IL-23/p19-knockout mice. Interestingly, similar to T-bet, IL-23 seems to connect Th1 and Th17 cells and regulate their effector function, as cells isolated from draining lymph nodes of

MOG-immunized IL-23/p19-knockout mice were greatly defective in production of IFN-γ and IL-17A (186).

In summary, both Th1 and Th17 lineage cells are implicated in the pathogenesis of EAE. The encephalitogenicity of the pro-inflammatory Th subsets seems to depend on the combinatorial expression of various transcription factors, including RORγt and T-bet as well as cytokines IL-23, GM-CSF, and TNF-α (187).

1.2.5 Plasticity of T cells

Although CD4+ T cell subsets have elements of stability and are regarded as distinct lineages, there is increasing evidence of substantial plasticity among the subsets (162,164,188). Among all CD4+ T cell subsets, Th17 cells seem to be the most plastic cells that can produce IFN-γ in addition to IL-17, in combination with co-expression of RORγt and T-bet, suggesting a relationship between Th1 and Th17 cells (189–191) (Figure 10). Polarized Th17 cells can convert to Th1 or Th2 cells in the presence of IL-12 or IL-4, respectively (192,193). This plasticity was further demonstrated in *in vivo* models for colitis and diabetes in which IL-17+IFN-γ- cells rapidly converted into a subset of IL-17+IFN-γ+ double positive cells upon adoptive transfer into naïve recipient mice (192,194,195). The transcription factor T-bet was suggested to link Th1 and Th17 cells and to be responsible for the differentiation potential and encephalitogenicity of both cell lineages in EAE (196,197).

A relationship between Th17 cells and Tregs was also proposed as TGF-β is an essential cytokine in the polarization of both Th17 and Tregs (198,199). Of note, considerable numbers of human CD4+ T cells co-express FoxP3 and RORγt and exhibit suppressive activity (200). The speculation that T cell plasticity and lineage transcription factor co-expression is an *in vitro* artifact could be counteracted by isolation of CD4+ T cells, co-expressing RORγt and FoxP3 in mice and human *in vivo* (200–202).

Epigenetic modulations were proposed to control phenotypic stability of CD4+ T cells. Complex methylation patterns were found in CD4+ lineage-committed cells that can be associated with activation and silencing of genes with considerable intrinsic instability of i.e. the *Ifng* locus of Th17 cells (162,192,203).

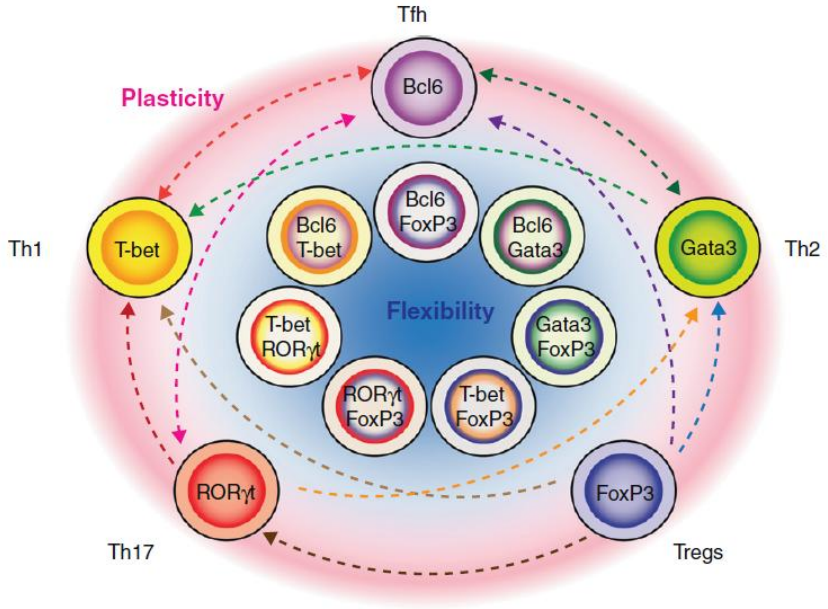

Figure 10: Plasticity of T helper cells.
Th cells can rapidly switch between different phenotypes and even express more than one "lineage-specific" master transcription factor. Adapted from Nakayamada et al., 2012 (162).

1.2.6 Nuclear factor of activated T cells (NFAT) and its role in autoimmune diseases

The nuclear factor of activated T cells (NFAT) was originally characterized as a putative transcription factor in nuclear protein extract from activated Jurkat T cells in which it was bound to the human IL-2 promotor (204). The NFAT family consists of five different members: NFATc1 (NFAT2; NFATc), NFATc2 (NFAT1; NFATp), NFATc3 (NFAT4; NFATx), NFATc4 (NFAT3), and NFAT5 (TonEBP; OREBP). NFATs are ubiquitously expressed in all cell types but only NFATc1-c3 are expressed in lymphocytes (205). All of the family members share a highly conserved DNA binding domain that is structurally related to the Rel/NFκB DNA binding domain which harbors a sequence for the interaction with other transcription factors such as AP-1 (Fos/Jun) (206,207). NFATc1-c4 build a distinct family of transcription factors due to their regulatory domain to which the Calcium (Ca^{2+})/calmodulin-dependent protein phosphatase calcineurin can bind for NFAT activation.

In T lymphocytes, NFAT proteins regulate gene expression for T cell development, activation, differentiation, as well as induction and maintenance of T cell tolerance (208–210). TCR-mediated signaling induces a rise of intracellular calcium and the activation of the phosphatase calcineurin and, in the presence of secondary signals, activation of the Ras/Raf/Erk signaling cascade. While calcineurin immediately translocates NFAT to the nucleus, components of the Ras/Raf/Erk pathway control its transcriptional activation and the induction of AP-1 (Fos/Jun) proteins (211–213). In the case of TCR activation in absence of secondary signals, an increase in intracellular calcium leads to the formation of NFAT homodimer complexes that direct the expression of a specific set of anergy-inducing genes, important for the inactivation of T cells that recognize self-antigens (209,214,215).

In Th17 cells, NFAT proteins regulate the expression of IL-17, IL-21, and IL-22 as well as the master transcription factor RORγt through combinatorial binding with other transcription factors to the promotor regions (208,216) (Figure 11).

The importance of calcium signaling and NFAT activation are exploited especially after organ transplantation or in autoimmune diseases when patients are treated with calcineurin inhibitors cyclosporin A (CsA) or FK506 that are efficient immune suppressors (217–220). As the NFAT proteins are multi-functional key regulators of immunological response and tolerance, deregulation can have dramatic effects and contribute to autoimmune diseases (221).

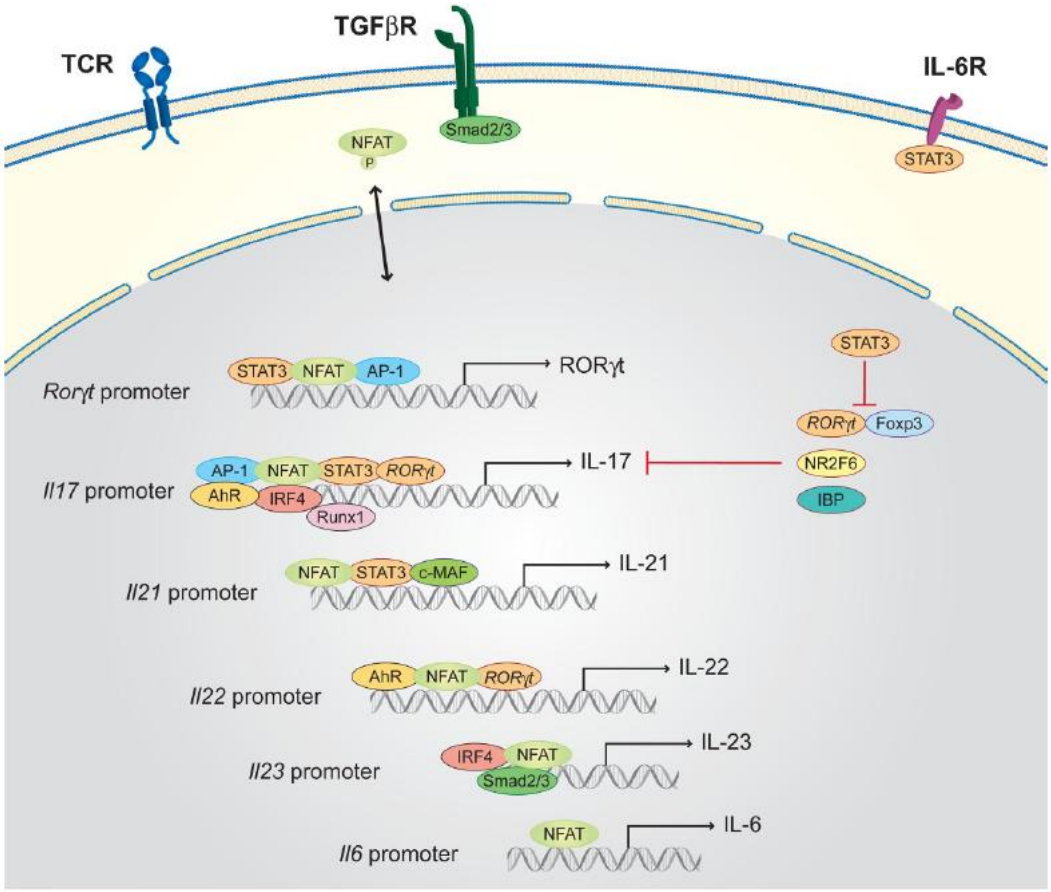

Figure 11: Schematic representation of Th17 lineage master transcription factor and cytokines.
After TCR signaling, differentiation into Th17 cells starts with activation of IL-6R, and STAT3, which together with NFAT and AP-1 activate RORγt expression. Subsequently, RORγt, together with NFAT, AP-1, STAT3, AhR, IRF4, and Runx1, bind to the IL-17 promoter to induce transcription. In parallel, NFAT, STAT3 and c-MAF, induce the transcription of IL-21. NFAT together with RORγt and AhR activates transcription of IL-22 and in combination with IRF4 and Smad2/3 activation of IL-23. Adapted from Hermann-Kleiter & Baier, 2010 (208).

1.3 Aim of this study

Glioblastoma multiforme and multiple sclerosis are two incurable diseases that affect the CNS. While GBM cells manipulate the cells of the immune system become tumor-protective, the immune cells exacerbate their actions against self-molecules and destroy the CNS, which leads to the symptoms of MS.

Glioma-initiating cells are low immunogenic, resistant to various kinds of therapy, and seem to be the main players in orchestrating immune escape mechanisms,

thus initiate and propagate the growth of brain tumors. Therefore, these cells need further characterization in order to understand their molecular mechanisms and resulting changes when pressured with anti-tumor therapies.

In the pathogenesis of MS, T cells are regarded as the main drivers. T cells were shown to undergo massive metabolic changes in the course of EAE that might even contribute to a more pathogenic phenotype. To better understand pathogenic mechanisms of Th17 cells and possibly identify new therapeutic targets, analysis of underlying whole transcriptional changes is needed.

The overall aim of this study was to evaluate immune escape mechanisms in glioma-initiating cells and transcriptional changes that control T cell plasticity and encephalitogenicity in autoimmunity. Further, functional studies for the contribution of key regulatory factors were performed to identify new therapeutic targets.

To address this aim, the thesis was divided into two parts:

1.3.1 Analysis of GIC properties and their interaction with the immune system in the context of ionizing radiation and the functional analysis of the immune gene *Ifitm3*

Radiotherapy belongs to the standard treatment of GBM after surgery. Due to radio-resistant GICs, new approaches yield at exploiting immunotherapies to specifically target tumor-associated antigens (TAAs). Malignant glioma cells have been shown to hardly express TAP and MHC class I molecules (222) thus have low immunogenic potential. Controversial evidence proposes that GICs highly express TAAs that can be used for dendritic cell vaccination resulting in eradication of tumors (223,224). However, up to now there have only been unsuccessful clinical trials and GICs are highly immunosuppressive (54,225). Ionizing radiation has been shown to immediately increase MHC I complexes on the cellular surface, thus proposing to combine radiotherapy with immunotherapy (226). As radiotherapy also leads to immunosuppression, this combination can only be applied in a sequential therapeutic setup. It was the aim of the study to investigate long-term effects of radiation on immunologic properties of GICs in a

model of patient-derived GICs that were radio-selected with fractionated ionizing radiation while control cells were left untreated.

The findings that ionizing radiation also influences expression of immune related, i.e. interferon-inducible, genes further increased the need to investigate in which way radiotherapy can trigger a change in immunological characteristics of GICs and foster immune escape mechanisms (90,92). In a comparative transcriptome analysis of the GIC cell line 1080 (GIC-1080) and their radio-selected counterparts (rsGIC-1080), increased expression of IFITM3 was observed after fractionated radiation (E. Kim, unpublished data). However, a general role of IFITM3 in glioma cells and especially in GICs had not been described at the time when this thesis was started.

The following questions were addressed in this part:

- What is the effect of ionizing radiation on proliferation and migration in a patient-derived glioma-initiating cell line?
- Does ionizing radiation influence the immunological properties of glioma-initiating cells?
- Is the interferon-induced transmembrane protein 3 (IFITM3) involved in the proliferation of glioma-initiating cells *in vitro*?
- Does the upregulation or knockdown of IFITM3 influence tumor growths, survival, or microglia activation *in vivo*?

1.3.2 Analysis of transcriptional changes underlying T cell plasticity as well as the influence of NFATc1 on the pathogenicity of T cells in the course of EAE

It is well established that *in vitro* primed IL-17-producing cells start to additionally express IFN-γ upon adoptive transfer into lymphopenic *Rag-1*$^{-/-}$ mice in the course of EAE. This transformation towards a Th1 phenotype was accompanied by synchronously expression of Th17 and Th1 transcription factors RORγt and T-bet (162,189). In a melanoma model, this Th17 cell lineage flexibility was even

associated with a more pathogenic phenotype, necessary to eradicate the tumor (227).

With the advent of microarray technology, this useful and hypothesis-free method has been used to identify differentially expressed genes that contribute to T cell differentiation and pathogenesis in autoimmunity (228). Yet, whole transcriptional changes in combination with signaling network analysis that control Th17 cell plasticity and encephalitogenicity in the course of EAE have not been investigated. Further, the involvement of MS susceptibility risk associated genes in T cell differentiation and the course of EAE has only been addressed with the characterization of few single genes. Another goal of this work was the functional investigation of candidate genes that play a major role in T cell plasticity and encephalitogenicity.

The following questions were addressed in this part:

- Which phenotypic changes and molecular mechanisms underlie the plasticity and encephalitogenicity of Th17 cells in the course of EAE?
- Which MS susceptibility genes are regulated in the differentiation of Th17 cells and are involved in their pathogenic effector function in the context of EAE?
- What is the impact of the deletion of Nuclear factor of activated T cells c1 (NFATc1) to the activation, differentiation and effector function of Th17 cells in the course of EAE?

2 Materials and Methods

2.1 Materials

2.1.1 Chemical and reagents

Chemicals / Reagents / Kits	Company	Number
4',6-Diamidino-2-Phenylindole, Dilactate (DAPI)	Invitrogen	D3571
^{51}Chromium (2 mCi=74 MBq)	Perkin Elmer	NEZ 030S002MC
AB-Serum	Lonza	14-491E
Accutase	PAA The Cell Culture Company	L11007
Agarose	Applichem	A8963, 0500
Bovine serum albumin	Serva	11930.03
Bradford Ultra TM	Biozol	EXP-BFU05L
Brefeldin A	Sigma-Aldrich	D7651
Bromphenol blue	Roth	A512.1
Carprofen (Rimadyl®)	Pfizer	P693088G
CFSE	Invitrogen	C1157
Collagenase	Sigma-Aldrich	C5138
Collagenase-Dispase	Roche	11097113001
Complete Freund`s adjuvant (CFA)	BD Difco	263810 (0638-60)
Complete protease inhibitor	Roche	11836145001
Dithiothreitol (DTT)	Roth	6908.2
DNase I recombinant RNase-free	Roche	14070500
Dulbeccos' PBS (1x) with Ca+Mg	PAA The Cell Culture Company	H15001
ECL Western Blotting Detection Reagents	GE Healthcare	RPN2106
EDTA	Roth	8043.2
Ethanol	Roth	9065.3
Ethylenediaminetetraacetic acid	Roth	8043.2

Fetal bovine serum Superior	Biochrom AG	S 0615
Fluorescent Mounting Medium	Dako North America	201110
Glycerol	Roth	3783.1
Glycin	Roth	3908.2
Goat Serum (Normal)	Dako North America	X0907
H37RA	BD Difco	231141
Hepes	Gibco	15630-056
Igepal Ca-630 (NP40)	Sigma	13021
Interferon-gamma	Sigma	I3265
Iscove's Mod Dulbecco's Medium (IMDM)	Gibco	21980-065
Ketamin-hameln	Hameln Pharma Plus GmBH	45481/37/10
L-Glutamine, 100x, 200 nM	Gibco	25030-024
MEM Non-essential amino acids solution	Gibco	11140035
Mercapto EtOH for electrophoresis	Sigma	M7154
Milk powder	Roth	T145.1
MOG_{35-55} (MEVGWYRSPFSRVVHLYRNGK)	Hookie	EK-2110
NaCl-solution (0.9%)	Braun	5/346177/0310
Neurobasal-A-Medium (1x)	Gibco	10888022
Nonident P-40	Sigma	I-3021
Ornithine-Poly-L-Hydrobromide	Sigma	P3655
PageRuler Prestained Protein Ladder	Thermo Scientific	26616
Paraforme aldehyde (PFA)	Merck	30525894
Pen Strep	Gibco	15140122
Percoll	Sigma	P1644-500ml
Pertussis toxin (PTX)	List Biologicals	180217A1
Propidium iodide (PI) solution	Sigma	P4864
RNaseOUT™ Recombinant Ribonuclease Inhibitor	Invitrogen	10777-019
Rotiphorese Gel 30	Roth	3029.2
RPMI Medium 1640 (1x) + L-Glutamine	Gibco	21875034

SDS Pellets	Roth	CN30.2
Sodium Chloride	Roth	3957.1
Superscript III First Strand Synthesis System	Invitrogen	18080-051
SYBRGreenER™ qPCR Supermix for iCycler	Invitrogen	11761500
TEMED	Roth	2367.3
Tris	Roth	4855.2
TritonX-100	Roth	3051.3
Trypan blue	Fluka	93595250ML
Trypsin-EDTA (10x)	PAA	L11003
Tween-20	Roth	9127.1
Xylazinhydrochloride (2%)	Bayer Vital GmbH	PZN-1320422

2.1.2 Buffers and solutions

Cell Culture

Neurobasal-A Medium Naked	Neurobasal-A Medium	500 ml
	B27 Supplement (50x)	10 ml
	Pen Strep (Pen: 10,000 units/ml; Strep: 10,000 µg/ml)	5 ml

Neurobasal-A Medium Complete	Neurobasal-A Medium Naked	500 ml
	0.1% BSA (10% stock)	5 ml
	10 ng/ml bFGF (100 µg/µl stock)	50 µl
	20 ng/ml EGF (500 µg/µl stock)	10 µl

DMEM Medium	DMEM Medium - Pyruvate	500 ml
	10% Fetal Calf Serum	50 ml
	Pen Strep (Pen: 10,000 units/ml; Strep: 10,000 µg/ml)	5 ml

RPMI 1640 Culture Medium	RPMI 1640 Medium	500 ml
	10% Fetal Calf Serum	50 ml
	Pen Strep (Pen: 10,000 units/ml; Strep: 10,000 µg/ml)	5 ml
	1% Hepes (1 M)	5 ml
	2 mM L-Glutamine	10 ml

RPMI 1640 Wash Medium	RPMI 1640 Medium	500 ml
	5% Fetal Calf Serum	25 ml
	Pen Strep (Pen: 10,000 units/ml; Strep: 10,000 µg/ml)	5 ml
	1% Hepes (1 M)	5 ml

Human AB Medium	RPMI 1640 Medium	500 ml
	5% human AB Serum	25 ml
	L-Glutamine	5 ml
	Pen Strep (Pen: 10,000 units/ml; Strep: 10,000 µg/ml)	5 ml
	1% Hepes (1 M)	5 ml

MACS Buffer	PBS	500 ml
	0.5% BSA	2.5 g
	2 mM EDTA	

FACS Buffer	PBS	500 ml
	0.5% BSA	2.5 g

SDS-PAGE and Western Blotting

Protein Lysis Buffer	50 mM Tris pH 7.4
	150 mM NaCl
	1% NP40
	0.5% Sodiumdeoxycholat
	20% Glycerol

Lipid Raft Lysis Buffer Brij98® pH 7.5 (1 l)	25 mM Tris	3.0 g
	140 mM NaCl	8.2 g
	0.5% Brij98®	0.5 g/100 ml
	1x Roche Complete (100x)	1 ml/100 ml
	1 mM EDTA	0.037 g

Lipid Raft Lysis Buffer Triton pH 7.5 (1 l)	25 mM Tris	3.0 g
	140 mM NaCl	8.2 g
	1% TritonX-100	10 ml/10%
	1x Roche Complete (100x)	1 ml/100 ml
	1 mM EDTA	0.037 g

5x Laemmli Buffer (10 ml)	1 M Tris pH6.8	2.5 ml
	DTT	0.77 g
	SDS	1 g
	Glycerol	5 ml
	Bromphenolblau	22 mg
	ddH_2O	4 ml

Separation Gel		10%	12%
	ddH_2O	4.2 ml	3.5 ml
	Acrylamid-Bisacrylamid (30%)	3.3 ml	4.0 ml
	1.5 mM Tris-SDS Buffer I pH 8.8	2.5 ml	2.5 ml
	APS (10%)	100 µl	100 µl
	TEMED	10 µl	10 µl

5% Stacking Gel	ddH_2O	1.725 ml
	Acrylamid-Bisacrylamid (30%)	415 µl
	1.5 mM Tris-SDS Buffer II pH 6.8	315 µl
	APS (10%)	25 µl
	TEMED	2.5 µl

10x Running Buffer (1 l)	Tris	30.3 g

	Glycine	144 g
	SDS	10 g
1x Transfer Buffer (1 l)	Tris	3.03 g
	Glycine	14.4 g
	Methanol	150 ml
10x TBS-T pH 7.5 (1 l)	Tris	60.5 g
	NaCl	87.6 g
	Tween20	10 ml
Primary Antibody Solution	TBS-T	50 ml
	5% BSA	2.5 g
	0.1% Sodiumazide (5%)	1 ml
Secondary Antibody Solution	TBS-T	100 ml
	3% BSA	3.0 g

Immunocytochemistry

Blocking buffer	1% BSA	0.1 g
	4% Normal Goat Serum	400 µl
	0.5% NP-40 (10%)	500 µl
	PBS	9.1 ml
Antibody buffer	1% BSA	0.1 g
	0.5% NP-40 (10%)	500 µl
	PBS	9.5 ml

2.1.3 Antibodies

Human Primary Antibodies	Source	Company	Order No.	Application & Dilution
anti-beta Actin	mouse	MP	691001	WB: 1:3000
anti-Cav1	rabbit	Sigma	C4490	WB: 1:3000
anti-CD16-FITC	mouse	Beckman Coulter	6604894	FACS: 1:3
anti-CD3-APC (clone UCHT1)	mouse	BD	555335	FACS: 1:4
anti-CD4-FITC	mouse	BD	345768	FACS: 1:400
anti-CD4-V450 (clone RPA-T4)	mouse	BD	560345	FACS: 1:40
anti-CD56-PE	mouse	Beckman Coulter	A07788	FACS: 1:3
anti-CD69-PeCy7	mouse	BD	557745	FACS: 1:100
anti-CD8-PerCP (clone SK1)	mouse	ebioscience	9043-0087	FACS: 1:6
anti-Flot1	rabbit	Sigma	HPA001393	WB: 1:500
anti-GAPDH	mouse	Millipore	MAB374	WB: 1:5,000
anti-GFAP (clone GA5)	mouse	Sigma	G3893	IF: 1:200
anti-HLA A1	mouse	OneLambda	0544HA	FACS: 1:100
anti-HLA A2-PA2.1	mouse	Hybridoma	AG Wölfel	FACS: 100 µl
anti-HLA B1.23.2	mouse	Hybridoma	AG Wölfel	FACS: 100 µl
anti-HLA B15	mouse	OneLambda	0044HA	FACS: 1 µl
anti-HLA W32/6	mouse	Hybridoma	AG Wölfel	FACS: 100 µl
anti-IFITM3	rabbit	Abgent	AP1153a	FACS: 1:50; IF: 1:200
anti-IFITM3	rabbit	Abcam	ab15592	WB: 1:1000
anti-IgG1	mouse	Beckman Coulter	IM 0571	FACS: 1:50
anti-myc-tag (clone 9B11)	mouse	Cell Signaling	2276	WB: 1:1000
anti-Nestin	mouse	R&D	MAB1259	FACS: 1:200; IF: 1:200
anti-Nestin	rabbit	Abcam	ab28944	FACS: 1:200; IF: 1:200
anti-Sfr6/B8	mouse	Hybridoma	AG Wölfel	FACS: 100 µl
anti-Sox2 (clone L1D6A2)	mouse	Cell Signaling	4900	IF: 1:50

anti-TAP1	mouse	Novus	NBP1-54435	WB: 1:500
anti-TAP2	mouse	MLB	K0137-3	WB: 1:1,000
anti-Vβ11-FITC	mouse	Beckman Coulter	IM1586	FACS: 1:3
anti-Vβ12-PE	mouse	Beckman Coulter	IM2291	FACS: 1:3
anti-Vβ13.1-PE	mouse	Beckman Coulter	IM2292	FACS: 1:3
anti-Vβ13.2-PE	mouse	Beckman Coulter	IM3603	FACS: 1:3
anti-Vβ13.6-FITC	mouse	Beckman Coulter	IM1330	FACS: 1:3
anti-Vβ14-FITC	mouse	Beckman Coulter	IM1558	FACS: 1:3
anti-Vβ16-FITC	mouse	Beckman Coulter	IM1560	FACS: 1:3
anti-Vβ17-PE	mouse	Beckman Coulter	IM2048	FACS: 1:3
anti-Vβ18-PE	mouse	Beckman Coulter	IM2049	FACS: 1:3
anti-Vβ1-FITC	rat	Beckman Coulter	IM2406	FACS: 1:3
anti-Vβ20-FITC	mouse	Beckman Coulter	IM1562	FACS: 1:3
anti-Vβ21.3-FITC	mouse	Beckman Coulter	IM1483	FACS: 1:3
anti-Vβ22-FITC	mouse	Beckman Coulter	IM1484	FACS: 1:3
anti-Vβ23-PE	mouse	Beckman Coulter	IM2004	FACS: 1:3
anti-Vβ2-PE	mouse	Beckman Coulter	IM2313	FACS: 1:3
anti-Vβ3-FITC	mouse	Beckman Coulter	IM2372	FACS: 1:3
anti-Vβ4-PE	rat	Beckman Coulter	IM3602	FACS: 1:3
anti-Vβ5.1-PE	mouse	Beckman Coulter	IM2285	FACS: 1:3
anti-Vβ5.2-FITC	mouse	Beckman Coulter	IM1482	FACS: 1:3
anti-Vβ5.3-PE	mouse	Beckman Coulter	IM2002	FACS: 1:3
anti-Vβ7.1-FITC	mouse	Beckman Coulter	IM2408	FACS: 1:3
anti-Vβ7.2-PE	mouse	Beckman Coulter	IM3604	FACS: 1:3
anti-Vβ8-FITC	mouse	Beckman Coulter	IM1233	FACS: 1:3
anti-Vβ9-PE	mouse	Beckman Coulter	IM2003	FACS: 1:3

anti-Yes	mouse	BD	610376	WB: 1:5,000

Secondary Antibodies	Company	Order No.	Application & Dilution
goat anti-m IgG HRP-conjugated	Thermo	31432	WB: 1:20,000
goat anti-rb IgG HRP-conjugated	Thermo	31462	WB: 1:20,000
goat anti-m AL488/AL568/AL647	Invitrogen	A-11001	FACS/IF: 1:1,000
goat anti-rb AL488/AL568/AL647	Invitrogen	A21244	FACS/IF 1:1,000

Murine Antibodies	Source	Company	Order No.	Application & Dilution
CD3e (clone 145-2C11)	hamster	BD	553058	Coating: 2.5 µg/ml
CD28 (clone 37.51)	hamster	BD	553295	Coating: 3.0 µg/ml
anti-CD3-APC (clone 145-2C11)	hamster	BD	553066	FACS: 1:200
anti-CD4-AF647 (clone RM4-5)	rat	BD	557681	FACS: 1:400
anti-CD8-FITC	rat	BD	553031	FACS: 1:100
anti-CD45.1-eF605 (clone A20)	mouse	ebioscience	48-0453-82	FACS: 1:400
anti-CD11b-PeCy7 (clone M1/70)	mouse	ebioscience	25-0112-81	FACS: 1:200
anti-CD45R-AF700	rat	BD	557957	FACS: 1:200
anti-FoxP3-PeCy7 (clone FJK-16s)	mouse	ebioscience	25-5773-82	FACS: 1:200
anti-IFNγ-V450	rat	BD	560661	FACS: 1:200
anti-IL17A-PE (clone TC11-18H10)	rat	BD	559502	FACS: 1:200
anti-TNFα-AF700 (clone MP6-XT22)	mouse	BD	558000	FACS: 1:200
anti-TNFα-APC	rat	BD	554420	FACS: 1:200
SA-V450	mouse	BD Horizon	560797	FACS: 1:200

2.1.4 Cytokines

Cytokine	Company	Order No.	Application & final conc.
rh IL-2	Tecin™ Roche	Ro23-6019	CD8+ cell culture; (100 IU/ml)
rh IL-7	R&D Systems	207-IL-025	CD8+ cell culture (5 ng/ml)
rh IL-12	R&D Systems	219-IL-005	CD8+ cell culture (1 ng/ml)
rh IL-15	R&D Systems	247-IL-025	CD8+ cell culture (5 ng/ml)
rm IL-23	R&D Systems	1887-ML	CD4+ cell culture
rm TGF-β	R&D Systems	7666-MB/CF	CD4+ cell culture
rm IL-6	R&D Systems	406-ML	CD4+ cell culture

2.1.5 MACS MicroBeads and Kits

Kit	Company	Order No.
anti-CD4 (L3T4) MicroBeads, mouse	Miltenyi Biotec	130-049-201
anti-CD4 T cell Isolation Kit II	Miltenyi Biotec	130-095-248
anti-CD62L Microbeads, mouse	Miltenyi Biotec	130-049-701
anti-CD8 Microbeads, human	Miltenyi Biotec	130-045-201
anti-CD90.2 MicroBeads, mouse	Miltenyi Biotec	130-049-101
ELISpot coating&detection antibody	Mabtech	3420-6-1000
Plasmid Purification Kit Maxi	Quiagen	12165
Plasmid Purification Kit Mini	Quiagen	12125
Quiaquick Gel Purification Kit	Quiagen	28706
RNeasy Mini Kit	Quiagen	74106
RNeasy MiniElute Cleanup	Quiagen	74207
Vectastain Elite Kit, standard	Vector Laboratories	PK-6100

2.1.6 qRT-PCR primer

Human qRT-PCR Primer:

Official gene name	Accession No.	Primer Name	Primer sequence	Prod. length
Homo sapiens interferon induced transmembrane protein 3 (IFITM3)	NM_021034.2	Hs-IFITM3-F	TTCAACACCCTCTTCAT	87
		Hs-IFITM3-R	GCCAACCATCTTCCT	
Homo sapiens peptide transporter (TAP1) mRNA	L21206.1	Hs-TAP1-F	AAGACACTCAACCAGAAG	101
		Hs-TAP1-R	CCACCAATGTAGAGGATT	
Homo sapiens TAP2 mRNA for ABC-transporter	AB073779.1	Hs-TAP2-F	CCAGGTGAACAACAAAGT	95
		Hs-TAP2-R	CAAGGACAAGGAAGAAGAA	

Housekeeping genes:

Homo sapiens actin, beta	NM_001101.3	Hs-ßACTIN-F	TTAGTTGCGTTACACCCTTTC	150
		Hs-ßACTIN-R	ACCTTCACCGTTCCAGTT	
Homo sapiens eukaryotic translation elongation factor 1 alpha 1 (EEF1A1/2)	NM_001402.5	Hs-EF1a-F	GATTACAGGGACATCTCAGGCTG	
	NM_001958.3	Hs-EF1a-R	TATCTCTTCTGGCTGTAGGGTGG	
Homo sapiens glyceraldehyde-3-phosphate dehydrogenase (GAPDH)	NM_002046.4	Hs-GAPDH-F	TATGACAACAGCCTCAAG	99
	NM_001256799.1	Hs-GAPDH-R	TTCCACGATACCAAAGTT	
Homo sapiens tyrosine 3-monooxygenase/tryptophan 5-monooxygenase activation protein, zeta polypeptide (YWHAZ)	NM_003406.3	Hs-YWHAZ-F	TCTTGATCCCCAATGCTTCAC	
	NM_145690.2	Hs-YWHAZ-R	GCCAAGTAACGGTAGTAATCTCC	
	NM_001135699.1			
	NM_001135700.1			
	NM_001135701.1			
	NM_001135702.1			

Mouse qRT-PCR Primer:

Official gene name	Accession No.	Primer Name	Primer sequence	Prod. length
Mus musculus aryl-hydrocarbon receptor (Ahr)	NM_013464.4	Mm-AHR-F	GATGCCTTGGTCTTCTATG	82
		Mm-AHR-R	ATACGCTCTGATGGATGA	
Mus Musculus BTB and CNC homology 2 (Bach2)	NM_001109661.1	Mm-BACH2-F	TGTAGCCTTCTCATCTCT	149
	D86604.1	Mm-BACH2-R	TGGACTGTGGACTCATAT	
Mus musculus CD86 antigen (Cd86)	NM_019388.3	Mm-CD86-F	GTTCGTGTTGCTATCTTA	135
	AF065900.1	Mm-CD86-R	ACTTAGGTCATTGTATTCAT	

Mus musculus CCAAT/enhancer binding protein (C/EBP), alpha (Cebpa)	NM_007678.3	Mm-CEBPA-F	AGGAACTTGAAGCACAAT	109
		Mm-CEBPA-R	ACACAGAGACCAGATACA	
Mus musculus FBJ osteosarcoma oncogene (Fos)	NM_010234.2	Mm-FOS-F	TTCTCATAGCACTAACTAATCT	102
		Mm-FOS-R	CAGGAACACAGTAGGTATT	
Mus Musculus ecotropic viral integration site 5 (Evi5)	NM_007964.2	Mm-EVI5-F	ACACTACATCCTCATCTA	135
	U53586.1	Mm-EVI5-R	ACTTACTGTCTGTCTCTA	
Mus musculus colony stimulating factor 2 (granulocyte-macrophage) (Csf2)	NM_009969.4	Mm-GMCSF-F	GCTACTACCAGACATACT	
		Mm-GMCSF-R	ATATCAGTCAGAAAGGTTT	
Mus Musculus hematopoietically expressed homeobox (Hhex)	NM_008245.3	Mm-HHEX-F	TCTTACATTGCTGCCTTA	84
		Mm-HHEX-R	CTTATCAACTATCTTGCTTGT	
Mus musculus interferon gamma (Ifng)	NM_008337.3	Mm-IFNg-F	AGACAATGAACGCTACAC	139
		Mm-IFNg-R	TCCACATCTATGCCACTT	
Mus musculus interleukin 1 receptor, type I (Il1r1)	NM_008362.2	Mm-IL1R1-F	GCCATATACAATGCTCTC	
	NM_001123382.1	Mm-IL1R1-R	TCTGCTTAATGAACTGAATA	
Mus Musculus interleukin 2 receptor, alpha chain (Il2ra)	NM_008367.3	Mm-IL2RA-F	AACATAAGTAAGGCAAAG	133
		Mm-IL2RA-R	CTGTCATAACGATTCATT	
Mus Musculus interleukin 12 receptor, beta 1 (Il12rb1)	NM_008353.2	Mm-IL12RB1-F	ATTTCCCGTTTATCCATCAT	81
		Mm-IL12RB1-R	GCCAATGTATCCGAGACT	
Mus musculus interleukin 17A (Il17a)	NM_010552.3	Mm-IL17A-F	GACTTCCTCCAGAATGTG	
		Mm-IL17A-R	TATCTATCAGGGTCTTCATTG	
Mus musculus interleukin 17F (Il17f)	NM_145856.2	Mm-IL17F-F	ACTTTCTGGCTTGCTTTA	
		Mm-IL17F-R	ACTGTGGTCATCATCTAAC	
Mus musculus interleukin 22 (Il22)	NM_016971.2	Mm-IL22-F	CCAGAGGTAGACTTGATAA	
		Mm-IL22-R	CTAAAGGAATGAGAGGTAAC	
Mus musculus interleukin 23 receptor (Il23r)	NM_144548.1	Mm-IL-23R	CAGTGAGTCAGTGGAGAT	
		Mm-IL23R-R	AAGCCTACCTACATAGATACC	
Mus musculus interferon regulatory factor 8 (Irf8)	NM_008320.3	Mm-IRF8-F	TGGTTGGAGAAGAAGAATC	109
		Mm-IRF8-R	CTGAGCCTGTGAGAATAC	
Mus musculus Kruppel-like factor 4 (gut) (Klf4)	NM_010637.3	Mm-KLF4-F	TTATTGTGTCGGAGGAAGAG	75
		Mm-KLF4-R	TCACCAAGCACCATCATT	
Mus Musculus c-mer proto-oncogene tyrosine kinase (Mertk)	NM_008587.1	Mm-MERTK.2-F	CTTGGATGAACTGTATGA	149
		Mm-MERTK.2-R	TATTGATGTAGATGATGGAT	
Mus Musculus myeloblastosis oncogene (Myb)	NM_001198914.1	Mm-MYB-F	AAGTGCTGAACCCTGAAC	94
	NM_010848.3	Mm-MYB-R	CAACGCTTCGGACCATAT	
	M16449.1			
Mus musculus nuclear factor of activated T cells, cytoplasmic, calcineurin dependent 1 (Nfatc1)	NM_016791.4	Mm-NFATC1-F	CAATGGTAACTCTGTCTT	95
	NM_198429.2	Mm-NFATC1-R	ACAACATCCTCTTATAGC	
	NM_001164109.1			
	NM_001164110.1			
	NM_001164111.1			
	NM_001164112.1			
	AF239169.1			

Mus musculus outer dense fiber 3b (Odf3b)	NM_001013022.1	Mm-ODF3B-F	GAAATGGCATCCCTGTAT	118
		Mm- ODF3B -F	GGTAGTCTGAGTGTCTGA	
Mus musculus pleckstrin (Plek)	NM_019549.2	Mm-PLEK-F	AAGTTGGAGGAAGAAGGT	91
	AF181829.1	Mm-PLEK-R	TAAGGCAGACAGGAATCA	
Mus musculus prostaglandin E receptor 4 (subtype EP4) (Ptger4)	NM_001136079.2	Mm-PTGER4-F	AGGATTGCTTCTGTGAAC	86
	NM_008965.2	Mm-PTGER4-R	ATCTTCTCTATGGCTTTACTG	
Mus musculus regulator of G-protein signaling 1 (Rgs1)	NM_015811.2	Mm-RGS1-F	GGAAGGAGATACTATGGT	115
		Mm-RGS1-R	CATACACATTATTCACAGTT	
Solute carrier family 30, member 7 (Slc30a7)	NM_023214.7	Mm-SLC30A7-F	CATACTGCTGAAGATGAAGGT	97
		Mm- SLC30A7-R	ACACATACAACGCCAACA	
Mus musculus spleen focus forming virus (SFFV) proviral integration oncogene (Spi1)	NM_011355.1	Mm-SFPI1-F	GGATGACTTGGTTACTTACGA	121
		Mm-SFPI1-R	ATGGTGTGCGGAGAAATC	
Mus musculus signal transducer and activator of transcription (Stat3)	NM_213659.2	Mm-STAT3-F	CCTTGCTAATATCCACAT	136
	NM_213660.2	Mm-STAT3-R	TTAACTGAGTATTCCTTGAT	
	NM_011486.4			
	U06922.1			
Thyroid adenoma associated (Thada)	NM_183021.3	Mm-THADA-F	TGGTAGGTGTTAGAGTTG	149
		Mm-THADA-F	CAGTAGGTCATCGTCATT	
Mus musculus vascular cell adhesion molecule 1 (Vcam1)	NM_011693.3	Mm-VCAM1-F	AGACTACACTGATGAAGAA	122
		Mm-VCAM1-R	GAGGCAAACAAGAGATTT	

Housekeeping genes:

Mus musculus actin, beta (Actb)	NM_007393.3	Mm-ß-ACTIN-F	AATCTTCCGCCTTAATACT	100
		Mm-ß-ACTIN-R	AGCCTTCATACATCAAGT	
Mus musculus eukaryotic translation elongation factor 1 alpha 1 (Eef1a1)	NM_010106.2	Mm-EF1alpha-F	TACAGTCAGAAGAGATACG	150
		Mm-EF1alpha-R	GAACCAAGGCATATTAGC	
Mus musculus glyceraldehyde-3-phosphate dehydrogenase (Gapdh)	NM_008084.2	Mm-GAPDN-F	CAGCAACTCCCACTCTTC	101
		Mm-GAPDH-R	TGTAGCCGTATTCATTGTCAT	

2.1.7 Instruments

Instrument	**Company**
Centrifuge Fresco21, Tabletop	ThermoScientific
Centrifuge Multifuge 3L-R/X1R	ThermoScientific
Confocal Microscope SP5	Leica
Flow Cytometer (FACSCanto II)	BD Biosciences
Flowbench MSC-Advantage	ThermoScientific

Incubator Heratherm	ThermoScientific
Incubator Incusafe	Sanyo
KS Elispot Automated Reader System	Carl Zeiss
Light microscope	Leica
MACS Separator	Miltenyi Biotech
Magnetic stirrer Ministar silverline	VWR
Neubauer counting chamber, improved	Roth
PCR cycler peqSTAR 96Universal	peqlab
Pipette aid Pipetus	Hirschmann Laborgeräte
Power Supply Consort EV231	peqlab
RealTime System CFXConnectTM	Biorad
SDS-PAGE Apparatus	Biorad
Spectrometer Infinite M200PRO	Tecan
Thermomixer comfort	Eppendorf
Ultracentrifuge Optima L-80 XP	Beckman Coulter
Ultracentrifuge rotor Sw-40 Ti, 40,000rpm	Beckman Coulter
UV detection system FusionFx7	peqlab
Vibratome Microm HM650V	ThermoScientific
Vortex Genie2	Scientific Industries
Waterbath Aqualine AL12	Lauda
Western Blot Wet Blot Chamber	Biorad

2.1.8 Consumables

Product	**Company**
6-, 12-, 24-, 48-, 96-well-plates	Greiner Bio-One
Cannulas, syringes	Braun
Cell strainer (100 µm, 70 µm pore size)	BD Biosciences

Culture Flasks (50 cm^2, 75 cm^2, 125 cm^2)	Nunc
ELISpot Multiscreen Filterplates S2EM0 04M 99	Millipore
Eppendorf tubes	Eppendorf
FACS tubes	BD Biosciences
Falcon tubes (15 ml, 50 ml)	BD Biosciences
MACS LS columns	Miltenyi Biotec
MACS pre-separation filters	Miltenyi Biotec
Petri dished (6 cm, 10 cm)	BD Biosciences
Pipette tips	Starlab
Pipettes	Eppendorf
Scalpels	Braun

2.2 Methods

2.2.1 Cell isolation and culture methods

2.2.1.1 Isolation of human PBMC

100 ml of blood was taken from healthy donors. For PBMC isolation the blood was diluted with equal amount of PBS (without Ca^{2+}/Mg^{2+}). 25 ml were carefully layered on top of 15 ml of Lymphoprep and centrifuged (RT, 764 x g, 40 min, without break). The lymphocyte rings (intermediate phase) were transferred into new 50 ml tubes, washed with 40 ml of PBS, and centrifuged (RT, 561 x g, 15 min). The supernatant was discarded and the pellet resuspended in 10 ml of RPMI wash medium for cell counting. $1x10^6$ cells were stored at -20°C for HLA Typing, $3x10^6$ cells were stored at -80°C for B cell isolation and immortalization.

2.2.1.2 Isolation of murine spleen and lymph node cells

For isolation of spleen and/or lymph node cells, mice were sacrificed by cervical dislocation. The fur was disinfected with 70% EtOH prior to opening the animal and removing the organs. Spleen and lymph nodes (usually inguinal, brachial, and axillary) were removed and transferred either separately (for lymphocyte

isolation) or together (for magnetic sorting) to 15 ml falcon tubes on ice containing 5 ml of mouse washing medium (WM). Next, the organs were meshed through a cell strainer in a petri dish to generate a single cell suspension. This and all the following steps were performed under the laminar flow hood and all centrifugation steps were carried out at 4°C, 550 x g for 5 min. The cell strainer and the petri dish were rinsed with WM and the single cell suspension was transferred to a 50 ml falcon tube. The single cell suspension was centrifuged. The lymph node cells were directly taken up in WM for counting. The spleen cells alone or when mixed with lymph node cells were lysed in order to remove the erythrocytes. For this, the spleen cells or the spleen and lymph node cell mixture were taken up in 10 ml of lysis buffer. 5 ml of WM were added immediately to stop lysis and the cell suspension was centrifuged. The spleen cells were taken up in WM, centrifuged again and resuspended in WM or MACS buffer for counting.

2.2.1.3 Isolation of lymphocytes from mouse CNS

For isolation of lymphocytes from the central nervous system, mice were lethally anaesthetized with an intraperitoneal injection of a ketamin/xylazine-mixture (415 mg/kg; 9.7 mg/kg). For transcardial perfusion the animal was disinfected with 70% EtOH and the fur was cut open. Next, the sternum was removed to expose the heart. The right atrium was opened, a 20-gauge needle was inserted into the left ventricle, and mice were transcardially perfused with 30 ml of ice-cold PBS. Brain and spinal cord were removed and placed in a 15 ml Falcon tube on ice containing 5 ml of IMDM. All the following steps were performed under a laminar flow hood. First, the brain and spinal cord were transferred along with the 5 ml of IMDM into a petri dish. The CNS tissue was cut into small pieces using a scalpel and retransferred along with the 5 ml of IMDM into the 15 ml Falcon tube. The IMDM medium was then supplemented with 360 U/ml of collagenase, 200 U/ml of DNase, and 5 µg/ml of collagenase/dispase. After incubation at 37°C for 30 min under continuous rotation on a MACS-rotator, the CNS tissue was put through a cell strainer and washed with cold IMDM medium. Next, the gradient for the isolation of the lymphocytes was prepared. For that, the pellet was resuspended in 5 ml of 40% percoll-solution (percoll diluted in IMDM) and carefully layered on top of 5 ml of 70% percoll-solution (percoll diluted in PBS) in a 15 ml falcon tube. After centrifugation (RT, 750 x g, 30 min, without break),

mononuclear cells were collected from the interphase of the gradient, washed with WM, and counted.

2.2.1.4 MACSBead isolation of specific lymphocyte populations

All specific T cell subsets were isolated using Miltenyi MACSBeads Separation Kits according to manufacturer's protocol.

For the positive isolation of human or murine CD4+ and CD8+ cells a maximum of $2x10^9$ cells were used per LS magnetic cell separation column. Cells were resuspended in 80 µl of MACS buffer per 10^7 cells. 20 µl of CD4- or CD8-MicroBeads were added and incubated (4°C, 15 min). Excess beads were washed off by addition of 50 ml of MACS buffer and cells were centrifuged (4°C, 300 x g, 5 min). The supernatant was discarded, the pellet resuspended in 500 µl of MACS buffer and applied to an equilibrated (3 ml MACS buffer) LS Column. The column was washed 3 x with 3 ml MACS buffer and the flow-through collected. The positively sorted CD4+ and CD8+ cells were flushed in 5 ml of MACS buffer from the magnetic column by placing it onto an appropriate collection tube and pressing the plunger into the column. 100 µl of samples were taken before and after cell separation for a flow cytometry staining to check purity of cells.

In order to isolate naïve murine CD4+ T cells, spleen and lymph node cells were washed with MACS buffer and the cell pellet resuspended in 40 µl of MACS buffer per 10^7 cells. 10 µl of CD4+ T Cell Biotin-Antibody Cocktail per 10^7 cells were added, incubated (4°C, 10 min) and further 30 µl of MACS-buffer and 20 µl of Anti-Biotin MicroBeads per 10^7 cells were added without washing and again incubated (4°C, 15 min). Magnetic Cell Sorting was continued as described above. Here, the flow-through containing the untouched CD4+ T cells was collected. Thereafter, the flow-through of one column of the CD4+ untouched sort was washed with MACS buffer and then incubated with 960 µl of MACS buffer and 40 µl of CD62L MicroBeads (4°C, 15 min). Magnetic cell sorting was performed as described above and positively labeled CD4+CD62L T cells were isolated from the column like positively sorted CD4+ and CD8+ cells.

A surface staining with CD4-, or CD8-, CD3-, and CD62L-antibodies was performed to check the purity of the isolated populations.

2.2.1.5 GIC culture

Cell culture work was carried out at a sterile work bench. Human glioma-initiating cells were grown in Neurobasal-A Medium, supplemented with B27-Supplement, 0.1% Bovine serum albumin, Penicillin/Streptomycin, and the growths factors bFGF and EGF (20 ng/ml each) to select for stem and progenitor cells. The GICs grew in spheres. GICs were differentiated and adherently grown in Dulbecco's Modified Eagles Medium (DMEM), supplemented with FCS and Penicillin/Streptomycin. To split the cells, the medium was removed and adherent cells were washed once with PBS before being treated with Accutase at 37°C for 3 minutes. The reaction was stopped by adding an equal amount of medium. Cells growing in spheres were further separated by pipetting up and down. Cells were counted in a Neubauer Chamber and 400,000 – 500,000 cells were plated into a 10 cm^2 petri dish or T75 culture flask and stored in an incubator at 37°C, 5% CO_2.

2.2.1.6 Human mixed CD8+ lymphocyte tumor culture

Mini Mixed Lymphocyte Tumor Cultures (MLTCs) were performed to generate GIC-reactive human CD8+ T cells. Human CD8+ T cells that are HLA-A/B-matched with GIC-1080 were isolated from PBMCs as described above. GIC-1080 and rsGIC-1080 cells were brought to a single cell level and incubated with 1 µg/ml of IFN-γ 24 h prior to experiment for increased HLA expression. Next day, tumor cells were brought to a single cell level again, resuspended in 10 ml of human AB-Medium and irradiation with 120 Gy. For the first incubation week, CD8- cells from PBMC-sorted cells were used as feeder cells, resuspended as well in 10 ml of AB-Medium and irradiated with 30 Gy. 10^4 tumor cells, feeder cells and CD8+ T cells were plated per well in a U-shaped 96-well plate. 200 µl of AB-Medium per well were supplemented with IL-7 (5 ng/ml), IL-12 (1 ng/ml), and IL-15 (5 ng/ml).

Every week, CD8+ T cells were restimulated with fresh GICs, stimulated with 1 µg/ml of IFN-γ for 24 h and irradiated with 120 Gy. On day 7, AB-Medium was again supplemented with IL-7, IL-12, and IL-15 and T cells and tumor cells were kept in 96-well plates with a ratio of 1:1. IL-12 was exchanged by IL-2 (100 IU/ml) in all consecutive weeks.

If necessary, the medium was exchanged in the middle of the week without addition of cytokines. The cells were expanded, first to 96-well flat bottom plates, via 48-well plates to 24-well plates therein, stimulated with tumor cells with a ratio 1:5. On culture day 19, all wells were tested for tumor reactivity in an IFN-γ ELISPOT. 10 wells per tumor (GIC-1080 and rsGIC-1080) with high IFN-γ-producing cells were continued to be stimulated for further clonal expansion and test for tumor reactivity in a Chromium Release Assay on day 35.

2.2.1.7 Murine CD4+ lymphocyte culture

Naïve CD4+ T cells were isolated from B6.2d2 transgenic mice by magnetic sorting as described above and stimulated with irradiated (30 Gy) APC from C57BL/6 mice (ratio 1:5 - 1:10), MOG_{35-55} (12.5 µg/ml), rm IL-6 (20 ng/ml), rm IL-23 (20 ng/ml) and rh TGF-β (3 ng/ml) to generate MOG-specific Th17 cells. 3 Mio cells/ml and well were plated in 24-well plates. On day 7 and 14, the Th17 cells were restimulated with freshly isolated irradiated APC (ratio 1:3 -1:5), peptide, and cytokines (10 ng/ml of IL-6, 20 ng/ml of IL-23, 0.75 ng/ml of TGF-β on day 7 and 5 ng/ml of IL-6, 10 ng/ml of IL-23 on day 14). On days 3 and 5 after stimulation, the cells were split and fresh MM, supplemented with rh IL-2 (50 U/ml) and rm IL-23 (10 ng/ml), was added. On day 17, Th17 cells were harvested and 5 Mio or 30 Mio cells were injected intravenously in $Rag1^{-/-}$ or C57BL/6 recipient mice respectively. The expression of cytokines was checked throughout the culture and on the day of harvesting by intracellular staining with anti-CD4, anti-IL-17, and anti-IFN-γ antibodies and analyzed by flow cytometry, routinely yielding 15-50% IL-17- and no IFN-γ-producers.

2.2.2 *In vitro* studies

2.2.2.1 EdU Proliferation Assay

Proliferation of cells was measured by EdU incorporation over 3 h and 6 h of treatment and staining as well as analysis was pursued similar to as described in the Click-iT® EdU Flow Cytometry Assay Kit's manual.

Briefly, the cells were brought to a single cell level by Accutase treatment, counted and seeded into a 6-well plate at 100,000 cells per 2 ml culture medium per well. After 4 days incubation and colony formation time, 2 µM EdU were

added to according wells in duplicates for the desired amount of time. The cells were brought to a single cell level, washed with 2 ml of 1%BSA/PBS, pelleted (4°C, 400 x g, 3 min) and resuspended in either Component D fixative or 2% PFA/PBS at RT for 15 min. Fixative was washed off by addition of 2 ml of 1%BSA/PBS and centrifuged. The pellet was resuspended in 500 µl of Saponin-based permeabilization and wash reagent (Component E) and incubated at RT for 15 min meanwhile staining cocktail consisting of PBS, $CuSO_4$, anti-EdU-AL488 or anti-EdU-AL647, and Reaction Buffer Additive was prepared. Cells were centrifuged, supernatant discarded, pellets resuspended in 100 µl of staining cocktail per sample, and incubated at RT for 30 min. Staining cocktail was washed off by addition of 2 ml of Saponin-based permeabilization and wash reagent (Component E), pelleted and resuspended in 300 µl of Saponin-based permeabilization and wash reagent plus DAPI (1:500) before being analyzed at FACS Canto II.

2.2.2.2 Irradiation of GICs

Tumor spheres were brought to a single cell level by treatment with Accutase and counted. 70,000 cells were irradiated in 10 ml of medium in 15 ml tubes at a dose rate of 3 Gy/min in doses of 10 – 60 Gy and plated in triplicates at 20,000 cells per condition and well of a 48-well plate. 48 h after irradiation, cells were harvested, singularized and counted in a 1:1 ratio with Trypan Blue in a Neubauer Chamber. Dead and living cells were counted and total live cell count from each treatment condition was normalized back to its individual untreated tumor sphere line and expressed as a percentage difference (viability).

2.2.2.3 Migration Assay

For the measurement of migration of single cells out of a tumor spheroid tumor, spheres were grown in a 24-well plate at a density of 10,000 – 20,000 cells per well until they reached a diameter of 100 – 200 µm. An extracellular matrix gel was prepared on ice using 80% Collagen I (Pure-Col S; Advanced Biomatrix), 10% MEM-Medium, 10% $NaHCO_3$-Buffer (1.5 g $NaHCO_3$ in 20 ml PBS, sterile filtered), and 5 µg/ml of Fibronectin (Sigma Aldrich). When mixed correctly, the pH indicator reached a rosy neutralized color. 70 µl of ECM solution were pipetted per well in a 96-well plate and kept on ice while single tumor spheres were picked with a yellow pipet under a microscope and carefully dropped onto

the gel. 10 wells with single tumor spheres were used per cell type and condition. The ECM solution was gelatinized at 37°C for one hour and then covered by 150 µl of culture medium. The spreading of the spheroids was monitored on a brightfield microscope, 4 x magnification, at 0 h, and after 1, 3, and 5 days. For quantification, the areas of each spheroid at time 0 h and mean extension areas at indicated time points were measured and the radial migration distance calculated by subtracting the radius of the sphere at time 0 h. Migratory distances were expressed in micrometer.

2.2.3 Immunological methods

2.2.3.1 Immunocytochemistry

Immunofluorescent staining for localization and cellular marker analysis was performed on cells that were grown on ornithine-coated coverslips in 24-well plates. 60,000 – 80,000 cells were plated three to four days prior to staining. The medium was removed, the cells were washed twice with 0.5 ml of PBS for 2 min and subsequently fixed in 0.5 ml of 4% formalin/PBS at RT for 5 min. Formalin was removed and cells were washed again twice with 0.5 ml of PBS for 2 min. Cells were permeabilized in 0.5 ml of 0.3% TritonX-100/PBS at RT for 10 min and washed twice with 0.5 ml of PBS for 2 min. Coverslips were then transferred onto the lid of a 24- well plate that was prepared with hydrophobic painting. Unspecific binding was blocked with 25 µl of blocking solution (1% BSA, 4% NGS, 0.5% NP40/PBS) at RT for 30 – 45 min in a wet chamber. Blocking solution was removed and 25 µl of primary antibody (diluted in 1% BSA, 0.5% NP40/PBS) were applied overnight at 4°C in a wet chamber. Cells were washed three times with 25 µl of PBS for 2 min and incubated with 25 µl of secondary antibody (diluted in 1% BSA, 0.5% NP40/PBS) at RT in the dark for 30 – 45 min in a wet chamber. Cells were washed twice with 25 µl of PBS for 2 min and incubated in 25 µl of DAPI/PBS (1:1000 dilution) at RT in the dark for 10 – 15 min. DAPI/PBS was exchanged by new PBS solution and coverslips were mounted with Immumount® (Thermo Scientific) on object trays for confocal microscopy analysis.

2.2.3.2 Flow Cytometry

For extracellular, quantitative immunofluorescent staining on a single cell level $1x10^5$ – $2x10^6$ cells per sample were transferred to FACS tubes and washed with 1 ml of FACS-buffer or PBS and centrifuged. Centrifugation steps were always carried out at 4°C, 500 x g for 5 min. The supernatant was discarded and the cells were stained with 100 µl of primary antibody (diluted in FACS-buffer) at 4°C in the dark for 10 – 30 min. Cells were washed with 2 ml of FACS-buffer or PBS, and if needed, stained with 50 – 100 µl of secondary antibody at 4°C for 20 – 30 min in the dark. Cells were washed with 1 ml of FACS-buffer and human cells were fixed with 2% PFA at 4°C for 20 min. PFA was washed off with 1 ml of PBS and human cells resuspended in 300 µl of PBS to be measured at FACS Canto II. Murine cells were measured alive and resuspended in 300 µl of FACS buffer. If differentiation of dead and living cells was needed, 1 µl of PI (0.1 µg/µl) was added to the sample shortly before measuring to exclude dead and dying cells.

To stain intracellular proteins, human cells were permeabilized with 1 ml of Saponin-buffer for 20 min and then incubated with 70 µl of α-human IVIC in Saponin-buffer at 4°C for 10 min for blockage of unspecific antibody binding to Fc-terminals. After incubation, 20 µl of antibody-mixture (intracellular antibodies in Saponin-buffer) were added and the cells incubated at 4°C for 20 min. Cells were subsequently washed once with Saponin-buffer, once with PBS, and resuspended in 300 µl of PBS to be measured at FACS Canto II.

Intracellular proteins of murine cells were stained according to FoxP3 analysis Kit (ebioscience). Cells were incubated in 500 µl of Fix/Perm Solution at 4°C for 2 – 16 h. The solution was washed off by addition of 1 ml of 1x permeabilization solution two times. Antibodies were mixed in permeabilization solution and incubated at 4°C for 30 min. Antibodies were washed by adding 1 ml of permeabilization solution and cells resuspended in 300 µl of FACS buffer for analysis at FACS Canto II.

2.2.3.3 ELISpot

To detect tumor reactive-CD8+ T cells via secreted IFN-γ, an Enzyme Linked Immuno Spot (ELISpot) Assay was performed. One day prior to experiment, the PVDF membrane of 96-well plates was activated with 15 µl of 35% ethanol per

well, washed 3 x with 150 µl/well PBS and incubated in 50 µl of 10 ng/µl coating antibody overnight at 4°C. Next day, the plates were washed 3 x with 150 µl of PBS per well and unspecific binding sites blocked by incubation in 100 µl of RPMI+ (RPMI1640 supplemented with 10% FCS) per well at 37°C for 30 min. Meanwhile, 30,000 – 50,000 tumor cells per well and 50 µl were singularized, resuspended in appropriate amount of RMPI+ Medium and distributed onto the plate. CD8+ effector cells were resuspended, washed with fresh RPMI+, adjusted to 20,000 cells per 50 µl of RPMI+ and well and pipetted onto the target cells. The MLTC was incubated at 37°C, 5% CO_2 for 20 h. The cell solution was discarded and plates washed 6 x with PBS + 0.05% Tween20 to lyse all cells. Detection antibody was diluted in PBS + 0.5% BSA to a final concentration of 2 µg/ml and 60 µl per well were used for secondary antibody incubation (37°C, 2 h, incubator). Detection reagents were prepared 30 min before the end of the incubation time by adding 1 drop of solution A and 1 drop of solution B to 10 ml of PBS + 0.1% Tween20 and stored in the dark until use. The plates were washed 4 x with PBS + 0.05% Tween20, 100 µl of avidin-peroxidase complex per well were added, and incubated (RT, 1 h, dark). Plates were washed again 3 x with PBS + 0.05% Tween20 and 3 x with PBS. For visualization of spots, 100 µl of peroxidase-substrate solution per well (freshly supplemented with 25 µl of 30% H_2O_2 and filtered) were added and incubated for at least 10 min. Substrate solution was discarded and plates washed by rinsing them under tap water. The membrane was dried by incubation at 50°C for 10 – 20 min and spots analyzed using the KS Elispot Automated Reader System (Carl Zeiss).

2.2.3.4 ^{51}Chromium Release Assay

Chromium-release assays are used to determine the cytolytic activity of effector cells (=allogeneic CD8+). Target cells (=GICs) are first incorporated with the radioactive ^{51}Cr isotope and then incubated with the effector cells that are to be tested. If the target cells are lysed by the effector cells, radioactive ^{51}Cr is released into the supernatant and can be detected.

1 Mio GICs were radioactively labeled with 200 µCi of ^{51}Cr and incubated (37°C, 2 h, resuspended every 30 min). Effector T cells were counted, resuspended in 80 µl/well T cell culture medium and plated in the 96-well plate in serial dilutions with an effector:target ratio of 60:1, 20:1, 7:1, 2:1, and 1:1. 1,500 GICs per well

were added in 80 µl/well T cell medium and incubated (37°C, 5 h). Additionally, for minimal and maximal lysis, controls with only effector T cells or with 1% TritonX-100 were used. Effector T cells raised and stimulated with either GIC1 or GIC1-IR were tested for their lysis potential of both target cell lines. After 5 h, plates were centrifuged (900 rpm, 5 min, without brake), 80 µl of supernatants transferred to cytotox tubes and radioactivity measured on an automated reader.

2.2.4 Molecular biology methods

2.2.4.1 Cloning of IFITM3

A Glycerol Stock of bacteria expressing IFITM3 clone with the accession number BC070243.1 [Homo sapiens interferon induced transmembrane protein 3 (1-8U), mRNA (cDNA clone MGC:88228 IMAGE:30401041), complete cds], was purchased from BioSource. IFITM3 was cloned from the bacterial stock by colony PCR with forward primer 5' AAAATCTAGAATGAATCACACTGTCCAAA 3' and reverse primer 5' AAAAGGATCCCTACAGATCTTCTTCAGAAATAAGTTTTTGTTCCTCGAGTC CATAGGCCTGGAAGAT 3' in a thermo cycler (program: 95°C for 2 min, [95°C for 30 sec, 57°C for 30 sec, 72°C for 30 sec] 30 cycles, 72°C for 10 min). Forward primer includes a cutting site for restriction enzyme XbaI whereas the reverse primer includes cutting sites for BamHI and XhoI as well as a myc-tag.

The mammalian expression vector pCDH-Ef1a-MCS-IRES-copGFP was purchased from Biocat. Chemically competent E.coli TOP10 bacteria (Invitrogen) were transformed with the vector and grown on agar plates with Ampicillin. For vector amplification, colonies were picked and grown in 200 ml LB-Medium and plasmids isolated in a maxi preparation according to protocol (QUIAGEN® Plasmid Purification Kit). Both, vector and insert were digested with XbaI and BamHI and the vector subsequentially dephosphorylated. Both, vector and insert were separated on a 1% agarose gel and purified (Quiaquick Gel Purification Kit) before being ligated. The ligation product was transformed into E.coli TOP10 bacteria and grown on agar selection plates with Ampicillin. Five colonies were picked and grown in LB-Medium for mini plasmid preparation according to protocol (PEQLAB® Plasmid Mini Preparation Kit). A restriction enzyme digest revealed four positive clones of which two were sent for sequencing (StarSEQ,

Mainz). The clone with the correct DNA sequence was used for maxi plasmid amplification and purification for preparation of lentivirus.

2.2.4.2 Lentiviral Production and Transduction of Cells

Lentivirus was generated by Dr. Matthias Bros in the group of Prof. Dr. Angelika Reske-Kuntz at the University Medical Center Mainz, Department of Hematology, according to their standard protocol. 300,000 GICs were seeded onto Ornithine-coated 6-well plates and infected with the virus in the presence of polybrene. 48 hours after infection, cells were transferred to S1 area and successful transduction secured by visualization of GFP expression.

2.2.4.3 RNA Isolation and cDNA synthesis

To quantitatively analyze gene transcription, total RNA was isolated from cells using RNeasy Mini Kit for quantitative Real-Time PCR and performed according to manufacturer's protocol. RNA was eluted in 50 µl of RNAse-free water.

For DNAse treatment, 37 µl of RNAse-free water were added onto the membrane of the columns and membranes were washed off RNA via centrifugation. 13 µl of Reaction Mix (10 µl of 10x Incubation Buffer RT, 1 µl of RNaseOUT, 2 µl of DNAse-I, all Roche) were added to each RNA sample and incubated at 37°C for 15-20 min. The reaction was stopped by addition of 2 µl of 0.2 M EDTA and samples were kept on ice. RNA was cleared off enzymes via a modified QUIAGEN RNeasy MiniElute Cleanup protocol. 350 µl of Buffer RLT were added to 100 µl of DNAse-treated RNA samples and mixed thoroughly. 250 µl of 100% Ethanol were added to the mixture, mixed well by pipetting up and down. 700 µl of reaction mixture were applied to RNeasy spin columns that were placed into 2 ml collection tubes and centrifuged. RNA was washed with 500 µl of Buffer RPE followed by 500 µl of 80% Ethanol and centrifuged for 2 min and subsequently for 5 min with open caps. Columns were transferred into new 1.5 ml collection tubes and RNA eluted in 14 µl of RNAse-free water. RNA was kept on ice for RNA concentration measurements at the NanoDrop (Thermo Scientific).

For cDNA synthesis, 1 µg of RNA was used and diluted to a volume of 18 µl in RNAse-free water. RNA was incubated with 5 µl of random hexamer primers (50 ng/µl) at 65°C for 5 min. Tubes were stored on ice and the cDNA synthesis

mix prepared (10 µl of $MgCl_2$, 5 µl of 10x RT Buffer, 5 µl of 0.1 M DTT, 5 µl of dNTP mix (10 mM each), 1 µl of RNaseOUT and 1 µl of Superscript III reverse transcriptase (250 Units)). The cDNA mix was added to the RNA and cDNA reverse transcribed in a PCR cycler (at 25°C for 10 min, at 50°C for 50 min, at 85°C for 5 min, infinite storage at 8°C). 50 µl of cDNA were diluted with 150 µl of RNAse-free water and stored at -20°C until used.

2.2.4.4 Quantitative Real-Time Polymerase-Chain-Reaction

To optimize the qRT-PCR temperature gradients and different amounts of cDNA were tested. Primer stock solutions (100 µM) were diluted 1:10 to working solutions in autoclaved MilliQ. A reaction mastermix was created, consisting of 10 µl of SYBR Green (Biorad), 0.4 µl of forward primer, 0.4 µl of reverse primer and 5.2 µl of MilliQ per well. 16 µl of reaction mix and 4 µl of cDNA were added to each well of a 96-well qRT-PCR plate (Biorad, transparent). Plates were sealed with a sticky foil and centrifuged. The qRT-PCR reaction was carried out on a Biorad iCycler or CFX detection system (95°C for 3 min, 95°C for 10 sec, 54°C-62°C for 45 sec repeated in 39 cycles, 95°C for 1 min, 55°C for 1 min; Meltcurve measurements: 55°C to 95°C, increment 0.5°C, 10 sec) Relative mRNA amounts were calculated by normalizing to housekeeping genes Ef1α, β-actin, GAPDH and YHWAZ and taking efficiency coefficients into account.

2.2.4.5 Lipid Raft isolation

About $2x10^8$ cells were transferred from culture flasks to 50 ml tubes. Each half of the cells was lysed in either 1 ml of 1% TritonX-100 or 0.5% of Brij98® lysis buffer for 45 min on ice and kept cool throughout the procedure. Lysis was mechanically assisted by slowly pipetting up and down. 1 g of sucrose was added to each lysate for a final concentration of 50% and carefully solubilized by horizontal rotation. A discontinuing sucrose gradient was prepared in Beckman 12 ml ultracentrifuge tubes with 1 ml of 50%, 5 ml of 30%, and 5 ml of 5% sucrose. Floating ultracentrifugation (4°C, 40,000 rpm, 18 h, without brake) was carried out in a Beckman Coulter Ultracentrifuge Optima L-80 XP with a Sw-40 Ti (40,000 rpm) swing rotor. Lipid Rafts were located at the border of 30% and 5% sucrose. From top to bottom, 500 µl fractions were harvested from the gradient, protein concentration measured by Bradford protein assay, and proteins analyzed by Western Blot analysis. SDS-PAGE: 10% polyacrylamid gels; const. 40 mA/gel,

2 h; Semi-dry Western Blot onto nitrocellulose membranes; const. 180 mA/membrane, 1 h (more detailed description see chapter 2.2.4.7).

2.2.4.6 Cell lysis and protein concentration analysis with Bradford

200,000 – 6,000,000 cells were pelleted from culture flasks, transferred into 1.5 ml tubes and lysed depending on the cell number in 150 – 400 µl Lysis-buffer plus Protease Inhibitors (Roche, Complete) on ice for 30-45 min. Cell lysates were subsequently centrifuged (4°C, 10,000 rpm, 10 min) and supernatants transferred into new 1.5 ml tubes. Protein concentration measurement was performed with the Bradford protein assay. This assay is based on an absorbance shift of the dye Coomassie Brilliant Blue G-250 in which under acidic conditions the red form of the dye is converted into its blue form, in which proteins can be bound.

A serial standard curve was created with 8 different concentrations of BSA, from 1 µg/µl up to 20 µg/µl protein concentration in H_2O mixed with Lysis buffer+Proteinase Inhibitors in a final dilution of 1:50. H_2O with Lysis buffer alone was used as a blank. 100 µl of Standard Curve Mastermix was pipetted into a flat bottom 96-well plate in triplicates. For sample protein concentration analysis, 2 µl of protein sample were mixed with 98 µl of H_2O (1:50 dilution) in duplicates. The colorimetric reaction was started by adding 100 µl Bradford reagent, the mixture incubated at RT for 10 min and measured for absorbance at a spectrometer at 595 nm, which is the absorbance maximum for the Coommassie blue form.

2.2.4.7 SDS-PAGE and Western Blot Analysis

To prepare protein samples for gel electrophoresis, 10-30 µg were mixed with 5 x Laemmli buffer and H_2O for equal sample amounts and the proteins were denatured at 95°C for 5 min.

Proteins were separated on 10-15% gels under reducing conditions at constant 80-100 V, max mA for 2 hours. Proteins were then transferred onto nitrocellulose membranes by wet western blotting at 100 V, max mA for 1.5 hours. Unspecific binding sites were blocked with TBS-T + 5% skim milk powder at RT for 60 min on a shaker. Membranes were incubated with indicated primary antibodies in TBS-T + 5% BSA, 0.1% Sodiumazide at 4°C overnight. Next day, membranes

were washed 3 x in TBS-T and probed with the corresponding HRP-conjugated secondary antibodies in TBS-T + 3% BSA at RT for 1.5 hours. The HRP signal was detected by incubation of the membrane with advanced ECL solution and consecutive exposure to X-ray films.

2.2.5 *In vivo* experiments

2.2.5.1 Animals

NMRI nude mice were purchased from Janvier (France). For experiments, 6-10-weeks-old female animals were used.

Mice were housed under specifically pathogen free (SPF) conditions at the central animal facility of the University Medical Center of the Johannes Gutenberg University Mainz at a twelve-hour dark/light cycle with free access to food and water.

All animal experiments were approved by local authorities (Landesuntersuchungsamt Rheinland-Pfalz: G12-1-033 and G-10-1-008) and conducted according to the German Animal Protection Law.

2.2.5.2 Stereotactic injections of tumor cells

For intracranial injections, 6 to 10-weeks-old NMRI nude mice were used. Tumor cells were harvested by treatment with Accutase and 200,000 – 1,000,000 cells per mouse were resuspended in 4 µl of Neurbasal-A medium naked and stored on ice until injection with a 10 µl Hamilton syringe.

30 min before surgery, experimental mice were subcutaneously injected with 400 µl of Carprofen (Rimadyl®, 4 mg/kg) solution to decrease pain perception throughout and 24 hours after surgery. Mice were anesthetized with intraperitoneal injection of 100 µl/10 g weight Ketamin/Xylazin-mixture (40 mg/kg, 5 mg/kg) and placed into the stereotact. The scalp was disinfected, cut open, a burr hole drilled 2 mm lateral to the bregma into the left hemisphere and the needle introduced to a depth of 3 mm. 2 µl of cell suspension were injected at a flow rate of 400nl/min. The injected cells were allowed to settle for 5 min before the needle was removed and the wound sewed.

2.2.5.3 Anesthesia and perfusion of mice

At first signs of weight loss or neurological symptoms mice were sacrificed by anesthesia with 1 ml Ketamin/Xylazin-mixture followed by transcardial perfusion. Mice were perfused with 30 ml of PBS to clear the blood and fixed with 30 ml of 4% PFA. Brains were removed and fixed over night with 4% PFA at 4°C.

2.2.6 Microarray and statistical analysis

Statistical analysis was carried out with Excel or GraphPad Prism 6. Data are usually presented as MEAN ± SEM. To compare more than two means in a dataset, ANOVA variance test with Tukey correction for multiple comparisons was used. To compare two means, the student t-test was performed. P-values < 0.05 were considered significant.

Microarray analysis for significant regulated genes and interaction pathways was performed using DAVID (http://david.abcc.ncifcrf.gov/), Ingenuity (IPA) (www.ingenuity.com) Venn analysis tool (http://jura.wi.mit.edu/bioc/tools/), KEGG (http://www.genome.jp/kegg/), Gene Ontology (http://www.geneontology.org/), and Expasy (http://expasy.org/).

Primer design for PCR and qRT-PCR was done with Beacon Designer and primer3 (http://frodo.wi.mit.edu/). mRNA and protein analysis was done with NCBI Database (www.ncbi.nlm.nih.gov/), SDSC Biology Workbench (http://workbench.sdsc.edu/), and UniProt (http://www.uniprot.org/).

3 Results

3.1 Characteristics of GICs

3.1.1 Functional analysis of ionizing radiation effects of GICs *in vitro*

GICs were shown to be more resistant to ionizing radiation than the tumor bulk (54). Evidence even suggested that non-lethal radiation can promote tumor development (65). *In vitro* studies proposed to combine radiotherapy with immunotherapy as radiation can enhance antigen-presentation by MHC class I molecules on the surface of glioma cells (226,229). The long-lasting molecular and functional alterations induced in GICs by fractionated, therapy-relevant ionizing radiation doses on GICs have not been investigated. Therefore, an *in vitro* model of radio-selected and untreated control GICs was used to investigate cellular effects of radiation GICs.

3.1.1.1 Generation of radioresistant GICs

The protocol for the generation of radioresistant GICs from fresh tumor specimen was established by Prof. Alf Giese and Dr Ella Kim at the Department of Neurosurgery of the University Medical Center Mainz. Patient-derived GICs were cultured under neural stem cell conditions and grown as spheroids. Cell aggregates were singularized by enzymatic digestion and divided in half. One group was subsequently irradiated with 2.5 Gy and further cultured until new spheres have formed. This procedure was repeated for the next six passages to select for GICs with a more radioresistant phenotype (radio-selected GICs, rsGICs) in the course of multi-fractionated radiation (Figure 12A). The total dose of 17.5 Gy was chosen according to the irradiation dose in human therapy, calculated for direct cellular *in vitro* γ-radiation without protecting surrounding cells. The established GIC cell line 1080 (GIC-1080) and its radio-selected counterpart (rsGIC-1080) was provided by Prof. Dr. Alf Giese and Dr. Ella Kim and used as a model throughout this thesis.

To evaluate if rsGIC-1080 have a survival advantage over the control GICs, both cell groups were brought to a single cell level and 500 single cells per well were

plated into a 24-well plate. After two weeks, the number of spheres with a diameter of ≥ 50 µm was counted. As shown in Figure 12B, rsGIC-1080 had a significantly ($p < 0.05$) increased number of spheres compared to GIC-1080. This experiment was performed twice in triplicates. To show that rsGIC-1080 had a survival advantage when challenged with different intensities of γ-radiation, cells were singularized and irradiated with γ-radiation ranging from 10 Gy to 60 Gy, the highest irradiation dose used in human radiotherapy. 48 hours after irradiation, viable and dead cells were counted in a Neubauer hemocytometer using Trypan Blue staining for dead cells. This experiment was performed twice in triplicates. As shown in Figure 12C, 68% of GIC-1080 and 86% of rsGIC-1080 were viable in the untreated controls, indicating less spontaneous apoptosis of rsGIC-1080, resulting from the previous radio-selection process. Even after a dose of 60 Gy, 61% of rsGIC-1080 survived compared to 45% of GIC-1080. These results demonstrate that already GIC-1080 have the capability to combat cell death-inducing irradiation as almost half of the cells were able to stay viable after 60 Gy of irradiation. A clear survival benefit of rsGIC-1080 was not observed at the irradiation doses tested. Only at an irradiation dose of 120 Gy, as used for the mixed lymphocyte tumor cultures (MLTC) (chapter 3.1.1.5), viable tumor cells were observed in rsGIC-1080 co-cultures but not in GIC-1080 co-cultures (data not shown).

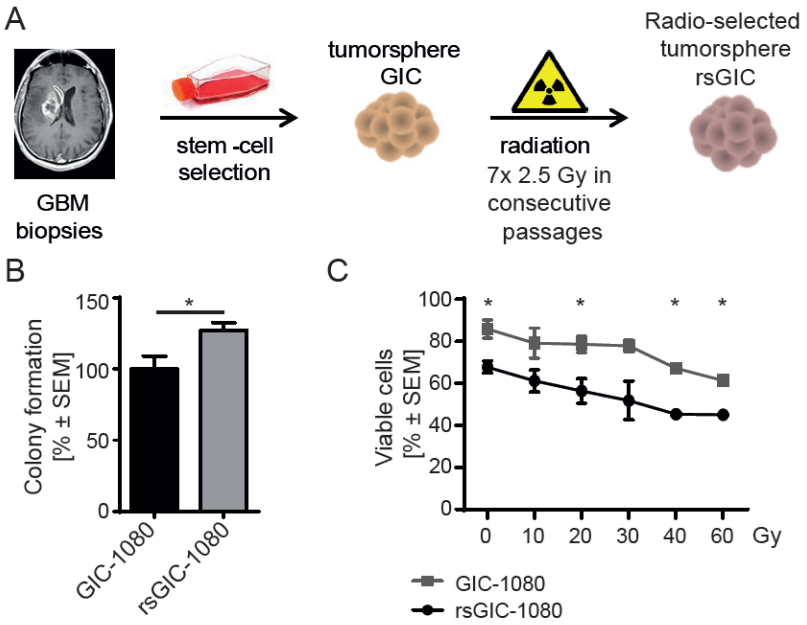

Figure 12: Schematic representation of radio-selection of GICs and viability test.
*(A) Tumor tissue of GBM patients was dissected and single cells cultured in medium under neural stem cell conditions. Each week, medium was refreshed. After 4 – 8 weeks, GICs proliferated, growing in spheroids, and were irradiated with 2.5 Gy (1 Gy/min) in 7 consecutive passages. (B) rsGIC-1080 showed enhanced sphere forming capacity compared to GIC-1080 as determined by colony formation assay. Data are shown as mean ± SEM. P-value * < 0.05. (C) rsGIC-1080 and control GIC-1080 were tested for survival 48 h after different doses of γ-radiation. P-value * < 0.05.*

3.1.1.2 Proliferation and migration potential of GICs

Only recently, efforts have focused on therapeutic intervention to target GICs. Analysis of resistance mechanisms revealed that ionizing radiation (IR) can activate NOTCH, hepatic growth factor (HGF) receptor, and c-MET signaling cascades, leading to increased proliferation, invasion and resistance to apoptosis (64,230,231). To determine the proliferation capacities of GIC-1080 and rsGIC-1080, EdU incorporation assays were used in which EdU instead of the nucleoside thymidine was inserted into the DNA in the synthesis phase of the cell cycle. Detection of EdU was based on a click reaction between an alkyne in the EdU and an azide coupled to a fluorescent dye. The number of cells that were EdU positive, and therefore had proliferated, was detected by flow cytometry on FACS Canto II (Figure 13). The results showed that rsGIC-1080 proliferated faster than the control GIC-1080. This was significant at the 3 hours' time point, but not anymore after 6 hours of incubation time, possibly due to a toxic effect of the dissolvent DMSO.

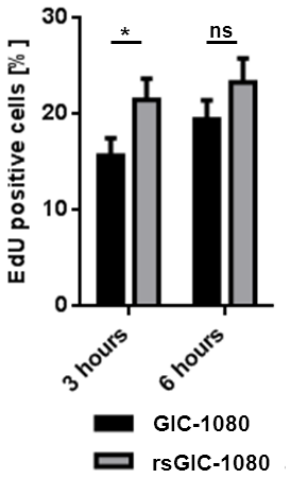

Figure 13: Proliferation measured by EdU incorporation in GIC-1080 and rsGIC-1080.
200,000 cells per well were cultured for 4 days to reach the exponential phase of proliferation. EdU was added to the cultures and cells were incubated for the indicated time. The EdU staining protocol was performed as described and EdU incorporation measured using a FACS Canto II flow cytometer. This experiment was performed 5 times in duplicates.

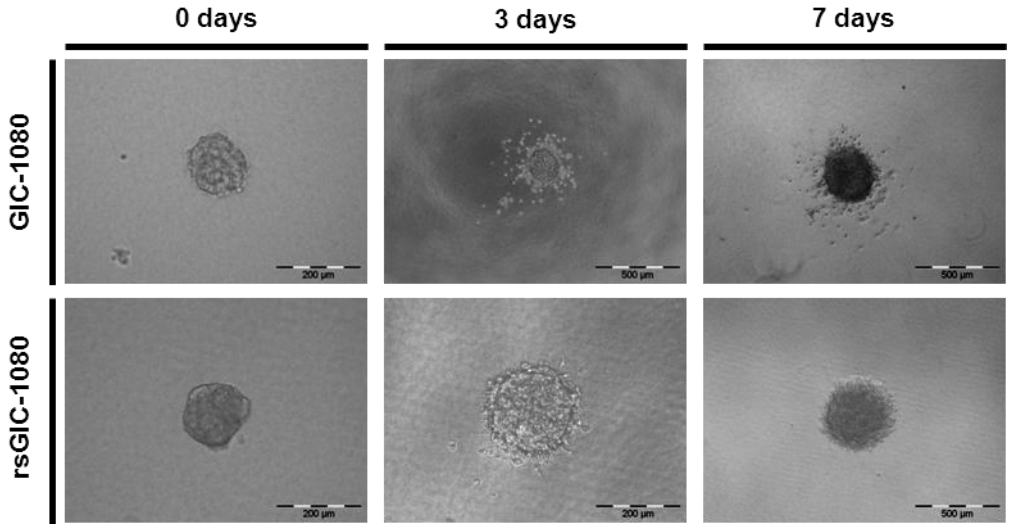

Figure 14: In vitro migration of GICs.
Spheres of 100 – 200 µm diameter have been carefully dropped onto a collagen matrix. Images were taken on day 0, 3, and 7 with an upright bright field microscope and 4x magnification. The results are representative for 4 experiments.

A collagen migration assay was used to determine the radial migration away from the tumor sphere. Spheres had been grown to a diameter of 100 – 200 µm, before they were picked and carefully dropped onto a collagen matrix. Images of the spheres were taken at day 0, 3, and 7 (Figure 14). The results showed that the rsGIC-1080 were incapable of migrating on the collagen matrix, whereas control cells moved away from the sphere. Taken together, fractionated irradiation increased the proliferation of rsGIC-1080 but unexpectedly diminished their migratory potential.

3.1.1.3 Differences in detergent-resistant membrane composition

It was published that radiation affects the composition of lipid rafts (63). The alteration of these detergent-resistant membranes (DRMs) subsequently leads to differences in downstream signaling pathways. Up to now, DRMs have not been analyzed in glioma cells, especially not in GICs. To evaluate a possible change in composition of DRMs after fractionated radiation in GICs, GIC-1080 and rsGIC-1080 were lysed using the detergent Brij98® and cellular components were separated on a discontinuous sucrose gradient with ultracentrifugation at 40,000 rpm for 18 hours. 500 µl fractions were collected and analyzed for lipid raft

proteins using Western Blot analysis. Fractions, including lipid raft marker proteins Yes, Flotilin1 (Flot1), and Caveolin1 (Cav1) were further processed for Mass Spectrometry analysis (Figure 15A). This experiment was performed twice.

454 proteins were detected via mass spectrometry to be present in the isolated DRMs in both isolation experiments. To evaluate, if the regulation of the detected proteins was stable, the $\log_2$ expression ratios (rsGIC-1080/GIC-1080) between experiment 1 and 2 were correlated (Figure 15B). The low correlation coefficient of $R = 0.2269$ indicated that rather few proteins were similarly up- or downregulated in the two experiments. This could reflect the variable nature of DRM composition. The detected proteins were annotated by using the STRAP protein annotation tool. Most of the proteins were associated with organelles, which contain detergent resistant membranes, such as plasma membrane (15.3%), other intracellular organelles, including the golgi apparatus (13.1%), endoplasmic reticulum (ER) (10.7%), nucleus (7.6%), cytoplasm (7.0%), or mitochondria (6.9%) (Figure 15C, upper graph). These proteins are mainly involved in biological processes, such as cellular processes (23.8%), regulation (21.3%), localization (12.1%), and metabolic processes (7.3%) (Figure 15C, lower graph). It was hypothesized that proteins, which were differentially regulated in rsGIC-1080 compared to GIC-1080 in both experiments were candidates influenced by fractionated radiation. The two most upregulated proteins in rsGIC-1080 were tetraspanin 6 (TSPAN6) and neuron-glia-related cell adhesion molecule (NRCAM), which were already associated with progression of GBM (232,233). Interestingly, proteins involved in antigen processing and presentation via MHC class I were among the most downregulated proteins in rsGIC-1080. This was further evaluated and confirmed using DAVID functional annotation and analysis tool. KEGG pathway analysis revealed a strong enrichment in “Antigen processing and presentation” as various proteins associated with MHC class I peptide loading and antigen presentation were identified and regulated in the dataset (Figure 16, Table 1).

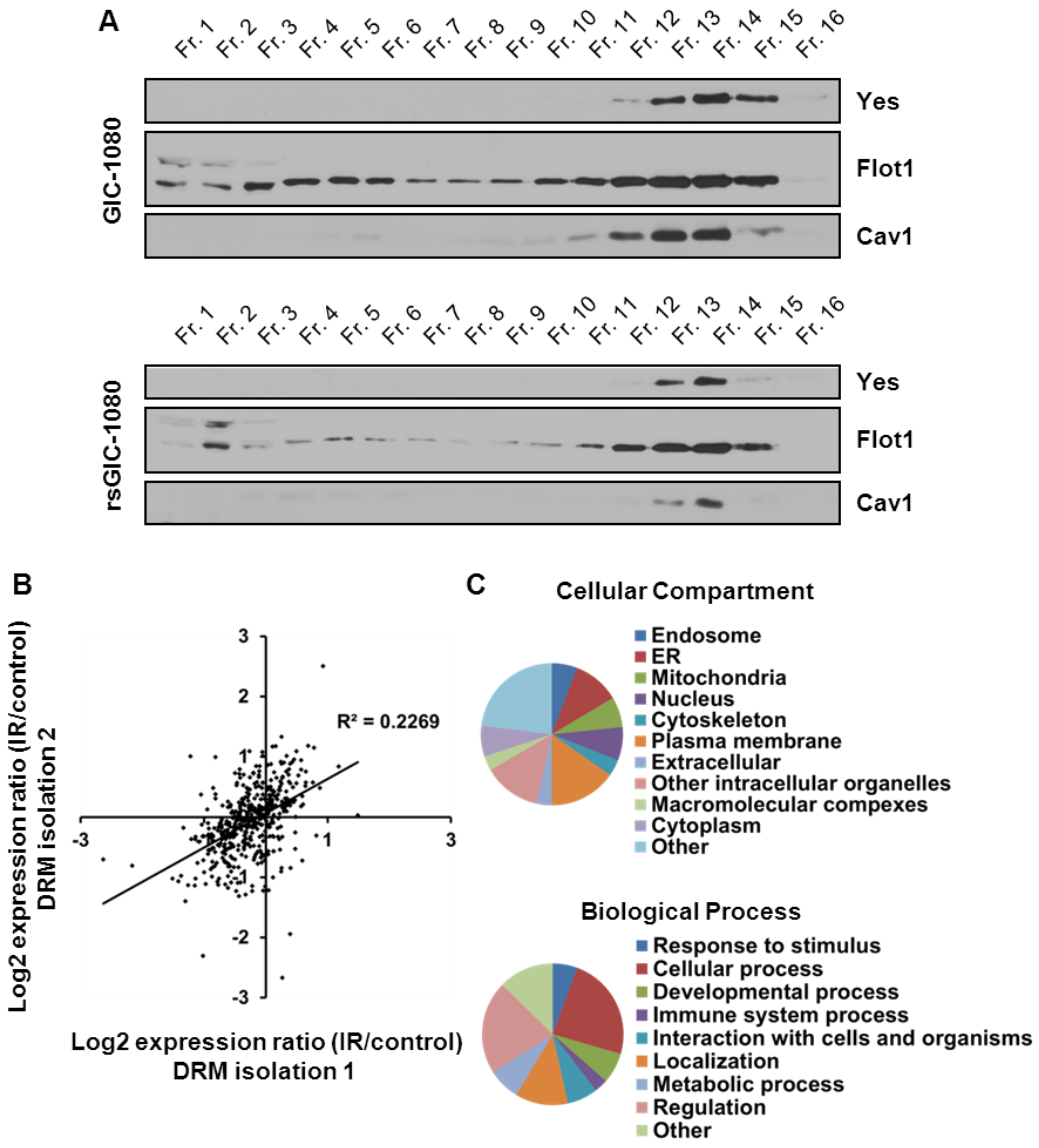

Figure 15: DRM isolation and evaluation of composition.
(A) Western Blot analysis of cellular fractionation. Cells were lysed in 0.5% Brij98® lysis buffer and 500 µl fractions taken from a discontinuous sucrose gradient. Shown by lipid raft markers YES, Flot1, Cav1, the DRM fractions are located between fractions no. 12-15. (B) The DRM isolation experiment was performed twice. 454 proteins were detected in both runs. Their log2 expression ratios, indicating differential or similar expression levels between rsGIC-1080 and GIC-1080 (control), correlated with a low correlation coefficient of R = 0.2269. Only few proteins were similarly regulated in both experiments. (C) 454 proteins were subjected to annotation and associated with various subcellular locations and biological processes.

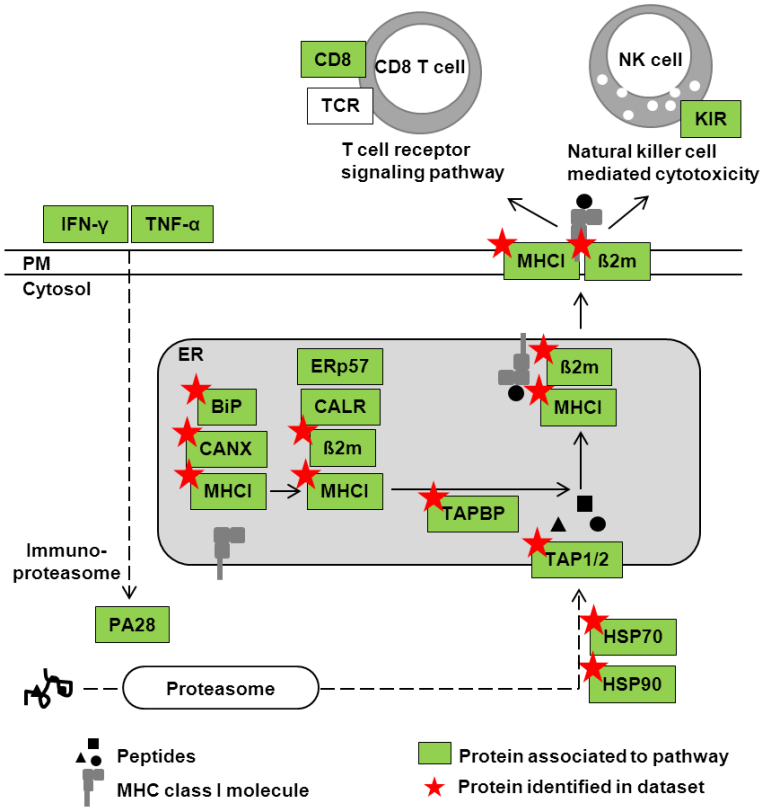

Figure 16: Regulation of "Antigen processing and presentation" KEGG pathway.
Analysis of LR proteins using DAVID Functional Annotation tool revealed distinct KEGG pathways that can be associated with the dataset. Proteins, isolated in the DRM fractions are marked with a red star.

Antigen processing and presentation KEGG pathway associated proteins

Accession No.	Description	Exp.1 [IR/control]	Exp. 2 [IR/control]	Mean [IR/control]
1A02_HUMAN	HLA class I histocompatibility antigen, A-2 alpha chain	-0.0579	0.4809	0.2115
1B08_HUMAN	HLA class I histocompatibility antigen, B-8 alpha chain	-1.0150	-2.3062	-1.6606
1C07_HUMAN	HLA class I histocompatibility antigen, Cw-7 alpha chain	-0.0616	-0.6051	-0.3333
B2MG_HUMAN	Beta-2-microglobulin	-0.4372	-0.8324	-0.6348
CALX_HUMAN	Calnexin	-0.2302	0.0385	-0.0958
HS71L_HUMAN	Heat shock 70kDa protein 1-like	-0.2651	0.1888	-0.0382
HSP71_HUMAN	Heat shock 70 kDa protein 1A/1B	-0.2160	-0.2627	-0.2393
HSP72_HUMAN	Heat shock-related 70 kDa protein 2	-0.4815	-0.0160	-0.2487
HSP76_HUMAN	Heat shock 70 kDa protein 6	-0.6122	-0.2145	-0.4134
TAP1_HUMAN	Antigen peptide transporter 1	-0.7549	-1.0215	-0.8882
TAP2_HUMAN	Antigen peptide transporter 2	-0.6017	-0.7768	-0.6893
TPSN_HUMAN	Tapasin	-0.9665	-1.1156	-1.0411

Table 1: Relative expression of proteins identified in dataset and involved in antigen processing and presentation.
All of the proteins identified in the dataset exhibited reduced expression.

3.1.1.4 Reduced expression of proteins involved in antigen processing and presentation

To validate the mass spectrometry results, RNA and proteins were extracted from GIC-1080 and rsGIC-1080. As shown in Figure 17A+B, TAP1 and TAP2 were significantly downregulated after radio-selection on mRNA- and protein-level.

Diminished expression of TAP transporter molecules in the ER possibly results in a lower number of shuttled peptides into the ER, a decreased function of the MHC I peptide loading complex machinery, and lower MHC class I molecule expression on the cellular surface (for reference see Figure 2). Interestingly, the radio-selection seemed to have had a direct effect on the genes involved in antigen processing and presentation. A lower protein expression was detected for the ER proteins ERp57, Tapasin, and β_2-microglobulin, but not for calreticulin in rsGIC-1808 compared to the control GIC-1080 (Figure 17B).

To analyze MHC class I expression on the cellular surface, the patient-specific Human Leukocyte Antigen (HLA) molecules were determined in a HLA diagnostics laboratory (Dr. Thiele, Institute for Immunology and Genetics, Kaiserslautern, Germany) (*HLA-A**01:02; *HLA-B**08:15; *HLA-C**03:07). Antibody stainings for HLA-A1, -A2, -B15, total HLA-A/B/C, and HLA-B/C were performed and expression measured by flow cytometry. As depicted in Figure 17C, a lower expression of total MHC class I molecules, especially HLA-A2, -B15, and general –B/C could be detected in rsGIC-1080 compared to the control GIC-1080. Of note, expression of HLA molecules could be increased by incubating the cells with 1 µg/ml IFN-γ for 24 hours in both, GIC-1080 and rsGIC-1080, although to a lesser extend in the latter (Figure 17D).

Together, these data demonstrated that fractionated ionizing radiation resulted in lower immunogenic potential and triggered an immune escape mechanism in this GIC cell line. The expression of MHC class I could be increased, also in rsGIC-1080 by administration of IFN-γ.

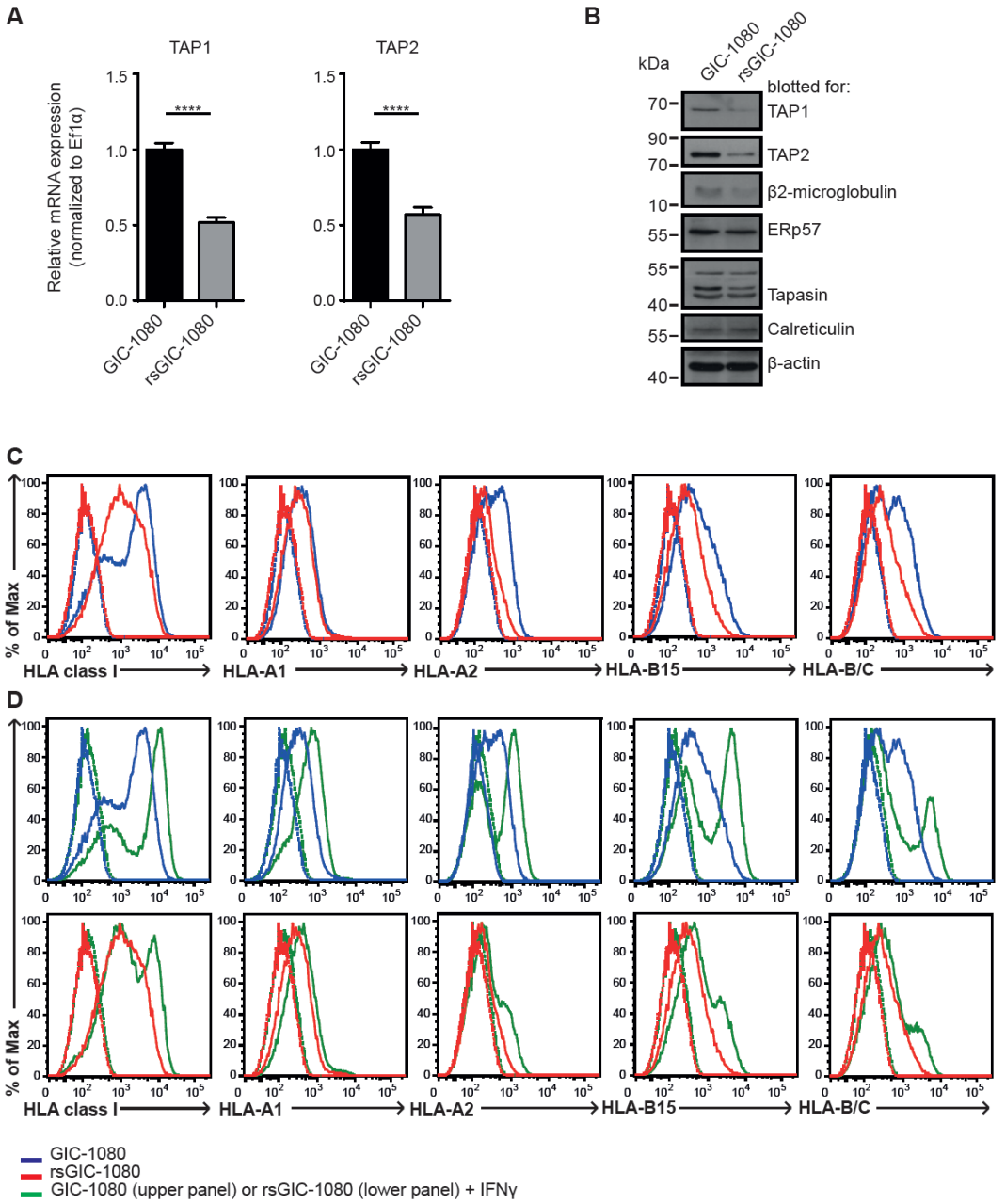

Figure 17: Immunological effects of radiation on GICs.
(A) Lower mRNA expression for TAP1 and TAP2 was detectable in rsGIC-1080 compared to GIC-1080. (B) Western Blot analysis of MHC class I peptide loading complex proteins demonstrated that almost all proteins involved in the antigen processing and presentation were downregulated after radio-selection. (C) Decreased expression of HLA molecules on the surface of irradiated rsGIC-1080 compared to control GIC-1080. (D) HLA expression on radio-selected and control GICs was increased after incubation with 1 µg/ml IFN-γ for 24 hours.

3.1.1.5 Decreased recognition of radio-selected GICs by cytotoxic CD8+ T lymphocytes

To test whether the decreased HLA expression on the surface of rsGIC-1080 had functional consequences in terms of a diminished recognition potential of these cells by cytotoxic CD8+ T lymphocytes, allogeneic mixed lymphocyte tumor cultures (MLTC) in the 96-well micro culture format were established for lysis potential testing using a ^{51}Chromium release assay. The micro culture format was chosen because under these conditions rare antigen-specific T cell clones have a better chance to become stimulated and expanded than in 48- or 24-well culture formats and per culture a lower diversity of T cells was expected. First, a blood donation from a HLA-A/B matched healthy donor was obtained from the German Red Cross Blood Donation Center, Bad Kreuznach, Germany. In this setting the most likely antigens targeted by the CTL were peptides presented by allo-HLA-C molecules or minor histocompatibility antigens (mHAG). PBMC were isolated, followed by a positive MACS sort for CD8+ T cells. For the MLTC, the target cells GIC-1080 and rsGIC-1080 served as APCs and therefore were stimulated with IFN-γ for 24 hours to increase HLA surface expression. Shortly before the co-culture, the tumor cells were freshly irradiated with 120 Gy to stop their proliferation. The T cells were co-cultured with the tumor cells and a cytokine cocktail and restimulated every week. To check the activity of the CD8+ T cells, an IFN-γ ELISpot Assay was performed on day 19. Ten T cell micro cultures, stimulated against GIC-1080 as well as ten cultures, stimulated against rsGIC-1080 with highest IFN-γ expression were chosen for further expansion. On day 40, the T cells were tested for their lysis potential of GIC-1080 as well as rsGIC-1080 in a ^{51}Chromium Release Assay. Effector T cells were incubated with radioactively labeled tumor cells in decreasing effector to target cell (E:T) ratios from 60:1 to 1:1 to see titration effects. After 5 hours of incubation, the amount of ^{51}Cr released into the supernatant of the cultures was detected. Lysis levels below 20% were regarded as unspecific background. The results of 16 cultures are depicted in Figure 18A+B. Four cultures did not yield sufficient T cell numbers or failed to lyse the tumor cells, as exemplarily shown by cultures A3 and D2. As expected, T cells raised against control GIC-1080 recognized these cells significantly better than the radio-selected counterparts. Interestingly, all active cultures that were raised against rsGIC-1080 recognized control GICs much

better than radio-selected GICs. Three cultures raised against rsGIC-1080 (C1, C2, and C5) were not able to lyse the radio-selected GICs, but exhibited lysis potential towards GIC-1080.

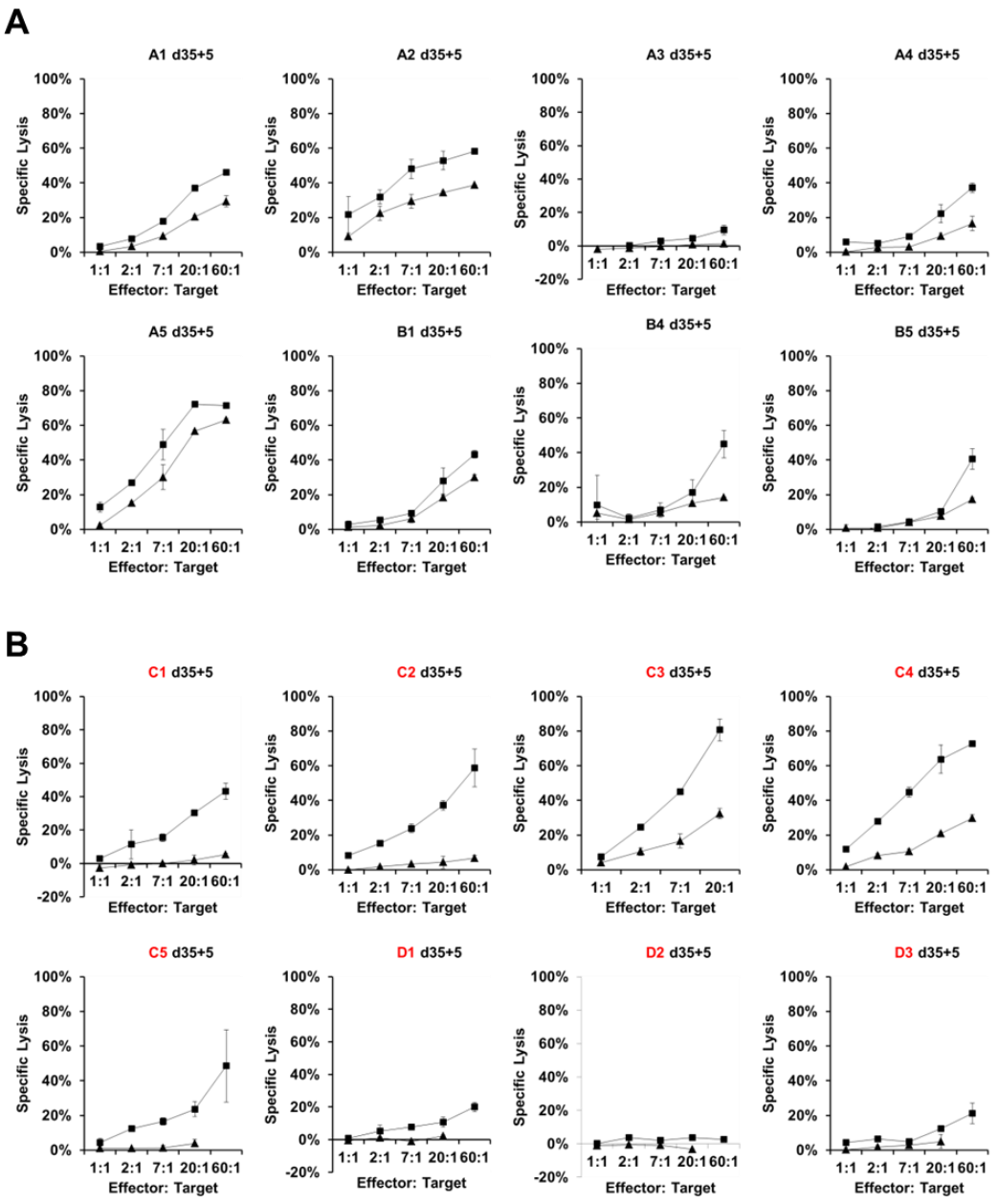

Figure 18: ^{51}Chromium release assay.
Lysis test of GIC-1080 and rsGIC-1080 by cytotoxic CD8+ cells. (A+B) Panel of 8 CD8+ cultures, stimulated with (A) GIC-1080 or (B) rsGIC-1080 and tested for lysis of GIC-1080 (squares) and rsGIC-1080 (triangles). The titration effect of Effector to Target ratio was visible in all active cultures.

To check the clonality of the CD8+ T cell cultures, a panel of 24 T cell receptor variable beta (Vβ) chains were labeled using specific antibodies and measured

by flow cytometry (Figure 19). The CD8+ T cell culture B5 was stimulated with GIC-1080 whereas CD8+ T cell culture C4 was stimulated with rsGIC-1080. These cultures were used as an example. The results for T cell culture B5 showed that 13.4% of the cells expressed Vβ 13.2, and 4.9% of the cells expressed Vβ 17. CD8+ T cells from culture C4 expressed 1.86% of Vβ 13.2 and 78.3% of Vβ 17. No populations of other Vβ chains (Vβ 1, 2, 3, 4, 5.1, 5.2, 5.3, 7.1, 7.2, 8, 9, 11, 12, 13.1, 13.2, 14, 16, 17, 18, 20, 21.3, 22, and 23) were detected. As antibodies are not available for all Vβ chains, it is possible that an antibody to the Vβ chain of the predominating T cells in the B5 culture was missing in the panel staining. The results indicated that the C4 CD8+ T cell culture was highly enriched for TCR-Vβ17-positive T cells (78.3%) and the fact that there was still lysis at an E:T-ratio as low as 2:1 suggested that this population was responsible for the tumor cell-lysis. In contrast, no conclusion about the prevalent T cell clone in culture B5 could be drawn. As in all cases the control GIC-1080 were better recognized and lysed by the CD8+ T cells, a possible interpretation of the results is that reduced expression of components of the antigen processing and presentation pathway upon fractionated irradiation indeed had an impact on the recognition of rsGIC-1080. For other micro cultures, in particular those with no strong enrichment of single T cell-specificities, it is likely that different antigens were recognized on GIC-1080 and rsGIC-1080.

Overall the results indicate that sub-lethal fractionated ionizing radiation can lead to decreased expression of HLA molecules on the cellular surface of GICs, resulting in lower recognition potential of GICs by cytotoxic CD8+ T cells and therefore immune escape.

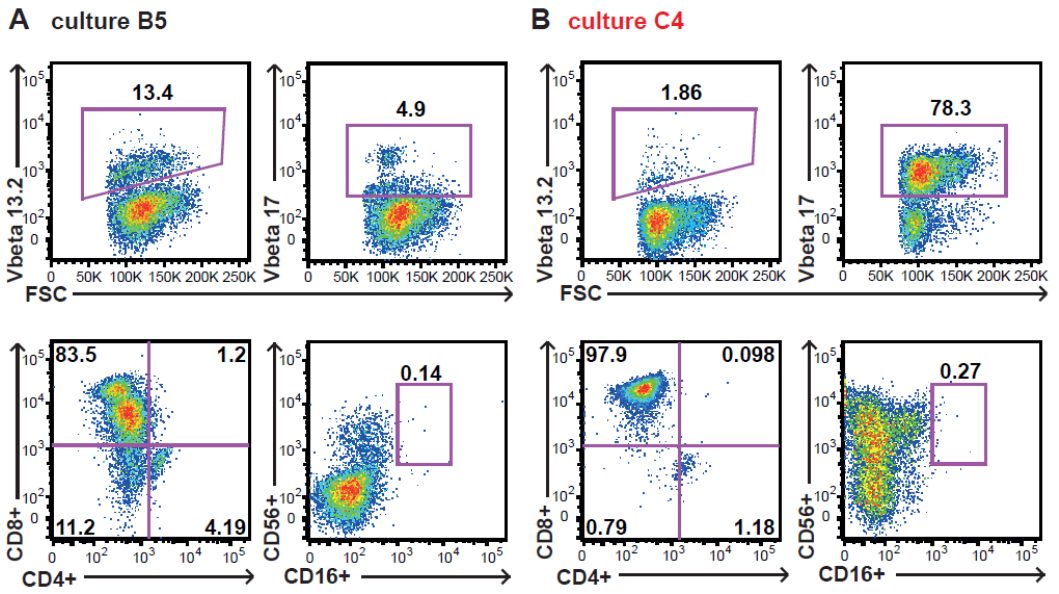

Figure 19: TCR variable beta chain staining of two selected CD8+ T cell cultures. *24 different Vβ chains were labeled with specific antibodies and their presence analyzed by flow cytometry to check clonality of CD8+ T cell cultures. Two cultures, stimulated either with GIC-1080 (B5) or rsGIC-1080 (C4) were tested. In both cultures, TCR-Vβ 13.2 and TCR-Vβ 17 revealed populations. The cultures were not contaminated by CD56+CD16+CD3- NK cells. (A) 84.7% of CD8+ T cells were present in the B5 culture with less than 5% CD4+ cells. 13.4% and 4.9% of the CD8+ T cells were positive for Vβ 13-2 and Vβ 17 chains respectively. (B) Culture C4 contained 98% of CD8+ T cells with only 1.2% of CD4+ cells. 1.86% of CD8+ T cells expressed Vβ 13.2 while 78.3% expressed Vβ 17 chain.*

3.1.2 Functional analysis of IFITM3 in GICs

The role of Interferons (IFNs), especially IFN-γ, is very important in immunotherapies as it stimulates differentiation and cytolytic effector function of CD8+ T cells (234,235). Interferons exhibit anti-proliferative signaling (50,236), but the role of interferon-induced transmembrane proteins (IFITM) in proliferation remains controversial. Data from different cell types suggested enhancing and diminishing effects of IFITM proteins on proliferation (85,87,88,237). Recently, expression of interferon-induced genes, including IFITM genes, was shown to be increased after treatment with ionizing radiation in breast, prostate, gliosarcoma cell lines (90), and head and neck tumors, suggesting a contribution to a more radioresistant phenotype (92).

Comparative whole genome transcriptome analysis (Affimetrix, HumanGene ST1.0 microarray) of GIC-1080 and rsGIC-1080 revealed an overall upregulation

of different interferon-inducible genes after radio-selection, including IFITM3, indicating a connection between radioresistance mechanisms and immune signaling pathways. This effect was confirmed in transcriptome analysis in a larger panel of radio-selected and control GICs (Ella Kim, personal communication). Up to now, contribution of IFITM3 to resistance mechanisms and proliferation has not been investigated in GICs. In this study, the expression of IFITM3 in GIC-1080 and rsGIC-1080 was analyzed. To investigate the contribution of IFITM3 to proliferation in GICs *in vitro* and *in vivo*, lentiviral vector systems were established for a stable upregulation and a stable knockdown of IFITM3.

3.1.2.1 Endogenous expression of IFITM3 in GICs

To analyze localization of IFITM3 in GICs, immunocytochemistry stainings and cellular fractionation was performed. Confocal Imaging showed that IFITM3 was located mainly at the plasma membrane, unevenly distributed in clusters. Immunostaining of the intermediate filament Nestin, located in the cytoplasm, served as a stem cell marker. The Nuclei were counterstained with DAPI (Figure 20A). Western Blot analysis of the subcellular fractions derived by ultracentrifugation as described in chapter 3.1.1.3 revealed that IFITM3 was detectable in fractions of lipid rafts/detergent resistant membranes (Figure 20B).

Increased expression of IFITM3 was observed in rsGIC-1080 compared to GIC-1080 on mRNA and protein level (Figure 20C+D). As expected, this expression was further increased by treatment with IFN-γ (data not shown).

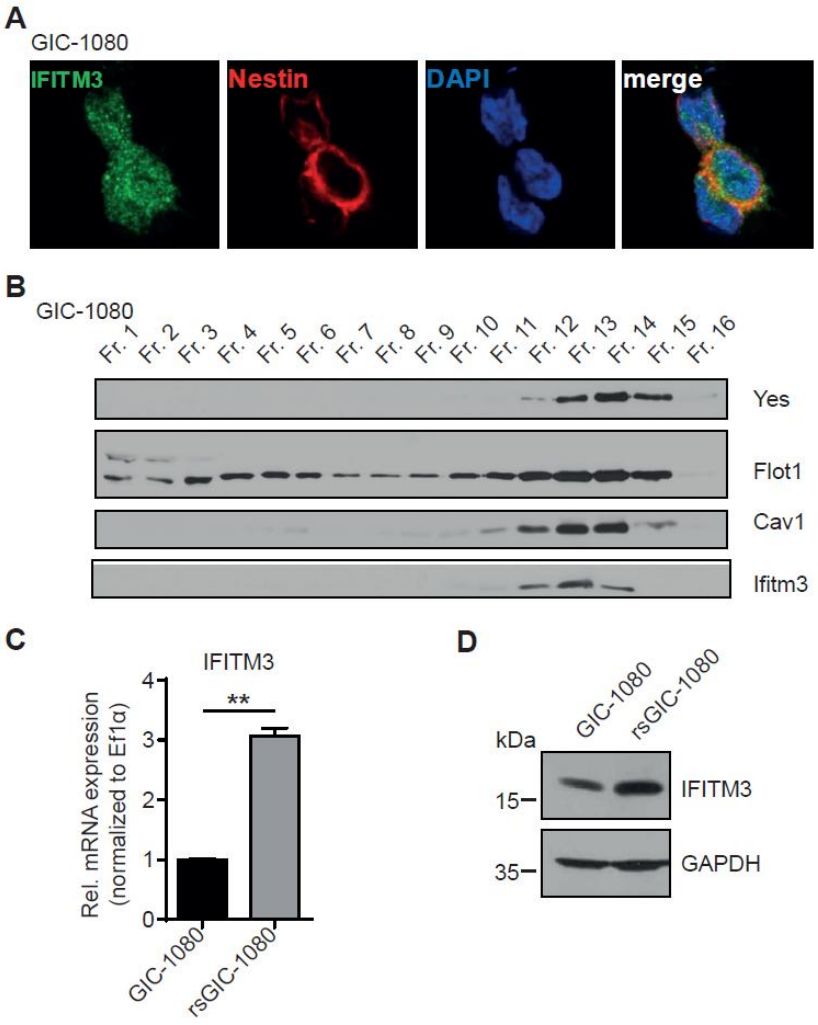

Figure 20: Expression and localization of IFITM3 in GIC.
(A) Tumor cells were immunostained with antibodies for IFITM3 and stem cell marker Nestin. Confocal analysis of immunocytochemistry staining showed dotted pattern of IFITM3 at the cellular surface. (B) Fractionation of cellular compartments and Western Blot analysis of the fractions showed overlap of lipid raft markers an IFITM3. (C+D)Fractionated ionizing radiation of GIC-1080 led to an increased expression of IFITM3 at mRNA- and protein levels.

3.1.2.2 Generation of overexpression and knockdown constructs for IFITM3

One of the aims of this study was to investigate the function of IFITM3 in GICs. An IMAGE clone with the reference sequence of IFITM3 was purchased from BioCat (Heidelberg, Germany). Several lentiviral vectors with different promotors were tested for the overexpression of IFITM3. Unfortunately, the strong CMV-promotor of the pCDH-vector seemed to be silenced in GIC and this vector could

not be used. Similarly, no expression of the construct was achieved with a vector containing the high expression MSCV-promotor, developed to function especially in hematopoietic and stem cells. Therefore, in this analysis, IFITM3-cDNA was inserted into the multiple cloning site (MCS) of the lentiviral pCDH-vector using the XbaI and BamHI restriction enzymes. This vector included a medium but robust expression Ef1alpha-promotor and copGFP as an expression reporter gene, coupled via an IRES cassette (Figure 21A+B). After lentiviral transduction of GIC-1080, spheres were grown, expression of IFITM3 was checked via expression of the reporter protein copGFP and cells were sorted for high GFP expression on a FACS Aria (Figure 21C). To have the possibility of targeting and isolating IFITM3 not only by IFITM3 antibodies, the protein was further tagged with a myc-tag at the c-terminus. Due to the larger size the constructed protein runs slightly higher in a SDS-PAGE, resulting in a double band of endogenous and artificial protein expression in Western Blot analysis. The total amount of IFITM3 protein was doubled by expression of the additional construct (Figure 21D).

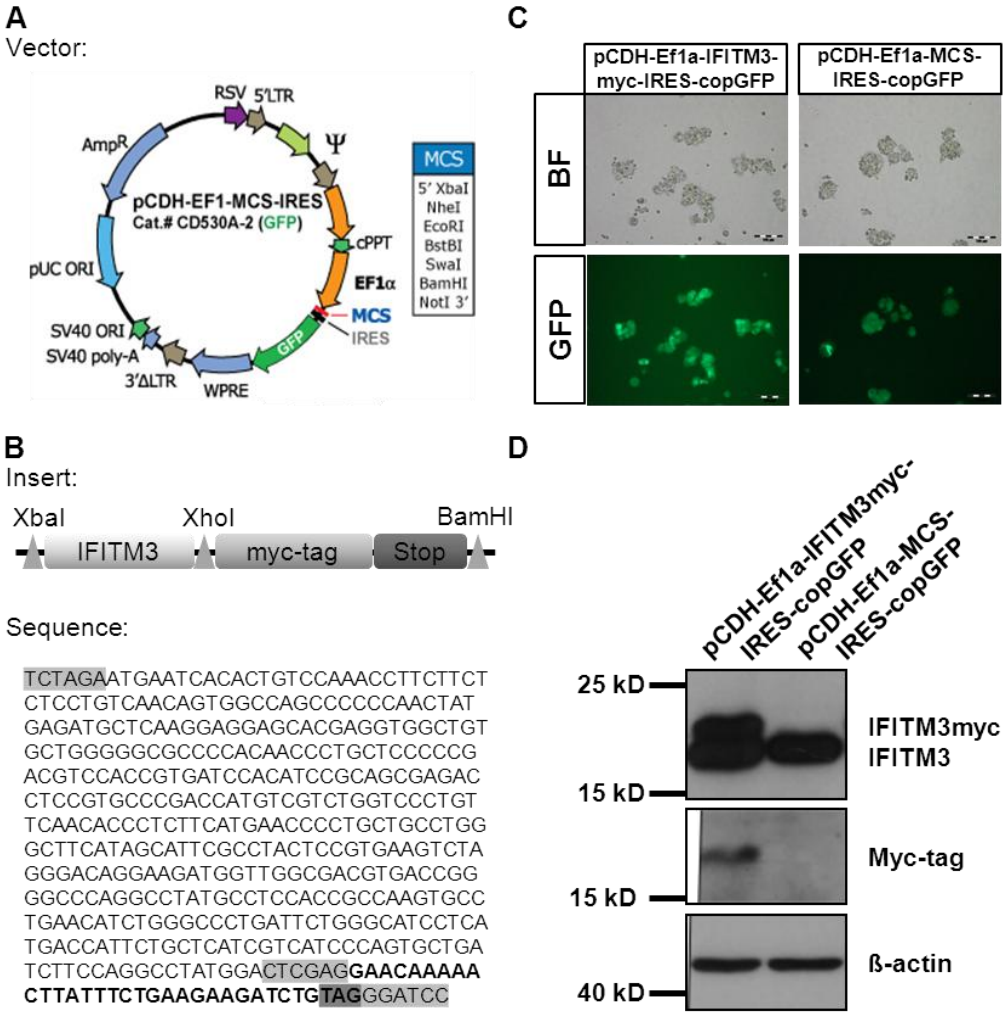

Figure 21: Lentiviral construct for overexpression of IFITM3.
(A) The vector was purchased from SBI. (B) A bacterial clone with the sequence of IFITM3 was purchased from BioCat and inserted into the vector. The IFITM3 insert was modified as follows: Xba1, XhoI, and BamHI cutting sites were added and are marked in light grey. The additional myc-tag and the stop codon are displayed in bold letters and the stop codon marked in dark grey. (C) Expression of IFITM3 was checked via the reporter gene copGFP expression in transduced GIC-1080. (D) SDS-PAGE and Western Blot analysis of GIC-1080 that were transduced with the IFITM3myc-enconding vector, displayed a double band of artificial and endogenous IFITM3 expression as well as myc-tag expression at the same height as IFITM3myc. GIC-1080, which were transduced with the empty control vector displayed the endogenously expressed IFITM3.

To stably silence IFITM3 expression five different pGIPZ short hairpin RNA (shRNA) clones for lentiviral transduction were purchased from Thermo Scientific (Schwerte, Germany). The expression of the shRNAs was driven by a human CMV-promotor and linked to turboGFP (tGFP) and Puromycin expression via an IRES sequence (Figure 22A). After lentiviral transduction of GIC-1080 and three

weeks selection with Puromycin, reporter GFP expression was checked with a fluorescence microscope (Figure 22C). IFITM3 protein expression was analyzed using SDS-PAGE and Western Blot analysis. Only shRNA sequence clones 1, 4, and 5 silenced IFITM3 expression by 40-70%. As shRNA clones 4 and 5 revealed the strongest knockdown of IFITM3, these constructs were used for the subsequent functional *in vitro* and *in vivo* assays.

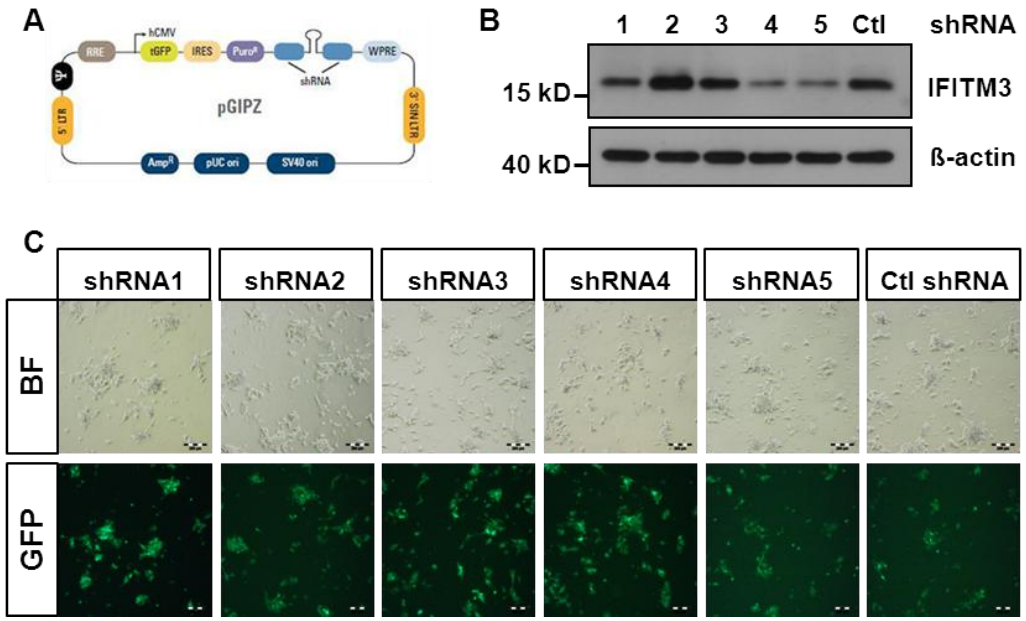

Figure 22: Lentiviral construct for stable knockdown of IFITM3.
(A) Five different pGIPZ shRNA vectors for the silencing of IFITM3 and a scramble control shRNA vector were purchased. (B) The knockdown of IFITM3 was analyzed via Western Blot in GIC-1080. ShRNA sequences number 4 and 5 revealed the strongest knockdown of IFITM3. (C) Transduced GIC-1080 were selected with Puromycin and GFP expression as a reporter checked on a fluorescence microscope. Transduction of all shRNA clones worked similarly well.

3.1.2.3 *In vitro* proliferation analysis of GICs with high expression and knockdown of IFITM3

As described above, IFITM3 was shown to have positive and negative effects on proliferation of various cancer cells. In glioma cell lines, knockdown of IFITM1 and IFITM3 by interfering RNA (RNAi) reduced proliferation and migration (88,89).

In this study, GIC-1080, transduced with the different constructs for overexpression and knockdown of IFITM3 as well as respective control cells, was tested for differences in proliferation using the EdU incorporation assay. The cells were incubated with EdU for 4 hours, fixed and stained with an anti-EdU antibody for detection by flow cytometry on FACS Canto II. As shown in Figure 23A, there was only a slight statistically not significant tendency of IFITM3 high expressing cells towards slower proliferation. Cells transduced with shRNA constructs for the knockdown of IFITM3 proliferated equally fast compared to their control (Figure 23B). Therefore, neither the doubled amount of IFITM3 nor the knockdown by about 70% resulted in significant changes in GIC-1080 proliferation potential.

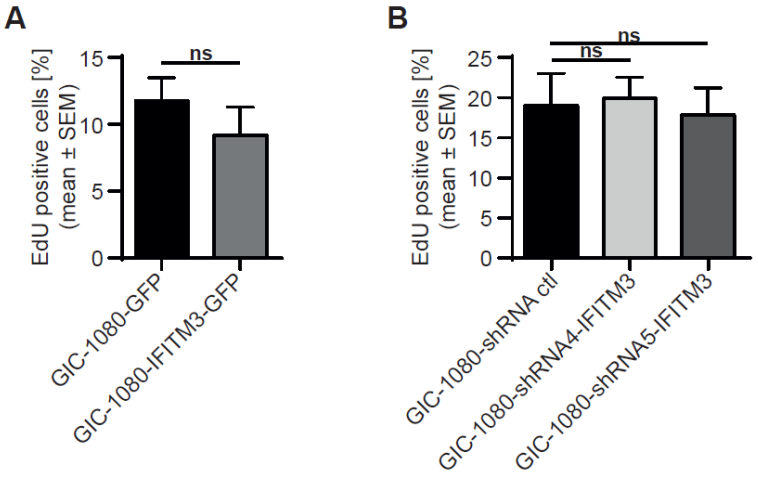

Figure 23: EdU proliferation assay of IFITM3 high expressing and knockdown cells. *GIC-1080 transduced with indicated constructs were incubated with EdU for 4 hours and EdU incorporation measured by flow cytometry. Proliferation of cells with high expression of IFITM3 (GIC-1080-IFITM3-GFP) (A) and cells with a knockdown of IFITM3 by shRNA (GIC-1080-shRNA-IFITM3) (B) was comparable to the respective control cells (GIC-1080-GFP: GIC-1080-shRNA ctl).*

3.1.2.4 Functional analysis of overexpression and knockdown of IFITM3 *in vivo*

Next to *in vitro* proliferation, the effect of IFITM3 high expression and knockdown on tumor growth was analyzed in a xenograft tumor model. Therefore, 100,000 GIC-1080 that had been transduced with the different constructs were intracranially implanted into immunodeficient NMRI nude mice. 10 mice were used per group and read out method. To compare the tumor volumes, tumors

were grown for 7 weeks in the xenograft model before mice were sacrificed. For the analysis, 50 µm coronal brain sections were prepared and at least 10 serial sections per brain imaged for tumor GFP expression on a confocal Leica SP5 microscope (Figure 24A). The area of each section was measured using ImageJ software and the result multiplied by the thickness of the slice and the distance between two slices measured. Of note, the tumor volumes inside the groups already showed a large variation between 2 – 200 mm^3. This might be one of the reasons leading to overall no significant differences of neither IFITM3 high expressing GIC-1080 nor IFITM3 knockdown GIC-1080 compared to their respective controls (Figure 24B+C).

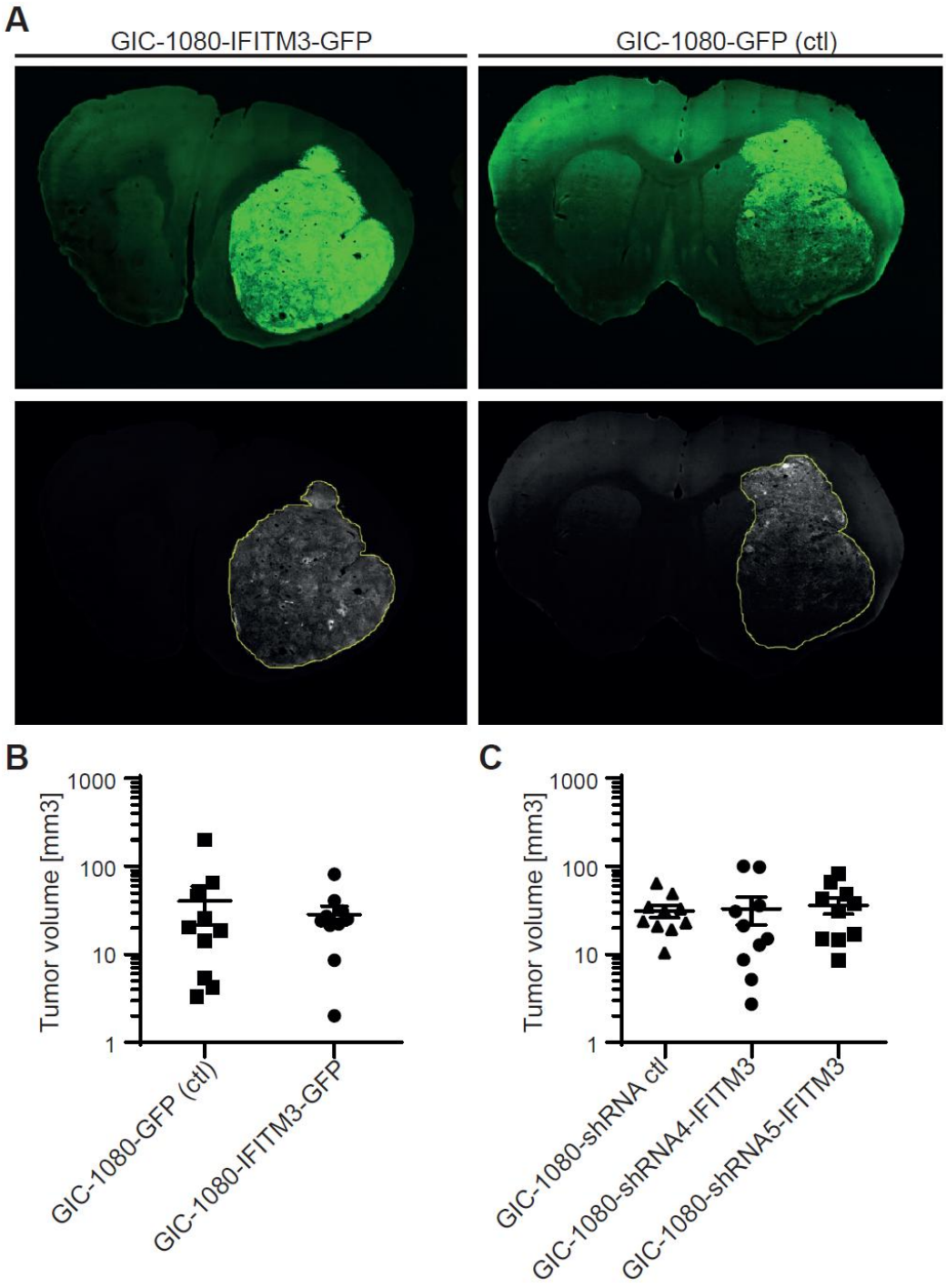

Figure 24: Tumor volume measurement.
(A) Coronal brain slices of GFP-expressing tumors consisting of IFITM3 high expression (left panel) and control cells (right panel). The tumor area of at least 10 slices per brain tumor was measured using ImageJ software. (B+C) Measurement of tumor volumes after 7 weeks incubation time revealed no significant difference between the experimental groups.

The overall survival as illustrated by the Kaplan Meier-survival curve was used as another read out for changes in tumor growth. Mice were implanted with the respective tumor cells as described above and the number of survival days measured. Mice with IFITM3 high expressing GICs seemed to survive longer than mice with control cells throughout the first weeks, showing the same tendency of slightly slower cell proliferation as seen in *in vitro* proliferation assays. This though did not reach statistical significance (Figure 25A). GIC-1080 transduced with shRNA constructs for IFITM3 resulted in equal survival of the knockdown groups compared to their control (Figure 25B), correlating as well to the *in vitro* results.

Overall, IFITM3 seems to be only a minor regulator of cell proliferation in GIC-1080.

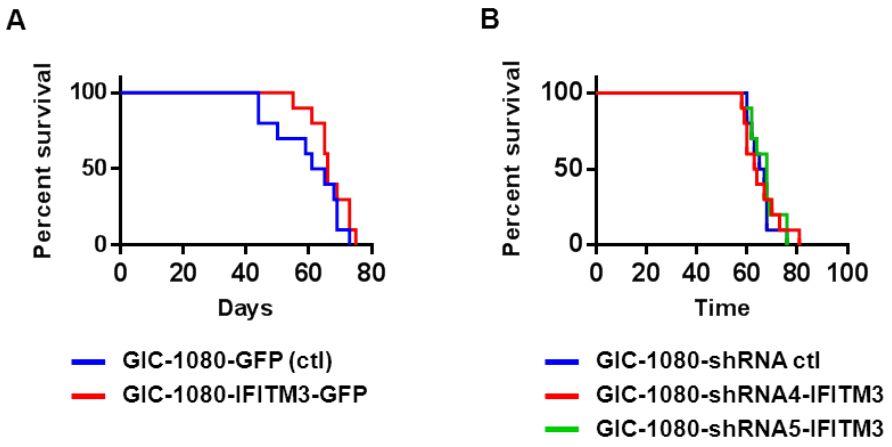

Figure 25: Kaplan-Meier-survival curve.
(A) The survival of mice harboring IFITM3 overexpressing cells only showed a tendency for slower tumor growth throughout the first incubation weeks but survival curves did not differ significantly. (B) Survival of mice harboring tumors of IFITM3 knockdown or control was comparable.

3.2 Multiple sclerosis and its animal model EAE

3.2.1 Evaluation of transcriptional changes in T cells in EAE

Data from various groups suggested that differentiated T cells undergo massive transcriptional changes in the course of EAE. Up to now, only single transcription factors or cytokines have been evaluated for their contribution on these variations in detail.

Herein, transcriptome analysis was performed in order to analyze whole genome expression levels of T cells at various stages of T cell differentiation and disease (Figure 8). Therefore naïve T cells (Tnaive) were isolated from spleen and lymph nodes of transgenic mice with MOG-specific T cell receptors (2d2.C57BL/6 mice) and differentiated towards Th17 cells *in vitro* with 3 stimulations using fresh antigen presenting cells (APCs), the peptide MOG_{35-55} and respective cytokines (Th17iv). The Th17iv cells were intravenously injected into lymphopenic *Rag1*$^{-/-}$ mice for induction of EAE (adoptive transfer model). At the peak of the disease, CD4+ T cells were re-isolated from the CNS of diseased mice (Th17eae). Similarly, CD4+ T cells were further isolated at the peak of disease from C57BL/6 wild-type mice, which had been actively immunized with the peptide MOG_{35-55} (CD4eae). The different cells were frozen and sent to Miltenyi Biotec for mRNA isolation and transcriptome analysis using Agilent Whole Mouse Genome Oligo 4x44K V2 microarray chips. Candidate genes were selected by two-fold differential gene expression a signal intensity variance error-model based p-value < 0.01 (238). This p-value calculation was chosen for evaluation of genes based on the indirect light signals measured on a microarray. This p-value can differ from statistical p-values.

3.2.1.1 Transcriptional changes in T cell lineage genes in the course of EAE

In vitro primed Th17 cells typically express IL-17 but no or low levels of IFN-γ. Interestingly, it has been shown that former high IL-17 producers co-expressed IFN-γ after re-isolation from the CNS of adoptive transfer EAE mice. These cells obtained an intermediate phenotype between Th1 and Th17 and were called “ex-

Th17" cells (189). To confirm the differentiation of naïve T cells into Th17 cells and changes of key lineage factor expression after induction of EAE, lineage markers of Th17 and Th1 were evaluated (Figure 26A+B). In the comparison of naïve T cells (Tnaive) to differentiated Th17 cells (Th17iv), there was an increase in expression of the master transcription factor for Th17 cells *Rorc* and associated *Stat3*. Similarly, typical Th17 lineage cytokines such as *Il17a*, *Il17f*, *Il21*, and *Il22*, and surface markers such as the receptors for IL-1 (*Il1r1*) and IL-23 (*Il23r*, *Il12b2*) were highly upregulated. Th1 lineage factors were not significantly regulated, except for *Il12rb2*, which is a receptor subunit necessary for both Th1 and Th17 polarizing cytokines IL-12 and IL-23 respectively, and slightly the receptor subunits for IL-12 (*Il12rb1*) and IFN-γ (*Ifngr1*). In the comparison of CD4+ T cells isolated from adoptive transfer EAE mice (Th17eae) with naïve T cells (Tnaive) Th17 cytokines and transcription factors were still upregulated, but reduced in their expression levels compared to Th17iv. Further, expression of *Ifng* as well as its receptor *Ifngr2* and the master transcription factor for Th1 lineage cells *Tbx21* increased. Similarly, a mixed Th1 and Th17 phenotype was detected in the comparison of naïve T cells (Tnaive) with CD4+ T cells isolated from active immunized mice (CD4eae), in which both Th1 and Th17 phenotypic markers were upregulated.

These results indicate that under the differentiation condition used, clear-cut Th17 lineage cells were produced. Throughout the course of EAE, these cells largely maintained their characteristics, but shifted towards an intermediate Th1-Th1 phenotype.

A

	Th17 properties	Th17iv vs. Tnaive	Th17eae vs. Tnaive	Th17eae vs. Th17iv	CD4eae vs. Tnaive
		Fold Change	Fold Change	Fold Change	Fold Change
Surface expression	IL-1R1	29.73	4.43	-3.96	20.10
	IL-12Rβ1	7.62	2.99	-2.57	3.69
	IL-23R	13.20	1.50	-7.13	5.46
	CCR6	-1.59	1.63	3.41	3.41
	IL-13Rα1	1.50	22.76	15.56	40.95
	IL-13Rα2	-1.63	-3.08	-1.89	-5.36
Unique Cytokines	IL-17A	100.00	99.75	-2.99	100.00
	IL-17F	100.00	4.73	-57.14	11.36
	IL-21	89.96	95.10	1.09	7.70
	IL-22	8.27	-1.60	-15.06	14.34
TF	RORγt/Rorc	41.15	4.85	-7.37	10.40
Stats	STAT3	1.91	1.58	-1.23	1.60

B

	Th1 properties	Th17iv vs. Tnaive	Th17eae vs. Tnaive	Th17eae vs. Th17iv	CD4eae vs. Tnaive
		Fold Change	Fold Change	Fold Change	Fold Change
Surface expression	IL-12Rβ2	68.19	8.34	-7.64	13.56
	IL-12Rβ1	7.62	2.99	-2.57	3.69
	IFN-γR1	2.87	2.85	-1.08	4.53
	IFN-γR2	-1.24	2.04	2.59	1.60
Unique Cytokines	IFN-γ	1.68	11.45	1.99	32.98
TF	T-bet/Tbx21	2.15	7.03	1.71	8.33
Stats	STAT1	-1.07	-2.45	-2.21	-1.99
	STAT4	1.07	-1.87	-1.99	-1.13

- significantly increased gene expression FC >50
- significantly increased gene expression FC > 10 ≤ 50
- significantly increased gene expression FC > 1.5 ≤ 10
- no significant change in gene expression
- significantly decreased gene expression FC < -1.5 ≥ -10
- significantly decreased gene expression FC < -10 ≥ -50
- significantly decreased gene expression FC < -50

Figure 26: T cell lineage factor expression of T cells at various time points of adoptive transfer and active EAE protocols.
(A) Key lineage factors of Th17 cells were highly expressed after in vitro Th17 differentiation (Th17iv vs. Tnaive) but decreased in the course of EAE (Th17eae vs. Tnaive; Th17eae vs. Th17iv). (B) Expression of most Th1-associated factors was not significantly regulated in Th17 cell differentiation (Th17iv vs Tnaive), but was increased in CD4+ T cells isolated from adoptive transfer EAE cells (Th17eae) compared to naïve T cells. (A+B) Th17 and Th1 lineage factors were upregulated in CD4+ T cells isolated from actively immunized mice compared to naïve T cells (CD4eae vs. Tnaive).

3.2.1.2 Analysis of signaling networks regulated in the course of EAE

To identify underlying molecular mechanisms and key regulators of T cell plasticity and encephalitogenicity, the transcriptional alterations that were detected in *in vitro* primed Th17 cells (Th17iv) compared to re-isolated CD4+ T cells from the CNS of diseased mice (Th17eae) were analyzed in more detail. Ingenuity® Pathway Analysis (IPA) software was used as a tool to model and analyze complex biological systems. This software supports the interpretation of microarray datasets by identification of relationships between genes, mechanisms, functions, and relevant signaling pathways. Only candidate genes with a fold change > 2 and signal intensity p-value < 0.01 were analyzed. IPA mapped 5,149 of total 5788 Agilent microarray sequence codes (88.9%) of the candidate genes to a defined gene and excluded duplicate genes from analysis, thus resulting in a total of 4,343 analyzed genes. The genes were associated with key signaling networks according to Gene Ontology terms and experimental observations on the basis of known connections from immune cells or specifically T lymphocytes.

Two of the most prominent signaling networks are presented in Figure 27. In both networks, genes that were upregulated in Th17eae compared to Th17iv are displayed in graded reddish colors, downregulated genes in graded greenish colors, while genes associated with the network but not meeting the selection criteria (fold change > 2, signal intensity p-value < 0.01) are white. In network 1 (Figure 27A), most of the genes were upregulated in Th17eae cells compared to Th17iv, which indicated a general increased regulation of cellular function and maintenance, T cell development and differentiation, and proliferation. Key elements of network 1 were the enhanced expression of the T cell polarizing cytokines *Il2, Il6, Il9,* and *Il23* and the transcription factors *Aryl Hydrocarbon Receptor* (*Ahr)*, *Krüppel-like factor* (*Klf4*), *FBJ osteosarcoma oncogene* (*Fos*), *Nuclear factor of activated T cells c1* (*Nfatc1*), *Reticuloendotheliosis oncogene* (*Rel*), and *Spleen focus forming virus* (SFFV) *proviral integration oncogene* (*Spi1*, *Sfpi1, Pu.1*) that all have been reported to participate in the functions mentioned above. Interestingly, *Il6* and *Il23* are Th17 cell polarizing cytokines, while *Il2* is necessary for the differentiation of all other Th cells suppresses Th17 differentiation. While *Rorc* was decreased in the Th17iv cell transformation

towards Th17eae (Figure 26A), *Ahr* expression, necessary for Th17 differentiation, was upregulated, indicating that these cells did not completely lose their Th17 phenotype. However, many developmental changes occur as *Klf4*, *Spi1*, *Fos*, and *Nfatc1* were upregulated which are all implicated in thymocyte development. Key molecules in network 2 (Figure 27B) were the chemokines *Cxcl2*, *Cxcl3*, *Cxcl9*, *Cxcl10*, *Ccl2*, cytokines *Il2*, *Il1b*, *Il18*, *Il15*, *Il12b*, and *Ifnb2* in cooperation with the transcription factors *Spi1*, *Rel*, *Interferon regulatory factor 1* and *7* (*Irf1*, *Irf7*), and *Hematopoietically expressed homeobox* (*Hhex*). The expression of these chemokines and cytokines contributed to an inflammatory environment by recruiting and activating leukocytes. Although expression of co-stimulatory molecules *Cd40*, *Cd80*, and *Cd86* and Toll-like receptors (TLR) is rather associated with antigen presenting cells and cells of the innate immune system respectively, this data indicated an increased expression of *Tlr2*, *Tlr3*, *Tlr4*, and *Tlr6*, and the co-stimulatory molecules *Cd40*, *Cd80*, and *Cd86* on Th17eae cells. As highlighted by blue interaction lines in Figure 27D, an overlap of network 2 with canonical pathways suggested and interaction of the Th17 cells with cells from the innate immune system through the network-associated chemokines, TLR and co-stimulatory. Analysis of canonical pathways regulated in the transition of Th17iv cells to Th17eae cells revealed that LXR/RXR and PPAR Receptor signaling together with cholesterol biosynthesis were highly upregulated (Figure 27C and data not shown). Increased expression of cholesterol, which is necessary for membrane lipid raft formation, and therefore the building of T cell receptor signaling platforms, has been linked to enhanced pathologic T cell effector function and associated with a worse progression of EAE and MS. Of note, various MS risk-associated genes (see Chapter 3.2.1.4) were associated with the most prominent signaling pathways and involved in the developmental changes, including *Rgs1*, *Mertk*, *Cd80*, *Cd86*, *Il12b*, *Hhex* (network 1) and *Tnfrsf1a*, *Batf*, and *Cblb* (network 2).

Taken together, Th17iv cells underwent massive metabolic changes throughout the course of EAE that led to enhanced effector function to create a highly inflammatory environment. Further, developmental restructuring took place, possibly contributing to a more encephalitogenic T cell phenotype.

A Network 1

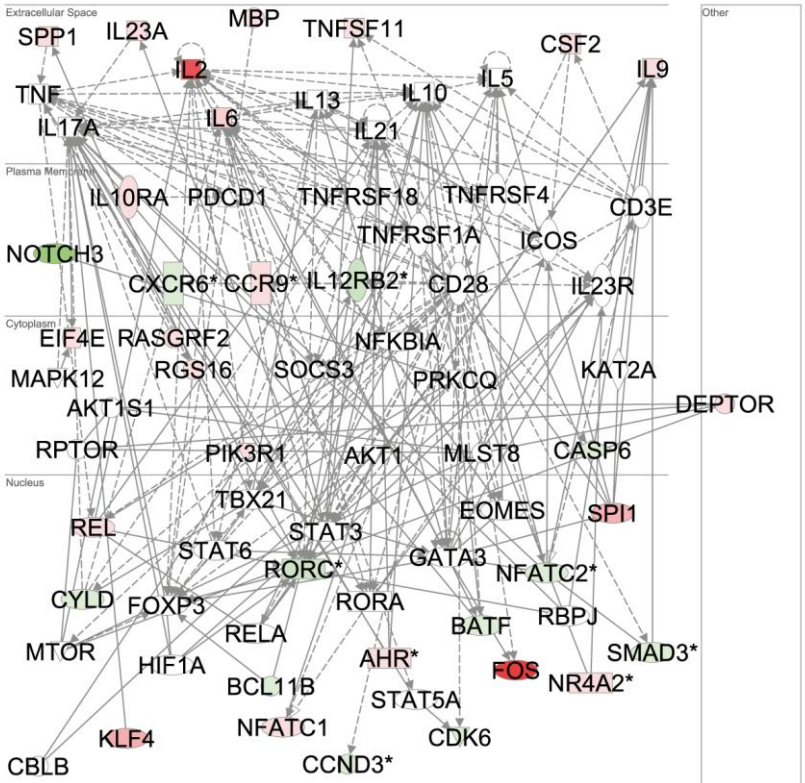

B Network 2

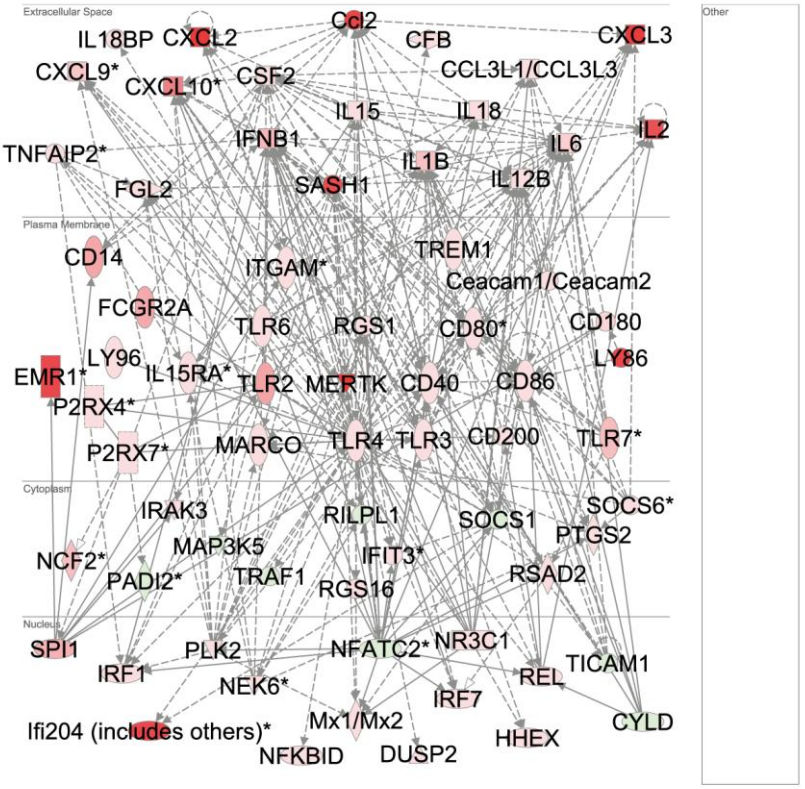

highly upregulated in Th17eae
highly downregulated in Th17eae
little upregulated in Th17eae
little downregulated in Th17eae
not differentially expressed in dataset

C Prominent canonical pathway
LXR/RXR Receptor Signaling

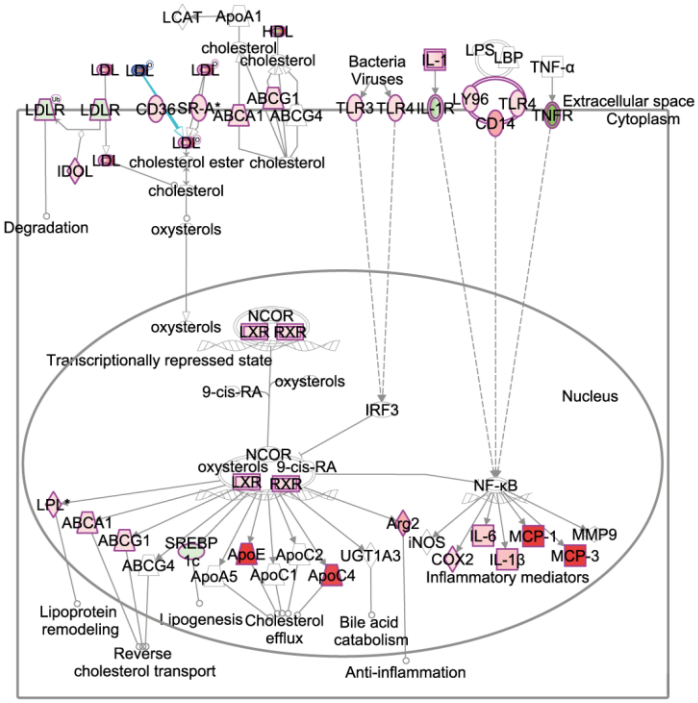

D Network 2 canonical pathway overlay
Communication between Innate & Adaptive Immune Cells

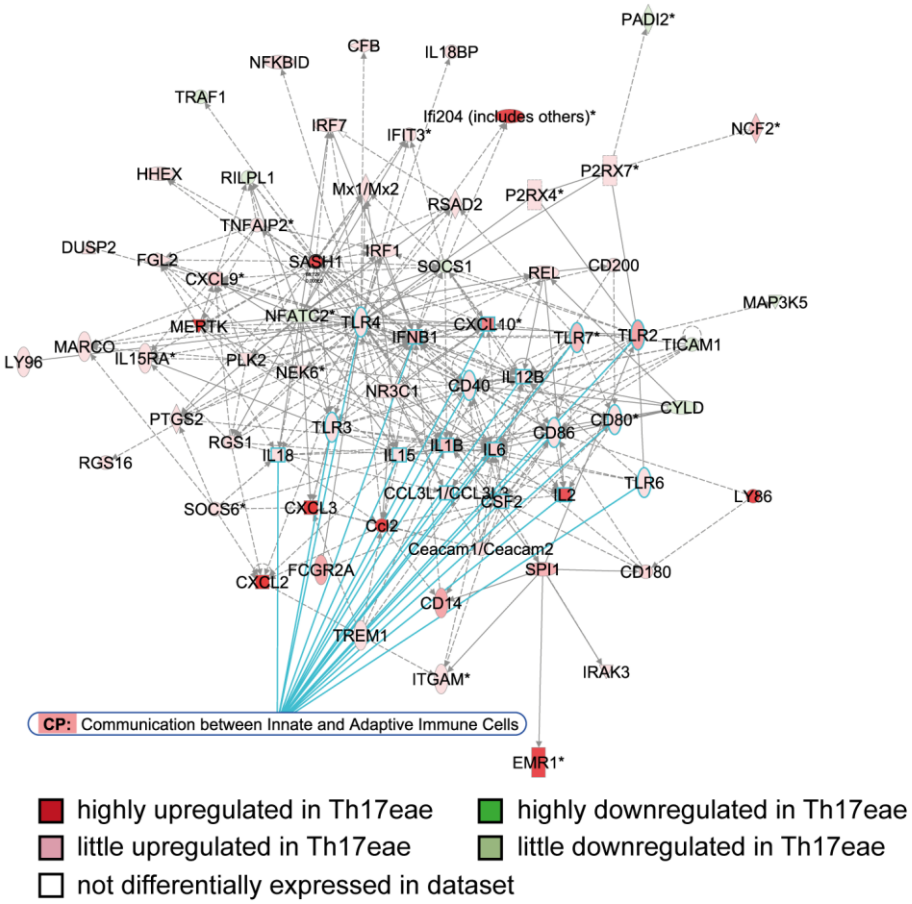

Figure 27: Representation of prominent signaling networks and canonical pathways associated with the transition of Th17iv cells to Th17eae.
(A) Network 1 was associated with changes in cellular development and hematological system development and function. Major transcription factors associated with these functions and highly upregulated in the dataset were Fos, Spi1, Klf4, and Nfatc1. (B) Network 2 was associated with cellular function and maintenance, cellular movement and trafficking. Therefore, many chemokines and cytokines and toll-like receptors (TLR) were increasingly expressed. Major transcription factors regulating these functions were Spi1, Hhex, Nr3c1, Irf1, Irf7, Rel, and Plk2. (C) LXR/RXR Receptor signaling was one of the most prominent canonical pathways that was activated in the transition from Th17iv cells to Th17eae cells, showing increasing metabolic activity to execute effector function. (D) Many genes, including chemokines Cxcl10, Ccl2, cytokines Il18, Il2, Il12b, Il15, Il1b, Il6, co-stimulatory molecules Cd40, Cd80, Cd86, and Tlr2, Tlr3, Tlr4, Tlr7 assist in the communication between cells of the innate and adaptive immune system as indicated by blue arrows.

3.2.1.3 Validation of transcription factor expression by qRT-PCR

A focus was set on the evaluation of key transcription factors (TFs) that were highly upregulated in the Th17 cell transition process and associated with the prominent signaling networks. Next to the TF *Fos*, *Klf4*, *Nfatc1*, and *Spi1*, *Cebpa* (encoding CCAAT/enhancer-binding protein alpha, C/EBPα), was the most upregulated transcription factor in Th17eae cells compared to Th17iv (Figure 28).

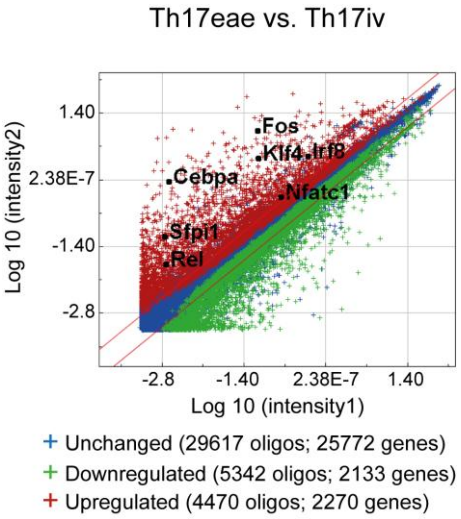

Figure 28: Transcriptional changes in the transition of Th17iv to Th17eae cells.
A total of 30,175 genes were spotted on the microarray, of which 2,133 genes were significantly downregulated (signal intensity p-value >0.01) and 2,270 upregulated as indicated by the two red lines. Fos, Cebpa, Klf4, Irf8, Spi1, and Rel belonged to the most upregulated transcription factors in this transition process. Nfatc1 was not highly upregulated but involved in signaling of prominent networks.

These transcription factors are generally implicated in T cell development, differentiation and proliferation. For the validation of microarray expression values with qRT-PCR, three independent adoptive transfer EAE experiments were

performed and RNA isolated from naïve T cells, *in vitro* primed Th17 cells, and CD4+ T cells re-isolated from the CNS of mice at the peak of disease (Figure 29). *Cebpa*, *Fos*, *Klf4*, *Nfatc1*, and *Spi1* were low expressed in Th17iv cells and highly upregulated in Th17eae cells in the microarray dataset, which was similarly observed in the qRT-PCR analysis, although the upregulation of *Nfatc1* did not reach statistical significance (One-Way ANOVA, post-hoc Tukey corrected for multiple comparisons). Expression levels of *Cebpa* and *Spi1* were similarly low in naïve T cells compared to Th17iv cells in both, the microarray and qRT-PCR analysis, indicating neither a major role in the maintenance of a naïve nor the Th17 cell status. Expression of *Fos*, *Klf4*, and *Nfatc1* was not significantly altered in naïve T cells compared to Th17iv although with a tendency towards higher expression levels. This tendency reached statistical significance for *Fos* and *Klf4* in the qRT-PCR analysis.

The results demonstrated that the expression of transcription factors *Cebpa*, *Fos*, *Klf4*, *Nfatc1*, and *Spi1* was not necessary for Th17 lineage commitment, but that these factors were involved in the transition process of Th17iv cells to Th7eae. *Fos*, *Klf4*, and possibly *Nfatc1* were also involved in naïve T cell associated molecular signaling processes. The regulation of these factors proposes a contribution to encephalitogenicity and/or plasticity of Th17 cells in EAE.

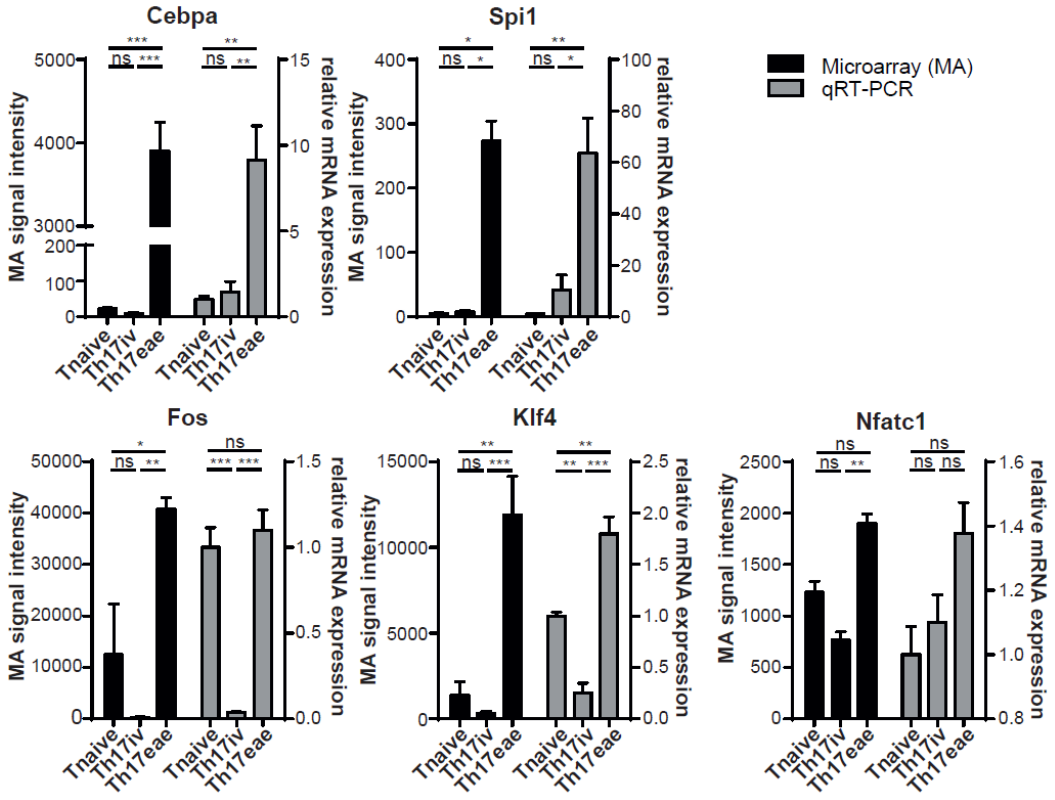

Figure 29: Validation of microarray TF expression via qRT-PCR.
*Cebpa and Spi1 were rather low expressed in naïve T cells and differentiated Th17 cells, but highly upregulated in Th17eae cells. This was validated in independent qRT-PCR experiments. The expression level of Fos varied in the Tnaive microarray samples, but was highly expressed in qRT-PCR samples, downregulated in Th17 cells and again high expressed in Th17eae cells. Expression of Nfatc1 in Tnaive samples decreased in Th17 cells and highly increased in Th17eae cells in the microarray samples, while a constant increase in its expression was observed in the qRT-PCR validation. The highly increased expression of all of these TFs hinted at a contribution in T cell plasticity and encephalitogenicity. Values are represented as mean ± SEM. Significance was determined using One-Way ANOVA, with post-hoc Tukey correction for multiple comparisons. P-values: * < 0.05; ** < 0.01; *** < 0.001; **** < 0.0001.*

3.2.1.4 Evaluation of the contribution of human MS susceptibility genes in the pathology of EAE

Throughout the last years, large multicenter genome-wide association studies (GWAS) evaluated the association of single nucleotide polymorphisms (SNPs) with different diseases including MS. In the most recent multiple sclerosis GWAS, 57 SNPs were reported to be associated with MS (109). These 57 SNPs were mapped to 55 human genes based on proximity (+/- 500 kb) using the ensembl database (release 75) (Table 2). 53 of the 55 genes were represented on the

murine whole genome microarray used in this study. The extent to which each SNP influences gene transcriptional activity and contributes to the disease is currently unknown.

Sawcer et al. 2011	Ensembl Database; release 75		NCBI Gene Database
SNP	**Human gene**	**Description**	**Murine Homolog**
rs12368653	AGAP2	ArfGAP with GTPase domain, ankyrin repeat and PH domain 2	Agap2
rs11154801	AHI1	Abelson helper integration site 1	Ahi1
rs12212193	BACH2	BTB and CNC homology 1, basic leucine zipper transcription factor 2	Bach2
rs2300603	BATF	basic leucine zipper transcription factor, ATF-like	Batf
rs7522462	C1orf106	chromosome 1 open reading frame 106	5730559C18Rik
rs2028597	CBLB	Cas-Br-M (murine) ecotropic retroviral transforming sequence b	Cblb
rs1335532	CD58	CD58 molecule	Cd48
rs650258	CD6	CD6 molecule	Cd6
rs9282641	CD86	CD86 molecule	Cd86
rs8112449	CDC37	cell division cycle 37 homolog (S. cerevisiae)	Cdc37
rs7200786	CLEC16A	C-type lectin domain family 16, member A	Clec16a
rs10466829	CLECL1	C-type lectin-like 1	---
rs669607	CMC1	COX assembly mitochondrial protein homolog (S. cerevisiae)	Cmc1
rs630923	CXCR5	chemokine (C-X-C motif) receptor 5	Cxcr5
rs2248359	CYP24A1	cytochrome P450, family 24, subfamily A, polypeptide 1	Cyp24a1
rs2303759	DKKL1	dickkopf-like 1 (soggy)	Dkkl1
rs11810217	EVI5	ecotropic viral integration site 5	Evi5
rs2119704	GPR65	G protein-coupled receptor 65	Gpr65
rs7923837	HHEX	hematopoietically expressed homeobox	Hhex
rs2243123	IL12A	interleukin 12a	Il12a
rs2546890	IL12B	interleukin 12b	Il12b
rs17066096	IL22RA2	interleukin 22 receptor, alpha 2	Il22ra2
rs3118470	IL2RA	interleukin 2 receptor, alpha	Il2ra
rs6897932	IL7R	interleukin 7 receptor	Il7r
rs13333054	IRF8	interferon regulatory factor 8	Irf8
rs7238078	MALT1	mucosa associated lymphoid tissue lymphoma translocation gene 1	Malt1
rs228614	MANBA	mannosidase, beta A, lysosomal	Manba
rs2283792	MAPK1	mitogen-activated protein kinase 1	Mapk1
rs17174870	MERTK	c-mer proto-oncogene tyrosine kinase	Mertk
rs874628	MPV17L2	MPV17 mitochondrial membrane protein-like 2	Mpv17l2
rs4410871	MYC	v-myc myelocytomatosis viral oncogene homolog (avian)	Myc
rs2425752	NCOA5	nuclear receptor coactivator 5	Ncoa5
rs11129295	no gene		
rs2019960	no gene		
rs140522	ODF3B	outer dense fiber of sperm tails 3B	Odf3b
rs13192841	OLIG3	oligodendrocyte transcription factor 3	Olig3
rs949143	PITPNM2	phosphatidylinositol transfer protein, membrane-associated 2	Pitpnm2
rs1520333	PKIA	protein kinase (cAMP-dependent) inhibitor alpha	Pkia

rs7595037	PLEK	pleckstrin	Plek
rs4613763	PTGER4	prostaglandin E receptor 4 (subtype EP4)	Ptger4
rs802734	PTPRK	protein tyrosine phosphatase, receptor type, K	Ptprk
rs1323292	RGS1	regulator of G-protein signaling 1	Rgs1
rs180515	RPS6KB1	ribosomal protein S6 kinase, 70kDa, polypeptide 1	Rps6kb1
rs11581062	SLC30A7	solute carrier family 30 (zinc transporter), member 7	Slc30a7
rs2744148	SOX8	SRY (sex determining region Y)-box 8	Sox8
rs10201872	SP140	SP140 nuclear body protein	Sp140
rs9891119	STAT3	signal transducer and activator of transcription 3	Stat3
rs1738074	TAGAP	T-cell activation RhoGTPase activating protein	Tagap
rs12466022	THADA	thyroid adenoma associated	Thada
rs2293370	TIMMDC1	translocase of inner mitochondrial membrane domain containing 1	Timmdc1
rs1800693	TNFRSF1A	TNF receptor superfamily, member 1A	Tnfrsf1a
rs1077667	TNFSF14	TNF (ligand) superfamily, member 14	Tnfsf14
rs4648356	TTC34	tetratricopeptide repeat domain 34	Ttc34
rs6062314	ZBTB46	zinc finger and BTB domain containing 46	Zbtb46
rs4902647	ZFP36L1	zinc finger protein 36, C3H type-like 1	Zfp36l1
rs1250550	ZMIZ1	zinc finger, MIZ-type containing 1	Zmiz1
rs354033	ZNF777	zinc finger protein 777	Zfp777

Table 2: Mapping of genes to 57 MS susceptibility associated SNPs.
57 SNPs were identified to be associated with increased MS risk in a large genome-wide association study in 2011 (109)*. These SNPs were mapped to human genes based on proximity (± 500 kb) according to the ensembl database (www.ensembl.org). The murine homologs were identified by NCBI gene database search (www.ncbi.nlm.nih.gov). The human gene annotation was kindly provided by Christina M. Lill.*

To investigate, if MS susceptibility genes were regulated at different time points in the T cell-based EAE these genes were compared to the candidate genes (fold change > 2; signal intensity p-value < 0.01) in the comparisons of Th17iv versus Th17eae, as well as Th17eae and CD4eae, each versus naïve T cells (Figure 30). The overall goal of this approach was to identify factors that play a role in the regulation of inflammation, T cell plasticity, and encephalitogenicity.

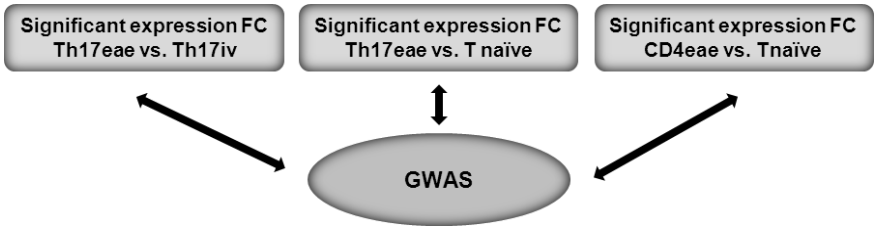

Figure 30: Comparison of MS susceptibility genes with genes involved in the course of EAE.
53 murine homologs to the MS associated genes were represented on the microarray chip. 15 genes were commonly differentially expressed in the comparisons of Th17eae versus Th17iv, Th17eae versus Tnaive, as well as CD4eae versus Tnaive. These genes were possibly involved in inflammation, T cell plasticity and encephalitogenicity.

15/53 MS susceptibility genes (28.3%), *Bach2*, *Cd86*, *Evi5*, *Hhex*, *Il12b*, *Il2ra*, *Il22ra1*, *Irf8*, *Mertk*, *Odf3b*, *Plek*, *Ptger4*, *Rgs1*, *Slc30a7*, and *Thada* were found to be differentially expressed in all of these three comparisons. *Il12b* and *Il22ra1* were excluded from further analysis due to microarray signal intensity values at background level.

To validate microarray expression levels of 13 overlapping candidate genes in naïve T cells (Tnaive), *in vitro* primed Th17 cells (Th17iv), and CD4+ T cells re-isolated from the CNS of adoptive transfer EAE mice (Th17eae), qRT-PCR analysis of three independent adoptive transfer EAE experiments were performed (Figure 31). Various expression patterns were observed. The transcriptional repressor *Bach2,* the zinc transporter of the *solute carrier family 30* (*Slc30a7*) (encoding ZnT7) and *thyroid adenoma associated gene* (*Thada*) were downregulated in Th17 cells and continued to be expressed at low levels in Th17eae cells. *Il2ra* and *Outer dense fiber of sperm tails 3B* (*Odf3b*) were strongly expressed in Th17 cells and downregulated to (*Il2ra*) or below (*Odf3b*) naïve T-cell expression levels during EAE. The *modulator of G-protein coupled receptors* (*Rgs1*) was strongly upregulated in Th17 cells isolated from the CNS of diseased mice (Th17eae), similar to the *tyrosine kinase Mer* (*Mertk*), *Plek* (encoding Plekstrin), and the transcription factor *Irf8* (Figure 31A). Discrepancies between the microarray expression pattern and the qRT-PCR validation were observed for *Cd86*, *Ecotropic viral integration site 5* (*Evi5*), *Hhex*, and *Prostaglandin E receptor 4* (*Ptger4*), in which the expected upregulation was not detected in the Th17eae qRT-PCR samples (Figure 31B).

Taken together, 9 MS susceptibility genes with implications in the modulation of a pro-inflammatory microenvironment, encephalitogenicity and T cell plasticity in the course of EAE could be identified and their expression patterns validated.

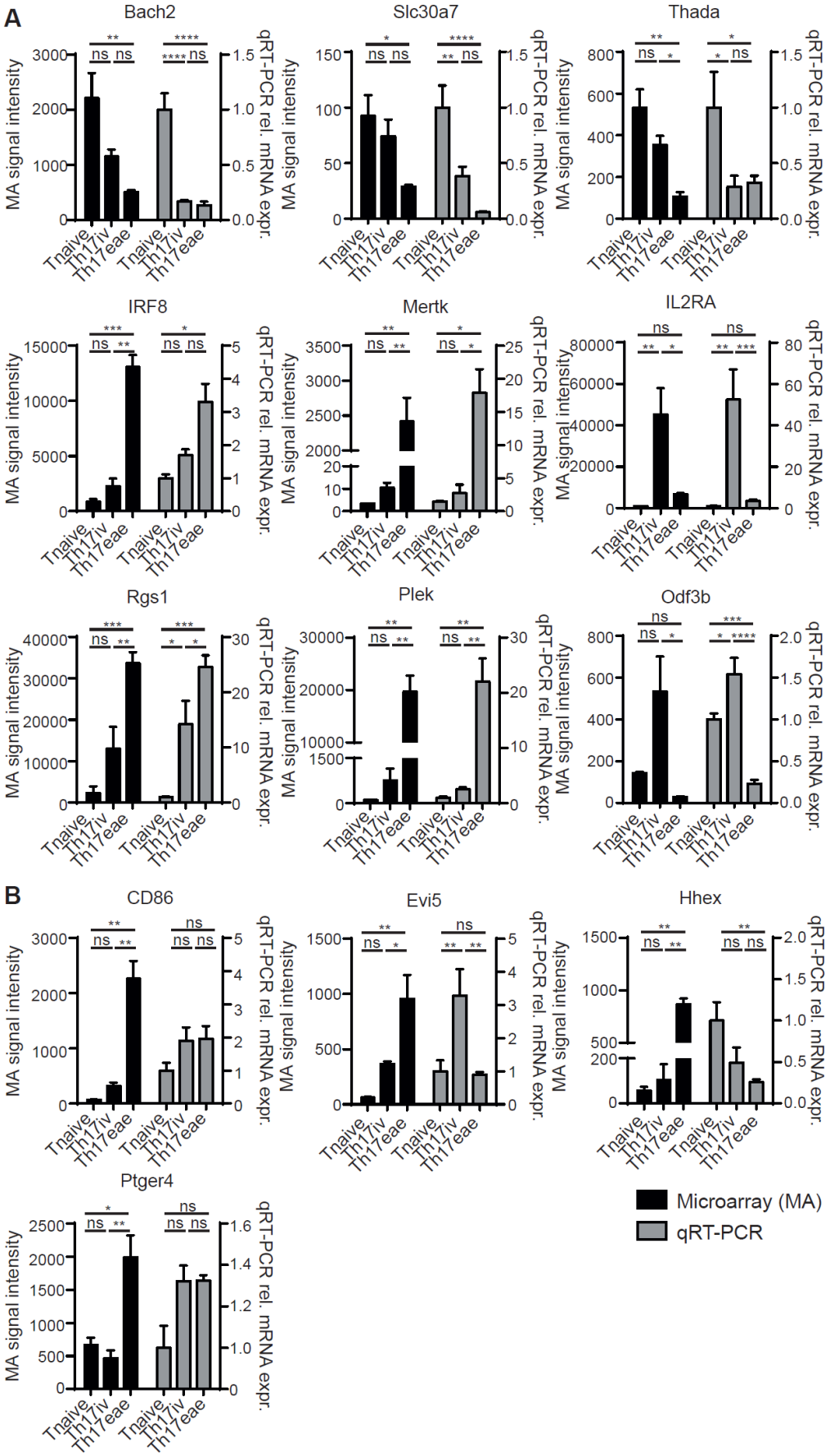
A
Bach2
Slc30a7
Thada
IRF8
Mertk
IL2RA
Rgs1
Plek
Odf3b
B
CD86
Evi5
Hhex
Ptger4
MA signal intensity
qRT-PCR rel. mRNA expr.
Tnaive
Th17iv
Th17eae
Microarray (MA)
qRT-PCR

Figure 31: Comparison of expression of candidate genes in the microarray and qRT-PCR analysis.
*(A) 9 MS susceptibility genes were identified and their expressional tendencies validated in independent qRT-PCR experiments. Various expression patterns were observed. All of these genes were probably involved in the pathogenicity and encephalitogenicity throughout T cell-based EAE. (B) 4 out of 13 tested MS susceptibility candidate genes were not validated in independent qRT-PCR experiments. Values are represented as mean ± SEM. Significance was evaluated using One-Way ANOVA, with post-hoc Tukey correction for multiple comparisons. P-values: * < 0.05; ** < 0.01; *** < 0.001; **** < 0.0001.*

3.2.2 Analysis of the impact of NFATc1 in CD4+ T cells in the context of EAE

In lymphocytes, three out of four calcium dependent NFAT proteins, NFATc1-c3, are expressed and activated upon T cell receptor stimulation through high influx in Ca^{2+}, resulting in cytokine expression and T cell activation and differentiation. Although these proteins are highly homologous, differences in their effector function were observed by the use of knockout mice. Yoshida et al. demonstrated that homozygous *Nfatc1*$^{-/-}$ embryonic stem cells showed decreased proliferation capacities upon immune receptor stimulation with various stimulating compounds including anti-CD3/anti-CD28 and Concanavalin A (ConA). Further, this group detected impaired Th2 (IL-4), but not Th1 (IFN-γ) cytokine production. Development of γδT cells and natural killer (NK) cells was comparable to wild-type cells (239). The effect of *Nfatc1* deletion though has not been investigated on the recently identified Th17 cells or Tregs. First hints that NFATc1 might not be necessary for Tregs, Th9 and Th17 cells come from a recent study showing that *Nfatc1* expression highly increased upon immune receptor stimulation in B, Th1, and Th2 cells, but only weakly in T regulatory, Th9, and Th17 cells (240). However, the effect of deletion of this transcription factor in Th17 also in the context of EAE is currently unknown. The microarray data analyzed herein nevertheless hinted at a role of NFATc1 in Th17 effector function if not plasticity due to its upregulation in Th17eae cells compared to Th17iv cells.

As the knockout of *Nfatc1* in the whole animal is embryonically lethal, *CD4-Cre.Nfatc1*$^{fl/fl}$ mice were used, with the specific knockout of *Nfatc1* in CD4+ T cells upon Cre recombinase activation.

3.2.2.1 Impact of *Nfatc1*-deficiency on the course of EAE

To investigate if the knockout of the transcription factor NFATc1 has an impact on the potential of CD4+ Th17 cells to induce EAE, *Cd4-Cre.Nfatc1*$^{fl/fl}$ mice were immunized with MOG_{35-55} peptide. Littermates with inactive Cre-recombinase were used as control. Littermates with active Cre-recombinase but only one allele of floxed *Nfatc1* (heterozygous littermates) were inspected for possible intermediate phenotypes. After immunization, animals were observed daily for the development of clinical symptoms over a period of 30 days. Control mice with inactive Cre-recombinase (*Cd4-Cre- Nfatc1*$^{fl/fl}$, ctl) started to develop symptoms of disease 12 days after immunization which resulted in plegia of tail and hind limps and defects in rightening reflex (score 3) between day 17 and 21 after immunization and a determination of experiment for this experimental group. Mice with active Cre-recombinase and partial knockout of *Nfatc1* in CD4+ T cells (*Cd4-Cre+ Nfatc1*$^{fl/wt}$, het) experienced an equal disease onset, but slightly less severe accumulation of disabilities that became stable around day 20 after immunization and led to a remission after day 26. Complete knockout of *Nfatc1* in CD4+ T cells (*Cd4-Cre+ Nfatc1*$^{fl/fl}$, k.o.) did not lead to clinical signs of disease over the test period of 30 days for most animals while some (3/15) showed slight tail paresis and disabilities in rightening reflex (Figure 32).

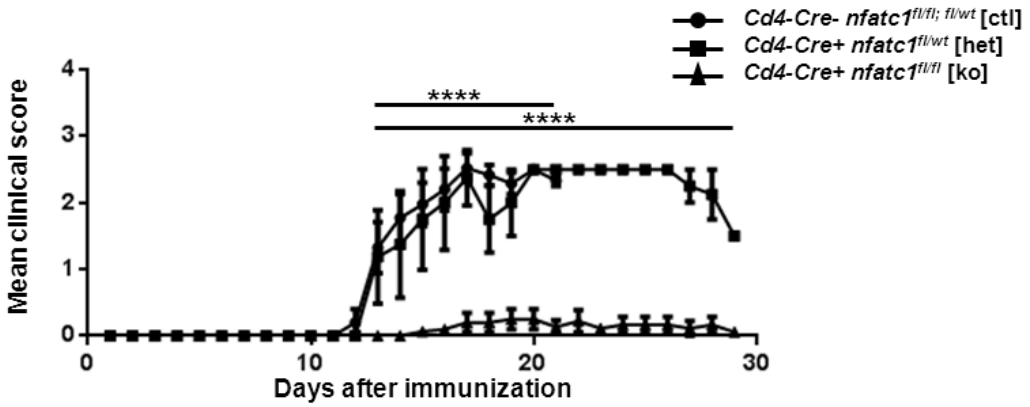

Figure 32: Disease course of Cd4-Cre.Nfatc1$^{fl/fl}$ mice after active immunization with MOG_{35-55}.
Control littermates with inactive Cre recombinase developed disease on day 12 after immunization and rapidly accumulated disabilities, resulting in termination of experiment on day 21. A full knockout of Nfatc1 in CD4+ T cells hampered these cells to induce EAE while a partial knockout resulted in a slightly milder course and stable disability with start of remission phase after day 26. Control mice: n=10; Heterozygous mice: n=4; Nfatc1 knockout mice: n=15. Data were pooled from two independent experiments and shown as

*Mean±SEM. Statistical significance was determined using two way ANOVA test, Bonferroni corrected; p-values <0.05 were considered significant; **** P < 0.0001.*

To investigate if the clinical sign-free course of *CD4-Cre+.Nfatc1*$^{fl/fl}$ mice resulted from defects in T cell differentiation or transmigration into the CNS, lymphocytes were isolated from the CNS of control, heterozygous, and *Nfatc1*-deficient mice at the peak of disease of control mice (Figure 33). Lymphocytes could be isolated from the CNS of all groups, although numbers were significantly reduced in mice with *Nfatc1*-deficient CD4+ T cells. In control mice, about 91% of isolated cells were CD45+ cells (nucleated cells), compared to 83% of *Nfatc1*-heterozygous mice and 67% of *Nfatc1*-deficient mice. These CD45+ cell populations were analyzed according to subpopulations which included CD4+ Th cells, CD8+ cytotoxic T cells and FoxP3+ Treg cells. *Nfatc1*-deficient CD45+ cells were composed of significantly less CD4+ T cells, which comprised only 35% of CD45+ T cells compared to 51% in heterozygous and 59% in control cells. The amounts of CD8+ T cells (0.8% k.o., 0.5% het., 0.6% ctl.) and Tregs (4.5% k.o., 11.6% het., 9.4% ctl.) were not significantly altered (Figure 33A).

Cells were further stained intracellularly with specific antibodies to determine typical Th1 or Th17 cytokine expression. As shown in Figure 33B, 24.6% of CD4+ T cells from control mice expressed IL-17A, compared to 12.1% and 2.2% of heterozygous and knockout mice. 13.6% of CD4+ T cells from control mice further were single IFN-γ producers, while this amount was decreased in heterozygous (3.2%) and *Nfatc1*-deficient cells (2.2%). Low amounts of IL-17A+IFN-γ+ double producing cells could be detected in CD4+ control (3.1%) and *Nfatc1*-heterozygous cells (0.6%) respectively, but not in *Nfatc1*-deficient cells.

Taken together, activated lymphocytes could be isolated from the CNS of all immunized mice, while *Nfatc1*-deficient cells were restricted in their cytokine production and induction of EAE. *Nfatc1*-heterozygous animals showed an intermediate phenotype.

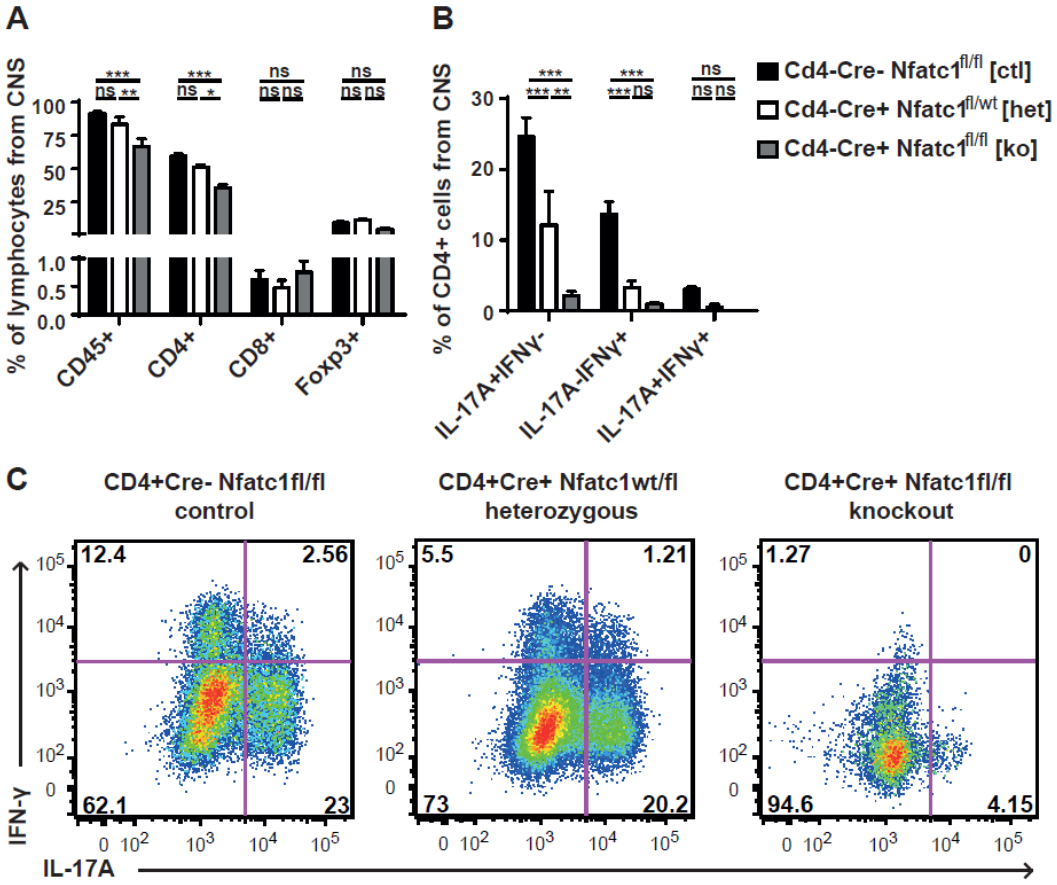

Figure 33: Percentage of lymphocytes isolated from the CNS of actively immunized mice and the cytokine profile of CD4+ T cells.
*(A) CD45+ cells could be isolated from the CNS of diseased control and Nfatc1-heterozygous mice as well as from healthy Nfatc1-deficient mice although the amount of CD45+ cells in Nfatc1-deficient mice was reduced. Among the CD45+ lymphocyte population fewer CD4+ T cells but equal numbers of CD8+ and FoxP3+ cells were detected in Nfatc1-deficient lymphocytes compared to the controls. (B+C) The amount of Th17 and Th1 phenotypic cytokines was significantly reduced in Nfatc1-heterozygous and even more in Nfatc1-deficient CD4+ T cells. (C) Depicted are representative cytokine profiles of CD45+CD4+ T cells of control, heterozygous and knockout mice. Data are shown as Means±SEM from 4 animals, representing one out of three experiments. Statistical significance was determined using one-way ANOVA, Bonferroni-corrected. P-values < 0.05 were regarded as significant: * P < 0.001; ** P < 0.0005; *** P < 0.0001.*

3.2.2.2 Adoptive transfer EAE of *Nfatc1*-deficient and control cells

To investigate effector function of *Nfatc1*-deficient CD4+ T cells without relying on *in situ* activation in the same animal, classical adoptive transfer EAE model was performed. Therefore, *CD4-Cre-.Nfatc1*$^{fl/fl;\ fl/wt}$ and *CD4-Cre+.Nfatc1*$^{fl/fl}$ mice were immunized with MOG_{35-55} peptide and incubated for 10 days. Shortly before expected disease onset, axillary and inguinal lymph nodes were isolated and the

lymph node cell mix (T and B cells, APCs) incubated with high amounts of MOG_{35-55} for *in vitro* stimulation and expansion of MOG-specific T cells. After 3 days, cells were polyclonally stimulated with anti-CD3/anti-CD28 (2.5 µg/ml; 3 µg/ml) to determine their cytokine expression potential. While ~6.2% and ~1.3% of control cells expressed IL-17 and IFN-γ respectively, these numbers were reduced to ~2.4% of IL-17 and 0.7% of IFN-γ producers in *Nfatc1*-deficient CD4+ T cells (data not shown).

350,000 T cells, mixed with other survivor cells from the lymph node culture, were adoptively transferred into immunodeficient *Rag1*$^{-/-}$ mice and monitored daily for development of disease symptoms. As shown in Figure 34, *Rag1*$^{-/-}$ mice that had been transferred with littermate control *Cd4-Cre-.Nfatc1*$^{fl/fl;\ fl/wt}$ cells (n=5) experienced disease onset on day 17/18 followed by a progressing course. The final disease score 2 with maximal tail plegia and defects in the rightening reflex was rather mild, but could be explained by the low number of transferred T cells. Mice that were injected with *Nfatc1*-deficient CD4+ T cells did not develop disease at all (n=3). These preliminary results suggest defects of T cell effector function upon *Nfatc1* deletion.

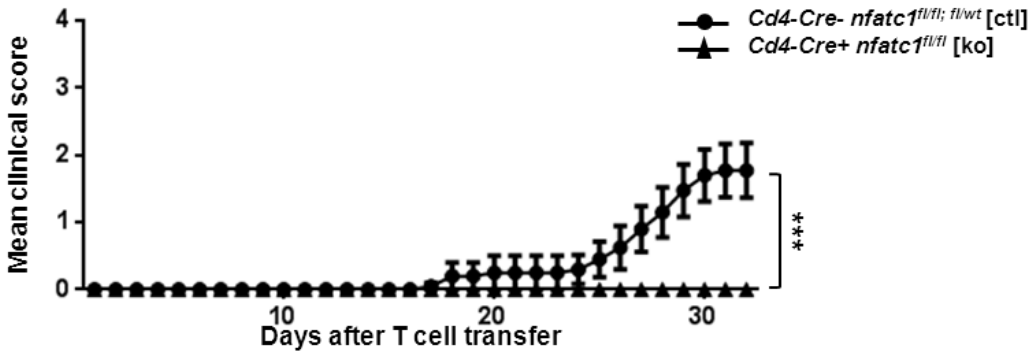

Figure 34: Disease course of Rag1$^{-/-}$ mice with adoptively transferred CD4+ T cells. *Cd4-Cre-.Nfatc1*$^{fl/fl;\ fl/wt}$ *and Cd4-Cre+.Nfatc1*$^{fl/fl}$ *mice were immunized with* MOG_{35-55} *and left for 10 days before cells from lymphnodes and spleens were isolated. The cells were stimulated in vitro with high amounts of* MOG_{35-55} *for three days before being transferred into Rag-1*$^{-/-}$ *mice (control: n=5; Nfatc1-ko: n=3). Preliminary data suggested that Nfatc1-deficient cells were not capable of inducing EAE symptoms.*

To clarify if the progression of *Rag1*$^{-/-}$ mice without clinical signs of disease was due to inefficient transmigration of *Nfatc1*-deficient cells into the CNS or a defect in their effector function, lymphocytes were again isolated from the CNS of

adoptively transferred *Rag1*$^{-/-}$ mice 32 days after T cell transfer. Lymphocytes could be isolated from all animals, indicating that also *Nfatc1*-deficient cells were activated and capable of migrating into the CNS. Nevertheless, the amount of *Nfatc1*-deficient cells re-isolated from the CNS was significantly lower compared to control cells (Figure 35A). The low amount of total *Nfatc1*-deficient CD4+ T cells made it impossible to analyze the number of IL-17+, IFN-γ+, and TNF-α+ cells. A defect in the homing to the spleen was not detected as comparable amounts of CD45+, CD4+, CD8+, and FoxP3+ lymphocytes could be isolated form the spleen (Figure 35B).

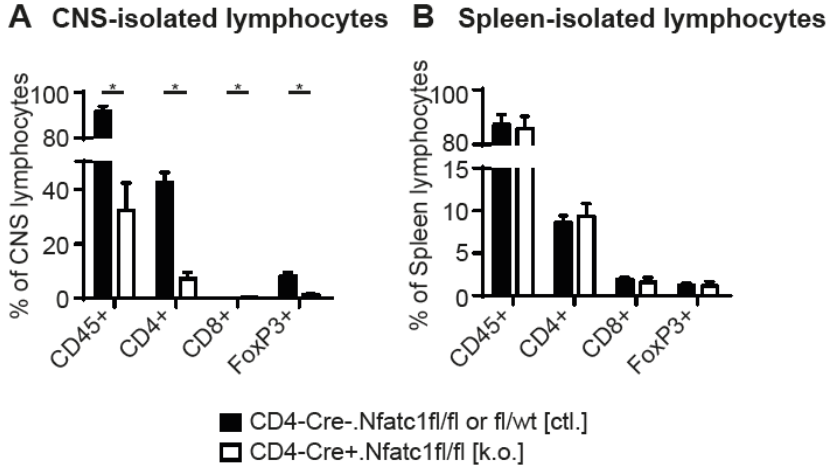

Figure 35: Lymphocytes isolated from the CNS of adoptive transfer EAE mice.
(A) Only very few cells could be re-isolated from the CNS of mice that had been transferred with Nfatc1-deficient cells which were comprised of only 32% CD45+ compared to 92% for control cells. Of the CD45+ population, only 7% were CD4+ compared to 42% of control CD45+CD4+ cells, additional to almost undetectable amounts of CD8+ T cells and Tregs. (B) Similar amounts of transferred Nfatc1-deficient and control cells recapitulated the spleens of Rag-1-/- mice.

3.2.2.3 Impact of *Nfatc1*-deficiency on T cell differentiation

In order to determine the effect of *Nfatc1*-deficiency on the activation and proliferation capacities of *in vitro* stimulated T cells, naïve CD4+ T cells were isolated from spleen and lymph nodes of *CD4-Cre.Nfatc1*$^{fl/fl}$ and littermate control mice (*Cre*-negative) and labeled with CFSE. This marker is divided in half with each symmetrical cell division, allowing the detection of a certain number of cell divisions by decreasing CFSE staining intensity using flow cytometry. The labeled cells were stimulated in an antigen-unspecific manner with plate-bound anti-

CD3/anti-CD28 antibodies (3 µg/ml; 2.5 µg/ml) and incubated for 3 days before being analyzed by flow cytometry. Stimulation with anti-CD3/anti-CD28 allows the formation of a signaling synapse, mimicking the binding of antigen presenting cells to T cells, providing a strong TCR activation signal. Five populations with distinct CFSE intensities were observed for both, control *Cd4+Cre-.Nfatc1*$^{fl/fl}$ and knockout *Cd4+Cre+Nfatc1*$^{fl/fl}$ after stimulation, indicating a total of four cell division cycles, while most cells underwent 2 – 3 cell divisions (Figure 36A+B). Thus, no proliferation differences between *Nfatc1*-deficient and control cells could be observed.

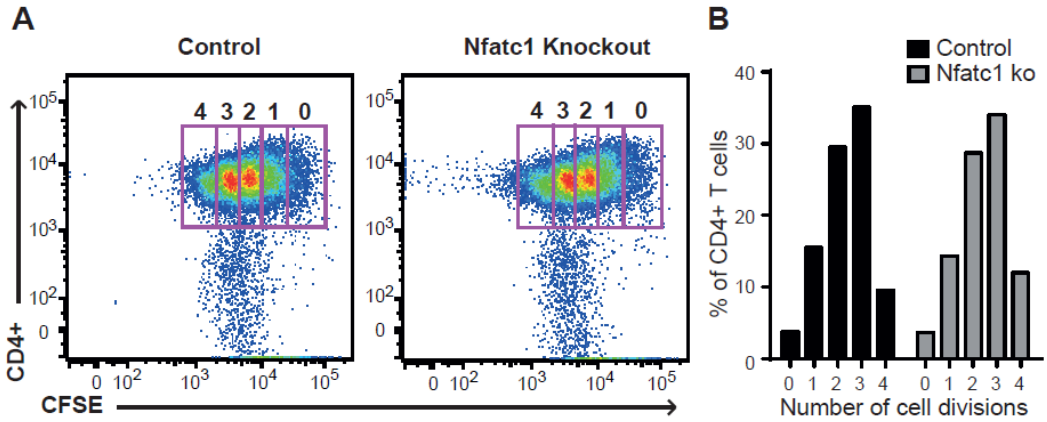

Figure 36: CFSE proliferation assay of Nfatc1-deficient and control Th17 cells.
Nfatc1-deficient and control cells were labeled with CFSE in similar efficiencies and stimulated with anti-CD3/anti-CD28 for 3 days. (A) Proliferation was characterized by decreasing CFSE intensity as measured by flow cytometry. The starting population was gate "division 0"; cells that proliferated 1 to 4 times were found in respective gates 1-4. (B) Control Cre- littermates and Cre+ Nfatc1$^{fl/fl}$ *cells proliferated similarly when stimulated with anti-CD3/anti-CD28,*

To investigate possible disturbances in Th17 cell differentiation, naïve CD4+ T cells were isolated from mice with *Nfatc1*-deficient CD4+T cells (*Cd4-Cre.Nfatc1*$^{fl/fl}$) and control (*Cre*-negative) littermates. The cells were incubated with plate-bound anti-CD3 (4 µg/ml) in medium supplemented with TGF-β (1 ng/ml), IL-6 (5 ng/ml), anti-IL-4 (10 µg/ml), and anti-IFN-γ (10µg/ml) for Th17 differentiation for three days, before mRNA was extracted. QRT-PCR analysis of key Th17 lineage factors revealed that TGF-β and IL-6 induced expression of the transcription factors *Ahr* and *Stat3* respectively, which was slightly increased in *Nfatc1*$^{-/-}$ cells. Both transcription factors are important for Th17 and iTreg differentiation and iTreg stabilization. Th17 lineage cytokines *Gmcsf*, *Il17a*, Il17f,

and *Il22* as well as the cytokine receptors *Il1r1* and *Il23r* were expressed at lower levels compared to control cells, which was statistically not significant. The results show a defect in proper Th17 lineage differentiation due to the observed decreased Th17 cytokine levels in *Nfatc1*-deficient cells (Figure 37) (241).

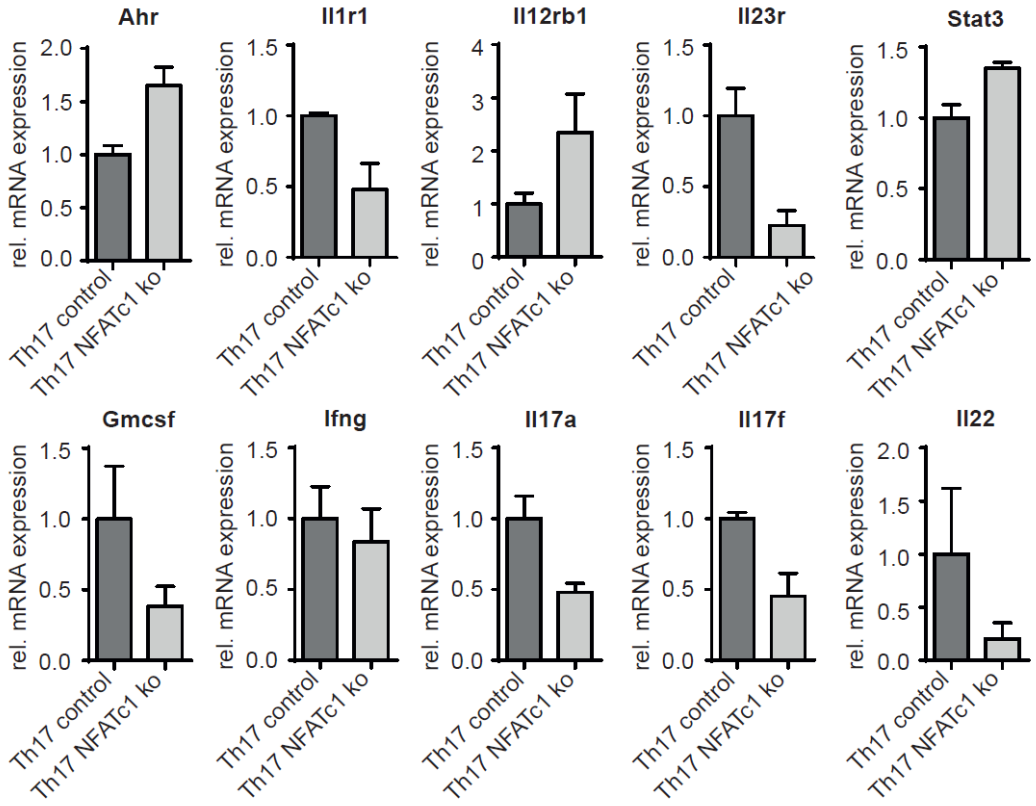

Figure 37: qRT-PCR analysis of Th17 lineage factors after in vitro differentiation. *Naïve CD4+ T cells were isolated from spleen and lymph nodes of CD4-Cre+.Nfatc1$^{fl/fl}$ and littermate control mice and differentiated into Th17 lineage cells using TGF-β, IL-6, anti-IL-4, and anti-IFN-γ. After 3 days, the mRNA was isolated and qRT-PCR analysis performed for Th17 lineage genes. Nfatc1-deficient cells expressed slightly lower levels of all tested cytokines (Gmcsf, Ifng, Il17a, Il17f, Il22) as well as Il1r1, Il23r, but slightly increased levels of the transcription factors Ahr and Stat3. None of the tendencies was statistically significant.*

4 Discussion

For a long time, the CNS was regarded as an immune privileged organ that is shielded from the entry of harmful agents by the blood-brain barrier. Recent investigations showed that the immune system can actively interact with the cells of the CNS: In case of infection/pathogen entry or malignancy, CNS-resident microglia recruit macrophages and lymphocytes to the CNS and activated T and B lymphocytes can cross the BBB (128,242) in order to specifically target and eliminate malignant transformed cells and harmful pathogens to prevent organ damage. While in the context of glioblastoma multiforme immune reactions fail to eradicate the tumor cells and are exploited for the formation of a tumor-protecting microenvironment, exuberant inflammatory responses against self-antigens lead to the destruction of the central nervous system of multiple sclerosis patients. The goal of this thesis was to investigate defective interactions between T lymphocytes and CNS-resident cells with a focus on molecular mechanisms in the context of glioblastoma multiforme and multiple sclerosis.

4.1 Glioblastoma multiforme

4.1.1 GICs resist anti-cancer treatments

Radiotherapy of up to 60 Gy, given in daily fractions of 2 Gy on five days per week over a period of six weeks, belongs to the standard therapy of GBM and lead to a median overall survival of 12 months (1). Various *in vitro* experiments showed that ionizing radiation enhances expression of MHC class I, suggesting to combine radiotherapy with immunotherapy (229,243). However, the results are based on single radiation and readout two to six days afterwards.

This study focused on the evaluation of long-term immune-relevant effects of ionizing radiation in a model of radio-selected and untreated GICs. In this model, which was established by Prof. Dr. Alf Giese and Dr. Ella Kim, Department of Neurosurgery, University Medical Center Mainz, patient-derived GICs were in part treated with therapeutic-relevant fractionated radiation doses of 2.5 Gy in seven consecutive passages to resemble patient's radiotherapy. Control GICs were left untreated. Evaluation of the resistance to different doses of γ-radiation of the model GIC line 1080 (GIC-1080) and its radio-selected counterparts

(rsGIC-1080) revealed that the fractionated radiation scheme applied led to less spontaneous apoptosis, increased sphere forming potential, and increased radioresistance. Nevertheless, also 45% of untreated GIC-1080 survived exposition to 60 Gy of γ-radiation. These findings are in line with other studies showing that GICs are more resistant to radiation than cells from the tumor bulk (54) and that sub-lethal radiation doses can select for a more resistant phenotype (65). In GIC-1080, fractionated radiation further led to increased proliferation but slower migration. An increased radiation-induced proliferation was also described in other studies, showing that c-MET and NOTCH, which promote proliferation, invasion, and resistance to apoptosis are activated by radiotherapy (230,231). The reduced migration, although being a desired effect, was though unexpected as latest studies showed an increase in migratory potential of GICs after *in vitro* radiation through increased expression of e.g. fatty acid binding protein 7 (FABP7) or urokinase plasminogen activator receptor (uPAR), which can interact with migration-associated proteins such as integrin (244,245). The discrepancy of radiation-induced effects on migration might result from differences in radiation schemes and doses.

For a long time, radiobiology studied mainly the damage of ionizing radiation on its primary target DNA. Recent reports revealed that also the integrity of (plasma) membranes with the signaling platforms lipid rafts/detergent-resistant membranes is also affected by ionizing radiation through lipid damage which can induce apoptosis. Moreover, deficiency in acid sphingomyelinase (A-SMase), resulting in defects in the apoptosis-inducing ceramide clustering was linked to radioresistance in carcinoma cells and lymphoblasts from Niemann-Pick-patients (63,246). In this study, detergent-resistant membranes (DRMs) were isolated from GIC-1080 and rsGIC-1080 and analyzed via mass spectrometry. Tetraspanin 6 (TSPAN6) and neuron-glia-related cell adhesion molecule (NRCAM) were identified as the two most upregulated DRM-associated proteins in rsGIC-1080. While a functional role of TSPAN6 needs to be elucidated it can be speculated that it plays a role in cell motility and maybe even proliferation and survival. Tetraspanin family members contribute to integrin-dependent cellular motility and changes in morphology by mediating post-ligand binding events such as integrin-mediated adhesion strengthening, which is necessary for the cell to become resistant to detachment (247). The tetraspanins CD81 and CD9 also positively regulate proliferation through activation of the extracellular signal-

regulated kinase 1/2 (ERK1/2)/ MAPK pathway (248–250). CD151 is upregulated in many types of tumors and on tumor-initiating cells e.g. in prostate cancer (251) and associated with tumor initiation, promotion and progression (232,252). An association of NRCAM with glioblastoma progression was made by the finding that this protein was overexpressed in GBM cells compared to normal brain tissue. Knockdown of NRCAM in a human glioblastoma cell line changed cell morphology, reduced the cell proliferation rate, and lengthened the cell cycle (233). Thus, the observed increased expression of TSPAN6 and NRCAM in GICs should be validated and their function evaluated to possibly identify new therapeutic intervention possibilities.

Expression of MHC class I molecules and proteins with a role in antigen processing and presentation was overall decreased with single members found among the most downregulated DRM-associated proteins after radio-selection. This was validated by Western Blot and FACS analysis. The most striking findings were the downregulation of TAP1/2 proteins through which peptides are transported from the cytosol into the ER, and β_2-microglobulin, the soluble but essential subunit of MHC class I molecules, which result in decreased MHC class I expression on the cellular surface. Downregulation of TAP1/2 was already described as immune surveillance evasion mechanism in gliomas (222) and murine fibroblasts after oncogenic transformation (253), similar to β_2-microglobulin in diffuse large B cell lymphomas and colorectal carcinomas (254,255). In this study, radiation-induced reduction of MHC class I molecule expression led to significantly diminished recognition of rsGIC-1080 by HLA-A/B-matched CD8+ cytotoxic T cells. Interestingly, CD8+ T cells stimulated with rsGIC-1080 also recognized untreated GIC-1080 much better than rsGIC-1080. Further, three CD8+ T cell cultures (C1, C2, C5) were able to lyse GIC-1080 but not rsGIC-1080 even though they had been stimulated with the latter and proliferated throughout the culture time. The proliferation of the T cells indicated proper activation, but effector functions seemed to be inhibited. Overall, these results suggest that sub-lethal fractionated ionizing radiation selects for GICs with a more radioresistant and less immunogenic phenotype, therefore discourage a combined radio-immunotherapy. These findings contradict other *in vitro* studies on differentiated tumor cell lines, which showed that single dose γ-radiation between 1 – 100 Gy enhances protein degradation, leading to a larger peptide pool, increased peptide presentation on the cellular surface, and better

recognition by CD8+ T cells, thus suggesting to combine radio- and immunotherapy (226,229,243). A first *in vivo* report on glioma-immune system interaction using two applications of radiation similarly showed an increased expression of β_2-microglobulin on GL261 glioma cells in combination with increased CD4+ and CD8+ lymphocyte infiltration 48 hours after radiotherapy in tumor-bearing mice. Unfortunately, the radiation scheme of 2 Gy of ionizing radiation exposed on established tumors on day 15 and 17 after implantation only minimally increased survival (256). Nevertheless, these *in vitro* and *in vivo* studies evaluated radiation effects two to six days after treatment, neglecting long-term effects of clinically relevant fractionated radiation. This, though, is essential as in a therapeutic setting patients have to recover from radiochemotherapy before being treated with immunotherapy. Fadul et al. showed that the standard therapeutic combination of radiation and temozolomide induces significant lymphopenia in GBM patients as measured four weeks after therapy (257). A method to increase TAP1/2 and MHC class I expression and therefore the success of immunotherapies might be the administration of IFN-γ, despite controversial clinical trials with IFN-γ administration for cancer patients (258). Next to the anti-proliferative capacities, many reports showed that IFN-γ enhances TAP1/2 and MHC class I expression, which, as shown herein, can also be achieved on radio-selected and untreated control GICs (50,52,259,260).

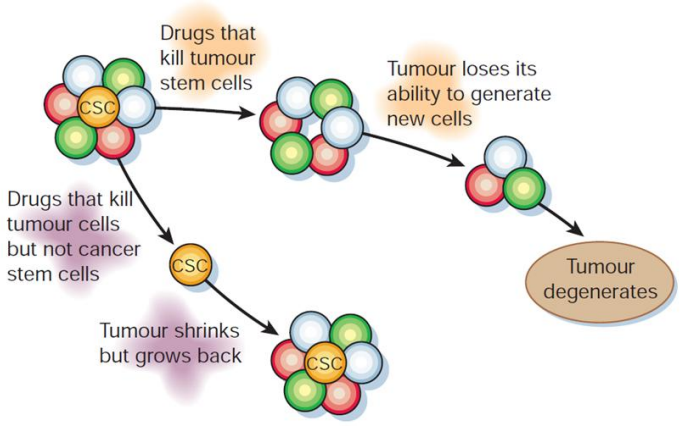

Figure 38: Targeting CSCs for effective anti-cancer treatment.
In standard therapeutic GBM treatment, therapeutic agents are applied that mainly target the more differentiated tumor cells but sparing CSC, leading to regrowth of secondary tumors. Drugs need to be developed that specifically target CSC for tumor eradication. Adopted from Reya et al., 2001 (19).

Further investigations on the (immune) characteristics of GICs in response to standard treatments will be essential in the development of new therapeutic combinations to target this specific subpopulation (Figure 38) (19,56,261).

4.1.2 Modulation of IFITM3 expression in GICs

So far, contribution of IFITM proteins to tumor initiation and progression remains controversial as increased and decreased expression of these proteins was described in different types of cancer compared to normal tissue (80–82) and their expression was associated with enhanced and reduced proliferation of cancer cells (85,87–89,237). In recent studies, IFITM1 and IFITM3 were proposed to positively contribute to glioma growths as knockdown of these proteins inhibited proliferation, migration, invasion and colony formation of glioma cell lines (88,89). Further, high expression of IFITM3 was linked to poor overall survival in GBM patients (TCGA database). If these proteins play a similar role in tumor-initiating cells has not been investigated.

In this study, the expression of IFITM3 in the subpopulation of glioma-initiating cells was analyzed. IFITM3 was found to be expressed in GIC-1080 and expression was even increased in rsGIC-1080. These findings are in line with recent observations that ionizing radiation can induce interferon-inducible genes. It was further suggested that interferon-induced genes also contribute to a more radioresistant phenotype (90,92,93). If enhanced IFITM3 expression also protects GICs from damage caused by ionizing radiation needs to be determined. In accordance with other studies, the detected distribution pattern of IFITM3 at the cell surface and in the cytosol, suggested its localization in lipid rafts/DRMs of the plasma membrane and intracellular vesicles. Western Blot analysis of cellular fractions confirmed IFITM3 to be present in the DRM containing fractions. While the topology of IFITM3 still needs to be clarified (72–74), the localization of this proteins suggests a function in signal transduction or microdomain organization also in GICs, possibly similar to IFITM1. IFITM1 was shown to interact with Caveolin1 in the caveolae via the hydrophobic IFITM transmembrane domain, which resulted in inhibition of ERK activation by enhancing the inhibitory function of Caveolin1 (262).

For the evaluation of the contribution of IFITM3 to proliferation and tumor growths GIC-1080 were lentivirally transduced for either stable upregulation or knockdown of IFITM3. Measurement of EdU incorporation revealed that comparable percentages of IFITM3-high expressing GICs, IFITM3-knockdown GICs, and respective control GICs proliferated throughout the 4 h incubation time. In line, IFITM3 high expressing and knockdown GICs gave rise to tumors of similar sizes compared to their controls in a xenograft model seven weeks after implantation. This was also reflected in comparable results for overall survival of tumor-bearing mice. Thus, the finding by others that knockdown of IFITM3 reduces proliferation and tumor growth in glioma cell lines was not confirmed in this study. This can be due to various reasons. A higher overexpression of IFITM3 driven by a strong CMV promotor was not achieved, possibly due to rapid methylation of the CMV promotor as was described for transduced human and mouse embryonic stem cells (263,264). Therefore, the medium expression EF1α promotor was used which resulted in a twofold higher expression of IFITM3 compared to the control GICs which probably was not sufficient to influence proliferation. An alternative explanation is that IFITM3 does not have a significant role in proliferation of glioma-initiating cells or that the forced up- and downregulation of IFITM3 expression is compensated by expression of the highly similar homologs IFITM1 or IFITM2 (68). Saitou et al. first described a role of IFITM3 in directing germ cell fate as IFITM3-positive murine primordial germ cells (PGCs) formed a community of cells through homotypic adhesion (83,265), separating them from somatic tissue-determined cells. They further found IFITM3 to be expressed in pluripotent embryonic stem cells and embryonic germ cells, proposing a role of IFITM3 in the propagation of the pluripotent state (266). More investigations are needed to clarify, if indeed IFITM3 does not influence proliferation, migration, and development in tumor-initiating cells. Eventually, the controversial findings of pro- and anti-proliferative roles of IFITM proteins in the different tumors might possibly depend on available interaction partners and signals from the tumor microenvironment (89).

4.2 Multiple sclerosis

4.2.1 Transcriptional changes controlling T cell plasticity and encephalitogenicity

T lymphocytes, especially the Th1 and Th17 subtypes, are regarded as the main players in induction and persistence of the autoimmune demyelinating disease multiple sclerosis. Despite intensive research, the molecular mechanisms underlying T cell pathology and encephalitogenicity are still not completely understood. As patient material is limited, animal models, such as EAE are a useful tool to analyze single genes or therapeutic molecules and their contribution and modulation of the disease course albeit the risk that effects might not occur or is even contradictory in humans (267,268). To better understand the whole picture of MS pathology, this study focused on the identification of whole signaling networks and transcriptional alterations of Th17 cells at distinct time points of T cell differentiation and in EAE. Thereby, key transcription factors and signaling networks that were implicated in T cell encephalitogenicity and plasticity could be identified. Transgenic naïve T cells with MOG-specific TCR were isolated from non-immunized mice (Tnaive; I.) and differentiated *in vitro* to generate Th17 cells (Th17iv; II.). These cells were adoptively transferred into lymphopenic *Rag1*$^{-/-}$ mice to induce EAE and re-isolated from the CNS at the peak of disease (Th17eae; III.), similar to CD4+ T cells from actively MOG_{35-55} immunized mice (CD4eae; IV.). Using whole mouse genome microarrays, expression levels of all transcribed genes could be compared in order to determine differential gene expression between these four groups.

Focusing on the evaluation of Th17 and Th1 phenotypic markers revealed that the T cell differentiation conditions used clearly led to the expression of Th17 cell phenotypic markers without major regulation of Th1 associated factors. In the comparison of naïve T cells and Th17eae cells, increased expression of Th1 markers *Tbx21* (T-bet) as well as *Ifng* and its receptor (*Ifngr*) in combination with minor reduction of Th17 lineage factor expression was observed. Nevertheless, the Th17eae cells, so-called “ex-Th17” cells, remained distinct from classical Th1 cells. These findings confirmed other studies showing that original Th17 cells can co-express the cytokines IFN-γ and IL-17, as well as the transcription factors T-

bet and RORγt under inflammatory conditions (269,270). This phenomenon was associated with a more pathogenic T cell phenotype in a melanoma model in which the transition was even essential for anti-tumor effectiveness against melanoma cells (227), suggesting not only an overlapping molecular pathway for differentiation and lineage plasticity, but a functional relationship between Th1 and Th17 cells. Although STAT1 and STAT4 have been described to be essential for *Tbx21* induction, in this study, *Tbx21* expression increased independent of *Stat1* and *Stat4* in the active and adoptive transfer EAE model, which endorsed a recently proposed STAT1-independent activation of *Tbx21* in active EAE (191). Duhen et al. recently also confirmed that encephalitogenic Th17 cells express IFN-γ and T-bet and showed that chronic stimulation of Th17 cells with IL-23 was essential to activate additional expression of IFN-γ independently of the Th1-associated transcription factors T-bet, Eomes, STAT1, and STAT4 (271).

The evaluation of whole transcriptional changes between Th17iv and Th17eae cells led to the identification of prominent signaling networks that could be associated with canonical signaling pathways. Among these were the “communication between cells of the innate and adaptive immune system”, mainly composed of increased expression by distinct cytokines and TLRs. TLRs belong to the group of pattern recognition receptors (PRR), which are widely expressed on antigen presenting cells. Few reports have shown that these receptors are also expressed on effector CD4+ T cells after activation and on CD4+CD45RO+ memory T cells (272–275). These reports suggested that TLR act as co-stimulatory molecules in TCR signaling to promote survival of activated CD4+ T cells, thus resulting in direct effects of pathogen-associated molecular patterns to mediate functional responses. Interestingly, enhanced TLR-TCR expression resulted in increased activation of naïve CD4+ T cells, which was recently associated with a faster relapsing-remitting course of MS (276). Thus, this rather unknown signaling pathway in T cells might contribute to stabilizing T cell activation to support a more effective inflammatory response.

Network analysis further revealed that metabolic changes were connected to the transition towards Th17eae cells including an upregulation of liver X receptor/ retinoid X receptor (LXR/RXR) signaling and modulation of cholesterol biosynthesis and transport. The modulation of cholesterol and lipid synthesis was suggested to be a promising therapeutic approach for MS (277) as increased

mRNA levels of LXRβ were measured in peripheral blood mononuclear cells (PBMCs) of MS patients compared to healthy controls (278) and higher serum levels of cholesterol, LDL, and triglycerides were even correlated to worsening disability (279).

Cholesterol is needed for membrane microdomain/lipid raft organization and responsible for proper TCR signaling. It was demonstrated that lipid raft organization by cholesterol levels varies in the different Th subsets, guiding T cell polarization and effector function e.g. by directly influencing the intensity of Calcium signaling and NFAT activation and translocation to the nucleus (280). Increased levels of cholesterol led to co-localization of IL-2Rα, IL-4Rα, and IL-12Rβ2 in the lipid rafts in antigen-specific, autoimmune Th1 cells promoting their organ-specific reactivity in a mouse model for diabetes while this mechanism did not increase the suppressive function of Tregs (281). The heterodimer of LXR/RXR maintains cholesterol homeostasis by regulating certain genes involved in cholesterol and fatty acid metabolism, such as *Abca1*, *Abcg1*, *Srebp1c*, and fatty acid synthase (282). Reciprocal activation of LXR and SREBP2 transcriptional pathways mediate cholesterol transport and synthesis, which is essential for cell proliferation and clonal expansion of T cells, thus, acquired immune responses. It was shown that *Lxrβ*-knockout mice had increased expression of *Srebp2* and enhanced proliferation of splenocytes (283). In line, increased expression of *Lxr/Rxr* and its downstream targets *Lpl*, *Abca1*, and *Abcg1* was observed in Th17eae compared to Th17iv cells, in combination with a decreased expression of *Srebp2* and its target *Ldlr*. Although the activation of LXR/RXR was published to also enhance *Srebp1c* expression (283), a downregulation of *Srebp1*, which could not further be divided into different isoforms, was observed in this dataset. Interestingly, forced expression of *Srebp1a* and *Srebp1c* inhibited Th17 cell differentiation, while the knockdown of either isoform of *Srebp1* led to increased Th17 cell differentiation (284). Thus, the observed modulation of genes involved in cholesterol homeostasis in Th17eae cells suggests that metabolic factors contribute to the expansion and reorganization of pro-inflammatory encephalitogenic CD4+ Th17 cells. However, the overall role of LXR/RXR in EAE is not clear yet. Administration of LXR agonists T0901317 or GW3965 was shown to inhibit differentiation and function of Th17 by downregulating RORγt and IL-23R and activating SREBP1 which can directly bind to the *Il17* promotor, inhibiting thereby the binding of AHR, thus

inhibiting *Il17* expression (284,285). However, this inhibition of Th17 function led to amelioration of EAE in MOG_{35-55}–immunized mice that were treated with LXR agonists, which could be associated with lower levels of IL-17A in the CNS and lymph nodes, and lower levels of IL-17A and IL-23R in splenocytes. LXR deficiency or antagonistic treatment had the opposite effect and exacerbated disease (284,285). This might be due to an independent anti-inflammatory effect of LXR signaling on APCs by inhibition of TLR signaling (286). The opposite effects might be due to distinct roles of LXR/RXR signaling in innate and adaptive immune cells.

It is commonly accepted that CD4+ T cell subsets are not as restricted in their lineage commitment as previously thought. In a certain range, the modulation of cytokine profiles and other effector molecules were described (287,288). In this respect Th17 cells showed strong plasticity as they can be reprogrammed into different lineages in various differentiation stages (164,289). Lineage flexibility might possibly be controlled by combinatorial re-expression of transcription factors that are highly expressed in naïve T cells or in even earlier thymocyte developmental stages and downregulated during T cell differentiation. Their upregulation might reprogram the differentiated Th cells back to a naïve stage as a basis for new commitments (289). In the direct comparison of Th17iv and Th17eae cells, we found the transcription factors *Cebpa* (C/EBPα), *Fos*, *Klf4*, *Nfatc1*, and *Spi1* (PU.1) among the most upregulated genes that were also linked and involved in prominent signaling networks, suggesting a contribution to the T cell transformation in EAE. We observed two expression patterns with *Fos* and *Klf4* being upregulated in Tnaive compared to Th17iv and *Cebpa*, *Nfatc1*, and *Spi1* being similarly low expression in Tnaive and Th17iv, which was validated by qRT-PCR. Interestingly, all of these transcription factors are involved in early T cell development (290–293). The observed expression pattern of *Fos* and *Klf4* is in line with the findings that c-Fos expression is associated with CD4+CD8- single positive (SP) thymocytes (293), while KLF4 was found to be high expressed in naïve CD8+ T cells to maintain a quiescent stage (294). Expression of KLF4 in combination with OCT3/4, SOX2, and c-MYC is essential for stem cells to maintain the pluripotency and re-expression of these factors in adult somatic cells was already shown to reprogram them into pluripotent stem cells (295). KLF4 expression might influence the course of EAE in various ways as *Klf4*-knockout mice showed a defect in the proliferation of CD4-CD8- double

negative (DN) thymocytes through missing inhibition of the cell cycle inhibitor Cyclin-dependent kinase inhibitor 1B (Cdkn1b), which also resulted in reduced numbers of Th17 cells in the spleen and the CNS, and a milder course of EAE. KLF4 was further shown to directly bind to the *Il17a* promotor to activate *Il17* expression (296), thus influencing T cell differentiation and effector function. PU.1 plays a central role in hematopoiesis, where it regulates gene expression through its interaction with other transcription factors including C/EBPα, IRF4, IRF8, and c-JUN, but is silenced in thymocyte development. The assumption that PU.1 remained inactive in T cell lineages was recently revised as low levels of PU.1 could be detected in Th2 cells, in which its expression was associated with low levels of IL-4, IL-5, IL-10, and IL-13 and heterogeneity of the Th2 population (287). PU.1 was also found to be essential for the expression of IL-9, the master cytokine of Th9 cells, which is associated with allergic inflammation (297,298). It can be speculated that PU.1 might have a similar role in encephalitogenic Th17eae cells as the transcriptome analysis revealed also an increased expression of IL-9, which might result from increased expression of the upstream regulator of *Spi1*, C/EBPα. As PU.1 was associated with TLR2 and CD14 expression in monocytes (299,300) which were also upregulated in Th17eae compared to Th17iv, PU.1 could also contribute to enhanced expression of these two factors and therefore to the communication between the innate and the adaptive immune system. The NFAT transcription factors are able to guide manifold cellular function due to their ability to integrate calcium signaling with other signaling pathways. By acting most often in cooperation with other transcription factors such as AP-1 (c-Fos and c-Jun) they regulate thymocyte development, T cell activation and differentiation and self-tolerance (208,221,292). *Nfatc1* was upregulated while *Nfatc2* was downregulated in encephalitogenic Th17eae cells. The specialty of *Nfatc1* is its expression of the short isoform NFATc1/αA, which is strongly enhanced through a positive-feedback loop, regulated by NFAT proteins, NF-κB, CREB, ATF-2 and Fos to sustain *Nfat* expression (301,302). Interestingly, it was shown that high levels of NFATc1/αA are important for lineage commitment in osteoclasts (303). Therefore, it can be speculated that the transcription factors *Cebpa*, *Fos*, *Klf4*, *Nfatc1*, and *Spi1* might contribute to the transformation process of Th17 cells via a more uncommitted, shapeable T cell stage in EAE.

Even though the causes of MS remain elusive, a genetic component for MS susceptibility is ascertained. Various single nucleotide polymorphisms (SNPs) were identified in large multicenter association studies that supposedly enhance MS risk. To which extend these polymorphisms affect gene expression and confer susceptibility to autoimmunity remains to be determined. In the MS GWAS 2011, 57 SNPs were identified which were annotated to 55 human genes based on proximity (± 500 kb) according to ensembl database (annotation search performed by Christina M. Lill). 53/55 murine homolog genes were represented on the murine microarray chip used in this study of which 15 genes were strong candidates for contributing to T cell encephalitogenicity and plasticity. Nine selected candidate genes were validated and also statistically significantly regulated. These genes could be grouped by their different expression patterns which suggested different roles and contributions to T cell pathology and plasticity in the context of EAE. Among these, the transcription factor *Bach2* was highly expressed in naïve T cells, which decreased in differentiated Th17 cells and in Th17eae cells, suggesting a role in maintaining a naïve T cell phenotype. In contrast to afore mentioned transcription factors, *Bach2* does not play a critical role in thymocyte differentiation, but contributes to maintaining T cells in a naïve state by suppressing effector-memory-related genes (304). Interestingly, Tsukumo et al. found elevated levels of S100A in *Bach2*$^{-/-}$ mice and suggested that Calcium-binding protein S100A is a putative direct target of BACH2. Increased expression of *S100a1* in Th17iv cells, which was further enhanced in Th17eae cells compared to naïve T cells, were also observed in this study, therefore negatively correlating to *Bach2* expression. S100A was proposed to increase inflammation and autoimmunity as its expression to the severity of inflammatory diseases including rheumatoid arthritis and artherosclerosis (305). Thus, a downregulation of *Bach2* in combination with increased levels of *S100a1* in Th17eae cells compared to Th17iv cells might contribute to the pathology of EAE and MS.

Among the MS susceptibility genes, *Irf8*, *Plek*, *Mertk*, and *Rgs1* were found to be increasingly expressed in Th17eae cells and involved in prominent signaling networks, suggesting a contribution to T cell encephalitogenicity and therefore MS pathology. A general role in differentiation of T, B, and dendritic cells was attributed to the transcription factor *Irf8* (306). *Irf8* was described to inhibit Th17 cell differentiation without affecting Th1 or Th2 differentiation thus, increased

expression of *Irf8* in Th17eae cells might contribute to the transition process towards a Th1-like phenotype (307). *Rgs1* was associated with a variety of T cell mediated pathologies including celiac disease, type I diabetes (T1D) and MS (308), and a contribution to T cell pathology was supported by recent findings showing that increased expression of RGS1 and other family members correlated with T cell activation and a slower *in vivo* migration of regulatory T cells (309). Increased expression levels of membrane-bound as well as soluble receptor tyrosine kinases MER (MERTK) and AXL were found in homogenates from established MS lesions (310). This indicated that the upregulation of *Mertk* might also contribute to Th17 cell encephalitogenicity. However, *Tyro3*, *Axl* and *Mertk* (TAM) triple knockout mice exhibited systemic autoimmune diseases, including increased production of the pro-inflammatory cytokine TNF-α, impaired integrity of the BBB, glial activation and protein degradation, associated with accumulation of autoantibodies and autoreactive lymphocyte infiltration into the brain (311). The function of PLEK (Pleckstrin/p47) is largely unknown, but it was found to be high expressed in platelets and leukocytes where it represents a major substrate of protein kinase C (PKC) (312). Interestingly, PLEK essentially contributes in the PKC signaling cascade for secretion of pro-inflammatory cytokines TNF-α and IL-1β in phagocytes and its deregulation is associated with the autoimmune disorder diabetes mellitus (313). Thus, PLEK might also contribute to secretion of pro-inflammatory cytokines in Th17 cells in the context of EAE and MS.

Among the MS risk genes, the cytokine receptor for IL-2 (*Il2ra*) was high expressed in Th17iv cells and low expressed in Tnaive and Th17eae cells, suggesting a negative regulatory role in the encephalitogenic process. A number of SNPs at the *IL2RA* locus were associated with increased risk of various autoimmune diseases including T1D (314) and Graves' disease (315), and also associated with increased levels of soluble IL-2RA (sIL-2RA) found in the serum of MS patients (316). sIL-2RA can sequester IL-2 and reduce IL-2-responsiveness and was shown to exacerbate EAE by promoting Th17 type responses and infiltration of both Th1 and Th17 cell subsets into the CNS (317). It would be interesting to evaluate if the observed decrease in *Il2ra* expression corresponds to increased levels of sIL-2RA in the CNS of EAE-affected animals, as a mechanism to reduce IL-2 signaling and restrict IL-2-mediated T cell tolerance, but increase autoimmunity by inducing enhanced proliferation of auto-reactive T cells, as suggested by studies using knockout animals (318–321).

Three of the confirmed candidates have been scarcely investigated up to date and their role in immune cell function is unclear. The *outer dense fiber of sperm tails 3b* (*Odf3b*) encodes a cytoskeletal coiled-coil protein, which has predominant importance for shear stress resistance in spermatocytes (322). The *solute carrier family 30 member 7* (*Slc30a7)* encodes ZnT7, which transports zinc from the cytosol into the golgi apparatus (323) and thus contributes to cellular zinc homeostasis and enzyme function in the secretory pathway (324). The *thyroid adenoma-associated gene* (*Thada*) was associated with death receptor signaling based on two-hybrid experiments (Puduvalli VK and Ridgway L, GenBank accession reference note) as well as with neoplasms (325). Its decreased expression in Th17eae cells might contribute to inhibition of apoptosis.

In summary, the analysis of whole transcriptional changes occurring in Th17 cells throughout the course of EAE substantially extended our knowledge by identifying key players and signaling networks controlling T cell plasticity and encephalitogenicity in EAE. Further, distinct MS risk-associated candidate genes were identified to play a role in these T cell processes. Functional analysis is now needed to evaluate the contribution of each gene to the pathology of MS in order to establish new therapeutic possibilities.

4.2.2 Knockdown of *Nfatc1* ameliorates EAE symptoms

Even though the transcription factor *Nfatc1* was not extremely upregulated in Th17eae cells compared to Th17iv, the analysis of the microarray data revealed that this factor was connected to various signaling networks and molecular processes taking place in the transition towards a Th1-like phenotype and the execution of Th17 cell effector function. A general regulation of NFAT proteins could be expected as NFAT proteins play a major role in T cell development, differentiation, cytokine expression, and tolerance (206,208–210). While a downregulation of *Nfatc2* was observed, this work focused on functional analysis of the positively regulated *Nfatc1*, which supports antigen-mediated proliferation and protects lymphocytes against rapid activation induced cell death (AICD), in contrast to all other NFATc proteins, which diminish lymphocyte proliferation, induce anergy and enhance AICD (205).

Herein, the effect of a knockout of *Nfatc1* in CD4+ T cells on Th17 cell differentiation and the course of EAE was analyzed. Active immunization of mice harboring *Nfatc1*-deficient CD4+ T cells (*CD4-Cre+.Nfatc1*$^{fl/fl}$) with MOG_{35-55} peptide did not lead to establishment of EAE symptoms. These results correlate with recent findings in which conditional ablation of *Nfatc1* in B cells led to a decrease in their capacity to stimulate T cells and a milder course of EAE (326). Despite the lack of clinical signs of disease, CD4+ T cells could be isolated from the CNS of immunized *CD4-Cre+.Nfatc1*$^{fl/fl}$ mice, excluding a defect in migration and activation as only activated lymphocytes can enter the CNS through the BBB (127,128). A defect in activation of *Nfatc1*-deficient CD4+ T cells could also be excluded as naïve CD4+ T cells that were stimulated *in vitro* with anti-CD3/anti-CD28 antibodies proliferated similarly well compared to control cells. These findings are in contrast with earlier findings obtained from *Nfatc1*-deficient T cells from *Nfatc1*$^{-/-}$*/Rag1*$^{-/-}$ somatic chimeric mice, which revealed about 30% diminished proliferation potential compared to wild-type mice, regardless of the stimulant used (239). In line with the results obtained in this study, Peng et al. found similar expression levels of activation markers and proliferation capacities of T cells from fetal liver *Nfatc1*$^{-/-}$*/Nfatc2*$^{-/-}$ chimeric mice and control cells, but showed inhibition of T cell development and multiple effector functions, including Th cytokine production, surface effector molecule expression, and cytolytic activity (327).

The evaluation of proper effector function of *Nfatc1*-deficient CD4+ T cells in an adoptive transfer EAE model revealed inflammatory cytokine expression (IL-17A and TNF-α) of CD4+ T cells before the transfer into lymphopenic *Rag1*$^{-/-}$ mice, although at lower levels than control cells. Also in this EAE model, *Nfatc1*-deficient cells were not capable of inducing EAE. While a defect in activation can be rather excluded by afore mentioned experiments, these results indicate a restriction in proper T cell differentiation and execution of effector function. Although the adoptive transfer EAE experiment has only been performed once and the results are rather preliminary, they correlate with the analysis of Th17 phenotypic marker expression after three days of *in vitro* differentiation of *Nfatc1*-deficient and control CD4+ T cells towards a Th17 cell phenotype. Here, a trend towards lower expression of receptors for IL-1 and IL-23 and cytokines IL-17A, IL-17F, IL-22, and GM-CSF was found. Thus, the data obtained herein established an essential role of NFATc1 in Th17 cell differentiation as well as

Th17 execution of effector function and initiation of EAE symptoms, without hampering T cell activation.

Inhibitors for the calcineurin-NFAT signaling cascade, cyclosporine A (CsA) or tacrolimus (FK-506) are widely in use to induce immune suppression e.g. to avoid transplant rejection. Using these broad Calcium-signaling inhibitors to ameliorate MS pathology might result in severe side effects and opportunistic infections, due to its contribution in a great variety of molecular functions. As the short inducible isoform NFATc1/αA is highly distinct in its generation and function from all the other NFAT proteins (205), it can possibly be specifically targeted in the treatment of MS and other immune disorders.

4.3 Summary and Outlook

In the first part of this thesis, molecular mechanisms underlying immune escape of GICs including a contribution of ionizing radiation were investigated. The model GIC cell line 1080 (GIC-1080) in comparison to the radio-selected counterpart (rsGIC-1080) was used to show that treatment with ionizing radiation can trigger the remodeling of plasma membrane signaling platforms, enhance proliferation of GICs, and reduce expression of molecules involved in antigen presentation, impairing immunogenicity. The decreased expression of MHC class I molecules on the cellular surface diminished the recognition potential by allogeneic cytotoxic CD8+ T cells. Ionizing radiation was suggested to affect immune responses as it can also regulate expression of immune-associated interferon-induced proteins. An upregulation of the interferon-induced transmembrane protein 3 (IFITM3) in radio-selected GICs compared to their untreated control was detected in this study. A contribution of this protein to proliferation *in vitro* and tumor growth *in vivo,* though, could not be demonstrated for this subpopulation.

In the second part of this thesis, gene expression studies were performed to dissect transcriptional alterations underlying Th17 cell encephalitogenicity and plasticity in the mouse model for MS, EAE. It was published before and confirmed herein that murine *in vitro* primed Th17 cells undergo massive metabolic changes and accumulate Th1 characteristics, while exhibiting exuberant myelin-destructive functions in the CNS. Analysis of associated signaling pathways

identified interaction partners that were involved in cytokine and chemokine expression for the establishment of a pro-inflammatory microenvironment and the communication with the innate immune system via TLRs. The transcription factors *Cebpa, Fos, Klf4, Spi1, and Nfatc1* seemed to play a role as key regulators in the encephalitogenicity and plasticity of Th17 cells. Further, analysis of differential regulation of MS-associated genes throughout the course of murine Th17 cell differentiation and disease revealed an overlap of 67.3%, emphasizing that MS is a T-cell-driven disease and nine MS-associated candidate genes, *Bach2, Il2ra, Irf8, Mertk, Odf3b, Plek, Rgs1*, *Slc30a7,* and *Thada,* were found to be regulated in Th17 cells throughout the course of EAE, suggesting their involvement in T cell pathogenicity. While the exact contribution of all of these candidate genes to T cell pathology needs to be determined, this study showed that knockout of the transcription factor *Nfatc1* in CD4+ T cells diminished the potential of these cells to fully differentiate into Th17 cells and to express high amounts of lineage cytokines, resulting in repression of EAE symptoms.

The main challenges in the treatment of the most aggressive primary tumor of the CNS, glioblastoma multiforme, are its penetration into the surrounding brain tissue, making complete surgical resection impossible, and its resistance to the standard treatment of radiotherapy combined with chemotherapy with temozolomide (1). Even though many tumors initially respond to the multimodal treatments, they recur as a more therapeutically resistant malignancy. Immunotherapies emerged as highly promising options because cells of the immune system can specifically trace, identify, and kill dispersed tumor cells based on recognition of tumor-associated antigen (TAA) -derived peptides on MHC class I molecules by cytolytic CD8+ T lymphocytes (CTL), a process independent of the cellular proliferation status. Unfortunately, immune modulatory capacities and low immunogenicity of the glioma cells have so far restricted clinical success (328,329). Resistance and regrowth of the tumors was suggested to be mainly caused by glioma-initiating cells. Therefore, the evaluation of molecular mechanisms underlying therapy resistance and immune modulation and evasion will be crucial to develop novel therapies to directly target these malignant cells.

The chronic inflammatory, demyelinating disease of the CNS, multiple sclerosis, already manifests in patients at the mean age of 29 years leading to progressive

disabilities over the years. The exact causes of MS are still unknown, but it is widely accepted that exposure of genetically susceptible persons to environmental factors, such as viral infections, triggers the disease. It is assumed that self-reactive, myelin-specific T lymphocytes, especially Th1 and Th17 cells, which have escaped the control mechanisms of the immune system, are responsible for the disease (122). A leakage in the BBB and peripheral activation of these T lymphocytes results in their transmigration into the CNS and destruction of myelin sheath and axons. Conventional treatments with Interferon-β, Glatiramer Acetate lead to the reduction of relapse frequencies and acute exacerbations, but cannot cure the disease. More potent drugs such as Natalizumab, a monoclonal antibody against α4β1 integrin to inhibit lymphocytes from entry into the CNS, or Fingolimod, a sphingosine-1-phosphate (S1P) analog that sequesters activated T cells in the lymph nodes to prevent their migration into the CNS, carry also the risk of life threatening side effects such as opportunistic infections (330,331). Therefore, more investigations on causes and triggers of MS and underlying pathogenic mechanisms are needed to develop novel strategies to ameliorate or stop the autoimmune attacks.

Understanding the molecular processes in both excess and restriction of immune responses within the CNS, is the basis for novel treatment strategies.

References

1. Stupp R, Mason WP, van den Bent MJ, Weller M, Fisher B, Taphoorn MJB, et al. Radiotherapy plus concomitant and adjuvant temozolomide for glioblastoma. N Engl J Med. 2005;352:987–96.
2. Furnari FB, Fenton T, Bachoo RM, Mukasa A, Stommel JM, Stegh A, et al. Malignant astrocytic glioma: genetics, biology, and paths to treatment. Genes Dev. 2007;21:2683–710.
3. Louis DN, Ohgaki H, Wiestler OD, Cavenee WK, Burger PC, Jouvet A, et al. The 2007 WHO classification of tumours of the central nervous system. Acta Neuropathol. 2007;114:97–109.
4. Behin A, Hoang-Xuan K, Carpentier AF, Delattre J-Y. Primary brain tumours in adults. Lancet. 2003;361:323–31.
5. DeAngelis LM. BRAIN TUMORS. N Engl J Med. 2001;344:114–23.
6. The Cancer Genome Atlas Research Network. Comprehensive genomic characterization defines human glioblastoma genes and core pathways. Nature. 2008;455:1061–8.
7. Parsons DW, Jones S, Zhang X, Lin JC-H, Leary RJ, Angenendt P, et al. An integrated genomic analysis of human glioblastoma multiforme. Science (80-). 2008;321:1807–12.
8. Verhaak RGW, Hoadley K a, Purdom E, Wang V, Qi Y, Wilkerson MD, et al. Integrated genomic analysis identifies clinically relevant subtypes of glioblastoma characterized by abnormalities in PDGFRA, IDH1, EGFR, and NF1. Cancer Cell. Elsevier Ltd; 2010;17:98–110.
9. Phillips HS, Kharbanda S, Chen R, Forrest WF, Soriano RH, Wu TD, et al. Molecular subclasses of high-grade glioma predict prognosis, delineate a pattern of disease progression, and resemble stages in neurogenesis. Cancer Cell. 2006;9:157–73.
10. Preston DL, Ron E, Yonehara S, Kobuke T, Fujii H, Kishikawa M, et al. Tumors of the nervous system and pituitary gland associated with atomic bomb radiation exposure. J Natl Cancer Inst. 2002;94:1555–63.
11. Hanahan D, Weinberg R a. Hallmarks of cancer: the next generation. Cell. Elsevier Inc.; 2011;144:646–74.
12. Bonnet D, Dick JE. Human acute myeloid leukemia is organized as a hierarchy that originates from a primitive hematopoietic cell. Nat Med. 1997;3:730–7.
13. Lapidot T, Sirard C, Vormoor J, Murdoch B, Hoang T, Caceres-Cortes J, et al. A cell initiating human acute myeloid leukeamia after transplantation into SCID mice. Nature. 1994;367:645–8.
14. Lorico A, Rappa G. Phenotypic heterogeneity of breast cancer stem cells. J Oncol. 2011;2011:135039.
15. Fang D, Nguyen TK, Leishear K, Finko R, Kulp AN, Hotz S, et al. A tumorigenic subpopulation with stem cell properties in melanomas. Cancer Res. 2005;65:9328–37.
16. Li C, Heidt DG, Dalerba P, Burant CF, Zhang L, Adsay V, et al. Identification of pancreatic cancer stem cells. Cancer Res. 2007;67:1030–7.
17. Al-Hajj M, Wicha MS, Benito-Hernandez A, Morrison SJ, Clarke MF. Prospective identification of tumorigenic breast cancer cells. PNAS. 2003;100:3983–8.

18. Vescovi AL, Galli R, Reynolds B a. Brain tumour stem cells. Nat Rev Cancer. 2006;6:425–36.

19. Reya T, Morrison SJ, Clarke MF, Weissman IL. Stem cells, cancer, and cancer stem cells. Nature. 2001;414:105–11.

20. Singh SK, Hawkins C, Clarke ID, Squire JA, Bayani J, Hide T, et al. Identification of human brain tumour initiating cells. Nature. 2004/11/19 ed. 2004;432:396–401.

21. Lathia JD, Gallagher J, Myers JT, Li M, Vasanji A, McLendon RE, et al. Direct in vivo evidence for tumor propagation by glioblastoma cancer stem cells. PLoS One. 2011;6:e24807.

22. Galli R, Binda E, Orfanelli U, Cipelletti B, Gritti A, Vitis S De, et al. Isolation and Characterization of Tumorigenic, Stem-like Neural Precursors from Human Glioblastoma. Cancer Res. 2004;64:7011–21.

23. Campos B, Herold-Mende CC. Insight into the complex regulation of CD133 in glioma. Int J Cancer. 2011;128:501–10.

24. Prestegarden L, Svendsen A, Wang J, Sleire L, Skaftnesmo KO, Bjerkvig R, et al. Glioma cell populations grouped by different cell type markers drive brain tumor growth. Cancer Res. 2010;70:4274–9.

25. Sanai N, Alvarez-Buylla A, Berger MS. Neural stem cells and the origin of gliomas. N Engl J Med. 2005;353:811–22.

26. Turner JD, Abla A a, Sanai N. Identification of the glioma cell of origin. World Neurosurg. Elsevier Inc.; 2012;78:200–1.

27. García-Verdugo JM, Doetsch F, Wichterle H, Lim D a, Alvarez-Buylla a. Architecture and cell types of the adult subventricular zone: in search of the stem cells. J Neurobiol. 1998;36:234–48.

28. Gage FH, Kempermann G, Palmer TD, Peterson D a, Ray J. Multipotent progenitor cells in the adult dentate gyrus. J Neurobiol. 1998;36:249–66.

29. Palmer TD, Willhoite AR, Gage FH. Vascular Niche for Adult Hippocampal Neurogenesis. J Comp Neurol. 2000;425:479–94.

30. Ramírez-Castillejo C, Sánchez-Sánchez F, Andreu-Agulló C, Ferrón SR, Aroca-Aguilar JD, Sánchez P, et al. Pigment epithelium-derived factor is a niche signal for neural stem cell renewal. Nat Neurosci. 2006;9:331–9.

31. Shen Q, Goderie SK, Jin L, Karanth N, Sun Y, Abramova N, et al. Endothelial cells stimulate self-renewal and expand neurogenesis of neural stem cells. Science (80-). 2004;304:1338–40.

32. Calabrese C, Poppleton H, Kocak M, Hogg TL, Fuller C, Hamner B, et al. A perivascular niche for brain tumor stem cells. Cancer Cell. 2007;11:69–82.

33. Bao S, Wu Q, Sathornsumetee S, Hao Y, Li Z, Hjelmeland AB, et al. Stem cell-like glioma cells promote tumor angiogenesis through vascular endothelial growth factor. Cancer Res. 2006;66:7843–8.

34. Becher B, Prat a, Antel JP. Brain-immune connection: immuno-regulatory properties of CNS-resident cells. Glia. 2000;29:293–304.

35. Gomez GG, Kruse CA. Mechanisms of malignant glioma immune resistance and sources of immunosuppression. Gene Ther Mol Biol. 2006;10:133–46.

36. Streit WJ, Kreutzberg GW. Response of Endogenous Glial Cells to Motor Neuron Degeneration Induced by Toxic Ricin. J Comp Neurol. 1988;263:248–63.

37. Wei J, Barr J, Kong L-Y, Wang Y, Wu A, Sharma AK, et al. Glioblastoma cancer-initiating cells inhibit T-cell proliferation and effector responses by the signal

transducers and activators of transcription 3 pathway. Mol Cancer Ther. 2010;9:67–78.

38. Seoane J. TGFbeta and cancer initiating cells. Cell Cycle. 2009;8:3787–8.

39. Crane CA, Ahn BJ, Han SJ, Parsa AT. Soluble factors secreted by glioblastoma cell lines facilitate recruitment, survival, and expansion of regulatory T cells: implications for immunotherapy. Neuro Oncol. 2012;14:584–95.

40. Yi L, Xiao H, Xu M, Ye X, Hu J, Li F, et al. Glioma-initiating cells: a predominant role in microglia/macrophages tropism to glioma. J Neuroimmunol. Elsevier B.V.; 2011;232:75–82.

41. Wu A, Wei J, Kong L-Y, Wang Y, Priebe W, Qiao W, et al. Glioma cancer stem cells induce immunosuppressive macrophages/microglia. Neuro Oncol. 2010;12:1113–25.

42. Li W, Graeber MB. The molecular profile of microglia under the influence of glioma. Neuro Oncol. 2012;14:958–78.

43. Gabrusiewicz K, Ellert-Miklaszewska A, Lipko M, Sielska M, Frankowska M, Kaminska B. Characteristics of the alternative phenotype of microglia/macrophages and its modulation in experimental gliomas. PLoS One. 2011;6:e23902.

44. Ye X, Xu S, Xin Y, Yu S, Ping Y, Chen L, et al. Tumor-associated microglia/macrophages enhance the invasion of glioma stem-like cells via TGF-β1 signaling pathway. J Immunol. 2012;189:444–53.

45. Fontenot JD, Rudensky AY. A well adapted regulatory contrivance: regulatory T cell development and the forkhead family transcription factor Foxp3. Nat Immunol. 2005;6:331–7.

46. Hussain SF, Yang D, Suki D, Aldape K, Grimm E, Heimberger AB. The role of human glioma-infiltrating microglia/macrophages in mediating antitumor immune responses. Neuro Oncol. 2006;8:261–79.

47. Facoetti A, Nano R, Zelini P, Morbini P, Benericetti E, Ceroni M, et al. Human leukocyte antigen and antigen processing machinery component defects in astrocytic tumors. Clin cancer Res. 2005;11:8304–11.

48. Wischhusen J, Friese M a, Mittelbronn M, Meyermann R, Weller M. HLA-E protects glioma cells from NKG2D-mediated immune responses in vitro: implications for immune escape in vivo. J Neuropathol Exp Neurol. 2005;64:523–8.

49. Lanier LL. NK cell recognition. Annu Rev Immunol. 2005;23:225–74.

50. Stark GR, Kerr IM, Williams BR, Silverman RH, Schreiber RD. How cells respond to interferons. Annu Rev Biochem. 1998;67:227–64.

51. Trowsdale J, Hanson I, Mockridge I, Beck S, Townsend A, Kelly A. Sequence encoded in the class II region of the MHC related to the ABC superfamily of transporters. Nature. 1990;348:741–7.

52. Epperson DE, Arnold D, Spies T, Cresswell P, Pober JS, Johnson DR. Cytokines increase transporter in antigen processing-1 expression more rapidly than HLA class I expression in endothelial cells. J Immunol. 1992;149:3297–301.

53. Grandea a G, Van Kaer L. Tapasin: an ER chaperone that controls MHC class I assembly with peptide. Trends Immunol. 2001;22:194–9.

54. Bao S, Wu Q, McLendon RE, Hao Y, Shi Q, Hjelmeland AB, et al. Glioma stem cells promote radioresistance by preferential activation of the DNA damage response. Nature. 2006;444:756–60.

55. Tamura K, Aoyagi M, Wakimoto H, Ando N, Nariai T, Yamamoto M, et al. Accumulation of CD133-positive glioma cells after high-dose irradiation by Gamma Knife surgery plus external beam radiation. J Neurosurg. 2010;113:310–8.

56. Hadjipanayis CG, Van Meir EG. Tumor initiating cells in malignant gliomas: biology and implications for therapy. J Mol Med (Berl). 2009;87:363–74.

57. Lucero H, Gae D, Taccioli GE. Novel localization of the DNA-PK complex in lipid rafts: a putative role in the signal transduction pathway of the ionizing radiation response. J Biol Chem. 2003;278:22136–43.

58. Corre I, Niaudet C, Paris F. Plasma membrane signaling induced by ionizing radiation. Mutat Res. Elsevier B.V.; 2010;704:61–7.

59. Staubach S, Hanisch F-G. Lipid rafts: signaling and sorting platforms of cells and their roles in cancer. Expert Rev Proteomics. 2011;8:263–77.

60. Brown DA, London E. Functions of lipid rafts in biological membranes. Annu Rev Cell Dev Biol. 1998;14:111–36.

61. Garcia-Barros M, Paris F, Cordon-Cardo C, Lyden D, Rafii S, Haimovitz-Friedman A, et al. Tumor response to radiotherapy regulated by endothelial cell apoptosis. Science. 2003;300:1155–9.

62. Bezombes C, Laurent G, Jaffrézou J-P. Implication of raft microdomains in drug induced apoptosis. Curr Med Chem Anticancer Agents. 2003;3:263–70.

63. Bionda C, Hadchity E, Alphonse G, Chapet O, Rousson R, Rodriguez-Lafrasse C, et al. Radioresistance of human carcinoma cells is correlated to a defect in raft membrane clustering. Free Radic Biol Med. 2007;43:681–94.

64. Rivera M, Sukhdeo K, Yu J. Ionizing radiation in glioblastoma initiating cells. Front Oncol. 2013;3:74.

65. Wild-Bode C, Weller M, Rimner A, Dichgans J, Wick W. Sublethal Irradiation Promotes Migration and Invasiveness of Glioma Cells : Implications for Radiotherapy of Human Glioblastoma. Cancer Res. 2001;61:2744–50.

66. Friedman RL, Manly SP, McMahon M, Kerr IM, Stark GR. Transcriptional and posttranscriptional regulation of interferon-induced gene expression in human cells. Cell. 1984;38:745–55.

67. Kelly JM, Gilbert CS, Stark GR, Kerr IM. Differential regulation of interferon-induced mRNAs and c-myc mRNA by alpha- and gamma-interferons. Eur J Biochem. 1985;153:367–71.

68. Lewin AR, Reid LE, McMahon M, Stark GR, Kerr IM. Molecular analysis of a human interferon-inducible gene family. Eur J Biochem. 1991;199:417–23.

69. Sällman Almén M, Bringeland N, Fredriksson R, Schiöth HB. The dispanins: a novel gene family of ancient origin that contains 14 human members. PLoS One. 2012;7:e31961.

70. Brem R, Oraszlan-Szovik K, Foser S, Bohrmann B, Certa U. Inhibition of proliferation by 1-8U in interferon-alpha-responsive and non-responsive cell lines. Cell Mol Life Sci. 2003;60:1235–48.

71. Smith RA, Young J, Weis JJ, Weis JH. Expression of the mouse fragilis gene products in immune cells and association with receptor signaling complexes. Genes Immun. 2006;7:113–21.

72. Diamond MS, Farzan M. The broad-spectrum antiviral functions of IFIT and IFITM proteins. Nat Rev Immunol. Nature Publishing Group; 2013;13:46–57.

73. Yount JS, Karssemeijer R a, Hang HC. S-palmitoylation and ubiquitination differentially regulate interferon-induced transmembrane protein 3 (IFITM3)-mediated resistance to influenza virus. J Biol Chem. 2012;287:19631–41.

74. Bailey CC, Kondur HR, Huang I-C, Farzan M. Interferon-induced transmembrane protein 3 is a type II transmembrane protein. J Biol Chem. 2013;288:32184–93.

75. Tanaka SS, Yamaguchi YL, Tsoi B, Lickert H, Tam PPL. IFITM/Mil/fragilis family proteins IFITM1 and IFITM3 play distinct roles in mouse primordial germ cell homing and repulsion. Dev Cell. 2005;9:745–56.

76. Frey M, Appenheimer MM, Evans SS. Tyrosine Kinase-Dependent Regulation of L-Selectin Expression Through the Leu-13 Signal Transduction Molecule. J Immunol. 1997;158:5424–34.

77. Sato S, Miller a S, Howard MC, Tedder TF. Regulation of B lymphocyte development and activation by the CD19/CD21/CD81/Leu 13 complex requires the cytoplasmic domain of CD19. J Immunol. 1997;159:3278–87.

78. Brass AL, Huang I-C, Benita Y, John SP, Krishnan MN, Feeley EM, et al. The IFITM proteins mediate cellular resistance to influenza A H1N1 virus, West Nile virus, and dengue virus. Cell. Elsevier Ltd; 2009;139:1243–54.

79. Amini-Bavil-Olyaee S, Choi YJ, Lee JH, Shi M, Huang I-C, Farzan M, et al. The antiviral effector IFITM3 disrupts intracellular cholesterol homeostasis to block viral entry. Cell Host Microbe. Elsevier; 2013;13:452–64.

80. Hisamatsu T, Watanabe M, Ogata H. Interferon-inducible Gene Family 1-8U Expression in Colitis-associated Colon Cancer and Severely Inflamed Mucosa in Ulcerative Colitis. Cancer Res. 1999;59:5927–31.

81. Andreu P, Colnot S, Godard C, Laurent-Puig P, Lamarque D, Kahn A, et al. Identification of the IFITM family as a new molecular marker in human colorectal tumors. Cancer Res. 2006;66:1949–55.

82. Hatano H, Kudo Y, Ogawa I, Tsunematsu T, Kikuchi A, Abiko Y, et al. IFN-induced transmembrane protein 1 promotes invasion at early stage of head and neck cancer progression. Clin Cancer Res. 2008;14:6097–105.

83. Evans SS, Lee DB, Han T, Tomasi TB, Evans RL. Monoclonal antibody to the interferon-inducible protein Leu-13 triggers aggregation and inhibits proliferation of leukemic B cells. Blood. 1990;76:2583–93.

84. Huang H, Colella S, Kurrer M, Yonekawa Y, Kleihues P, Ohgaki H. Gene Expression Profiling of Low-Grade Diffuse Astrocytomas by cDNA Arrays. Cancer Res. 2000;60:6868–74.

85. Krepler C, Certa U, Wacheck V, Jansen B, Wolff K, Pehamberger H. Pegylated and conventional interferon-alpha induce comparable transcriptional responses and inhibition of tumor growth in a human melanoma SCID mouse xenotransplantation model. J Invest Dermatol. 2004;123:664–9.

86. El-Tanani MK, Jin D, Campbell FC, Johnston PG. Interferon-induced transmembrane 3 binds osteopontin in vitro: expressed in vivo IFITM3 reduced OPN expression. Oncogene. Nature Publishing Group; 2010;29:752–62.

87. Li D, Peng Z, Tang H, Wei P, Kong X, Yan D, et al. KLF4-mediated negative regulation of IFITM3 expression plays a critical role in colon cancer pathogenesis. Clin Cancer Res. 2011;17:3558–68.

88. Yu F, Ng SSM, Chow BKC, Sze J, Lu G, Poon WS, et al. Knockdown of interferon-induced transmembrane protein 1 (IFITM1) inhibits proliferation, migration, and invasion of glioma cells. J Neurooncol. 2011;103:187–95.

89. Zhao B, Wang H, Zong G, Li P. The role of IFITM3 in the growth and migration of human glioma cells. BMC Neurol. 2013;13:210.

90. Tsai M-H, Cook J a, Chandramouli GVR, DeGraff W, Yan H, Zhao S, et al. Gene expression profiling of breast, prostate, and glioma cells following single versus fractionated doses of radiation. Cancer Res. 2007;67:3845–52.

91. Clave E, Carosella ED, Gluckman E, Socié G. Radiation-enhanced expression of interferon-inducible genes in the KG1a primitive hematopoietic cell line. Leukemia. 1997;11:114–9.

92. Khodarev NN, Beckett M, Labay E, Darga T, Roizman B, Weichselbaum RR. STAT1 is overexpressed in tumors selected for radioresistance and confers protection from radiation in transduced sensitive cells. Proc Natl Acad Sci U S A. 2004;101:1714–9.

93. Kita K, Sugaya S, Zhai L, Wu YP, Wano C, Chigira S, et al. Involvement of LEU13 in Interferon-Induced Refractoriness of Human RSa Cells to Cell Killing by X Rays. Radiat Res. 2003;160:302–8.

94. Compston A, Coles A. Multiple sclerosis. Lancet. Elsevier Ltd; 2008;372:1502–17.

95. Talley CL. The emergence of multiple sclerosis, 1870-1950: a puzzle of historical epidemiology. Perspect Biol Med. 2005;48:383–95.

96. Kumar DR, Aslinia F, Yale SH, Mazza JJ. Jean-Martin Charcot: the father of neurology. Clin Med Res. 2011;9:46–9.

97. Clanet M. Jean-Martin Charcot 1825-1893. Int MS J. 2008;15:59–61.

98. Frohman EM, Racke MK, Raine CS. Multiple sclerosis--the plaque and its pathogenesis. N Engl J Med. 2006;354:942–55.

99. Hauser SL, Chan JR, Oksenberg JR. Multiple sclerosis: Prospects and promise. Ann Neurol. 2013;74:317–27.

100. Brønnum-Hansen H, Koch-Henriksen N, Stenager E. Trends in survival and cause of death in Danish patients with multiple sclerosis. Brain. 2004;127:844–50.

101. Sospedra M, Martin R. Immunology of multiple sclerosis. Annu Rev Immunol. 2005;23:683–747.

102. Anderson DW, Ellenberg JH, Leventhal CM, Reingold SC, Rodriguez M, Silberberg DH. Revised estimate of the prevalence of multiple sclerosis in the United States. Ann Neurol. 1992;31:333–6.

103. Kingwell E, Marriott JJ, Jetté N, Pringsheim T, Makhani N, Morrow S a, et al. Incidence and prevalence of multiple sclerosis in Europe: a systematic review. BMC Neurol. 2013;13:128.

104. WHO. Atlas Multiple Sclerosis Resources in the World. WHO Press, Geneva; 2008.

105. Dyment DA, Ebers GC, Sadovnick AD. Genetics of multiple sclerosis. Lancet Neurol. 2004;3:104–10.

106. Bertrams J, Kuwert E. HL-A Antigen Frequencies in Multiple Sclerosis. Eur Neurol. 1972;7:74–8.

107. Naito S, Namerow N, Mickey M, Terasaki P. Multiple Sclerosis: association with HL-A3. Tissue Antigens. 1972;2:1–4.

108. Beecham AH, Patsopoulos N a, Xifara DK, Davis MF, Kemppinen A, Cotsapas C, et al. Analysis of immune-related loci identifies 48 new susceptibility variants for multiple sclerosis. Nat Genet. 2013;45:1353–60.

109. Sawcer S, Hellenthal G, Pirinen M, Spencer CC a, Patsopoulos N a, Moutsianas L, et al. Genetic risk and a primary role for cell-mediated immune mechanisms in multiple sclerosis. Nature. 2011;476:214–9.

110. O'Gorman C, Lucas R, Taylor B. Environmental risk factors for multiple sclerosis: a review with a focus on molecular mechanisms. Int J Mol Sci. 2012;13:11718–52.

111. Compston A. Risk factors for multiple sclerosis: race or place? J Neurol Neurosurg Psychiatry. 1990;53:821–3.

112. Sibley WA, Bamford CR, Clark K. Clinical viral infections and multiple sclerosis. Lancet. 1985;1:1313–5.

113. Lang HLE, Jacobsen H, Ikemizu S, Andersson C, Harlos K, Madsen L, et al. A functional and structural basis for TCR cross-reactivity in multiple sclerosis. Nat Immunol. 2002;3:940–3.

114. Albert LJ, Inman RD. Molecular Mimicry and Autoimmunity. N Engl J Med. 1999;341:2068–74.

115. Thomson A. FTY720 in multiple sclerosis: the emerging evidence of its therapeutic value. Core Evid. 2006;1:157–67.

116. Keegan BM, Noseworthy JH. Multiple sclerosis. Annu Rev Med. 2002;53:285–302.

117. Trapp BD, Peterson J, Ransohoff RM, Rudick R, Mörk S, Bö L. Axonal transection in the lesions of multiple sclerosis. N Engl J Med. 1998;338:278–85.

118. Ferguson B, Matyszak MK, Esiri MM, Perry VH. Axonal damage in acute multiple sclerosis lesions. Brain. 1997;120 (Pt 3:393–9.

119. Traugott U, Reinherz EL, Raine CS. Multiple Sclerosis : Distribution of T Cell Subsets Within Active Chronic Lesions. Science (80-). 1983;219:308–10.

120. Kuhlmann T, Lassmann H, Brück W. Diagnosis of inflammatory demyelination in biopsy specimens: a practical approach. Acta Neuropathol. 2008;115:275–87.

121. Benveniste EN. Role of macrophages/microglia in multiple sclerosis and experimental allergic encephalomyelitis. J Mol Med (Berl). 1997;75:165–73.

122. McFarland HF, Martin R. Multiple sclerosis: a complicated picture of autoimmunity. Nat Immunol. 2007;8:913–9.

123. Satoh J, Lee YB, Kim SU. T-cell costimulatory molecules B7-1 (CD80) and B7-2 (CD86) are expressed in human microglia but not in astrocytes in culture. Brain Res. 1995;704:92–6.

124. Hemmer B, Nessler S, Zhou D, Kieseier B, Hartung H-P. Immunopathogenesis and immunotherapy of multiple sclerosis. Nat Clin Pract Neurol. 2006;2:201–11.

125. Charo IF, Ransohoff RM. The many roles of chemokines and chemokine receptors in inflammation. N Engl J Med. 2006;354:610–21.

126. Ransohoff RM, Perry VH. Microglial physiology: unique stimuli, specialized responses. Annu Rev Immunol. 2009;27:119–45.

127. Wekerle H, Sun D, Oropeza-Wekerle RL, Meyermann R. Immune reactivity in the nervous system: modulation of T-lymphocyte activation by glial cells. J Exp Biol. 1987;132:43–57.

128. Engelhardt B, Ransohoff RM. The ins and outs of T-lymphocyte trafficking to the CNS: anatomical sites and molecular mechanisms. Trends Immunol. 2005;26:485–95.

129. Tompkins SM, Padilla J, Dal Canto MC, Ting JP-Y, Van Kaer L, Miller SD. De novo central nervous system processing of myelin antigen is required for the initiation of experimental autoimmune encephalomyelitis. J Immunol. 2002;168:4173–83.

130. Chastain EML, Duncan DS, Rodgers JM, Miller SD. The role of antigen presenting cells in multiple sclerosis. Biochim Biophys Acta. Elsevier B.V.; 2011;1812:265–74.

131. Kawakami N, Nägerl UV, Odoardi F, Bonhoeffer T, Wekerle H, Flügel A. Live imaging of effector cell trafficking and autoantigen recognition within the unfolding autoimmune encephalomyelitis lesion. J Exp Med. 2005;201:1805–14.

132. Kuhlmann T, Lingfeld G, Bitsch A, Schuchardt J, Bru W. Acute axonal damage in multiple sclerosis is most extensive in early disease stages and decreases over time. Brain. 2002;125:2202–12.

133. Hu D, Ikizawa K, Lu L, Sanchirico ME, Shinohara ML, Cantor H. Analysis of regulatory CD8 T cells in Qa-1-deficient mice. Nat Immunol. 2004;5:516–23.

134. Bitsch A, Schuchardt J, Bunkowski S, Kuhlmann T, Brück W. Acute axonal injury in multiple sclerosis Correlation with demyelination and inflammation. Brain. 2000;123:1174–83.

135. Korn T, Reddy J, Gao W, Bettelli E, Awasthi A, Petersen TR, et al. Myelin-specific regulatory T cells accumulate in the CNS but fail to control autoimmune inflammation. Nat Med. 2007;13:423–31.

136. Cepok S, Jacobsen M, Schock S, Omer B, Jaekel S, Böddeker I, et al. Patterns of cerebrospinal fluid pathology correlate with disease progression in multiple sclerosis. Brain. 2001;124:2169–76.

137. Hartung H-P, Kieseier BC. Atacicept: targeting B cells in multiple sclerosis. Ther Adv Neurol Disord. 2010;3:205–16.

138. Hauser SL, Waubant E, Arnold DL, Vollmer T, Antel J, Fox RJ, et al. B-Cell Depletion with Rituximab in Relapsing–Remitting Multiple Sclerosis. N Engl J Med. 2008;358:676–88.

139. Wootla B, Denic A, Keegan BM, Winters JL, Astapenko D, Warrington AE, et al. Evidence for the role of B cells and immunoglobulins in the pathogenesis of multiple sclerosis. Neurol Res Int. 2011;2011:780712.

140. Cross AH, Stark JL, Lauber J, Ramsbottom MJ, Lyons J-A. Rituximab reduces B cells and T cells in cerebrospinal fluid of multiple sclerosis patients. J Neuroimmunol. 2006;180:63–70.

141. Rivers TM, Sprunt DH, Berry GP. Observations on attempts to produce acute disseminated encephalomyelitis in monkeys. J Exp Med. 1933;58:39–53.

142. Batoulis H, Recks MS, Addicks K, Kuerten S. Experimental autoimmune encephalomyelitis--achievements and prospective advances. APMIS. 2011;119:819–30.

143. Ransohoff RM. Animal models of multiple sclerosis: the good, the bad and the bottom line. Nat Neurosci. Nature Publishing Group; 2012;15:1074–7.

144. Gao Z, Tsirka SE. Animal Models of MS Reveal Multiple Roles of Microglia in Disease Pathogenesis. Neurol Res Int. 2011;2011:383087.

145. Rangachari M, Kuchroo VK. Using EAE to better understand principles of immune function and autoimmune pathology. J Autoimmun. Elsevier Ltd; 2013;45:31–9.

146. Einstein ER, Robertson DM, Dicaprio JM, Moore W. The isolation from bovine spinal cord of a homogeneous protein with encephalitogenic activity. J Neurochem. 1962;9:353–61.

147. Laatsch BYRH, Kies MW, Gordon S, Alvord EC. The encephalomyelitic activity of myelin isolated by ultracentrifugation. J Exp Med. 1962;Apr 1; 115:777–88.

148. Tuohy VK, Sobel R a, Lu Z, Laursen R a, Lees MB. Myelin proteolipid protein: minimum sequence requirements for active induction of autoimmune encephalomyelitis in SWR/J and SJL/J mice. J Neuroimmunol. 1992;39:67–74.

149. Lebar R, Lubetzki C, Vincent C, Lombrail P, Boutry JM. The M2 autoantigen of central nervous system myelin, a glycoprotein present in oligodendrocyte membrane. Clin Exp Immunol. 1986;66:423–34.

150. Mendel I, Kerlero de Rosbo N, Ben-Nun a. A myelin oligodendrocyte glycoprotein peptide induces typical chronic experimental autoimmune encephalomyelitis in H-2b mice: fine specificity and T cell receptor V beta expression of encephalitogenic T cells. Eur J Immunol. 1995;25:1951–9.

151. Munoz JJ, Bernard CCA, Mackay IR. Elicitation of Experimental Allergic Encephalomyelitis in Mica with the Aid of Pertussigen. Cell Immunol. 1984;83:92–100.

152. Targoni OS, Baus J, Hofstetter HH, Hesse MD, Karulin a Y, Boehm BO, et al. Frequencies of neuroantigen-specific T cells in the central nervous system versus the immune periphery during the course of experimental allergic encephalomyelitis. J Immunol. 2001;166:4757–64.

153. Berard JL, Wolak K, Fournier S, David S. Characterization of relapsing-remitting and chronic forms of experimental autoimmune encephalomyelitis in C57BL/6 mice. Glia. 2010;58:434–45.

154. Krishnamoorthy G, Wekerle H. EAE: an immunologist's magic eye. Eur J Immunol. 2009;39:2031–5.

155. Starr TK, Jameson SC, Hogquist K a. Positive and negative selection of T cells. Annu Rev Immunol. 2003;21:139–76.

156. Drayton DL, Liao S, Mounzer RH, Ruddle NH. Lymphoid organ development: from ontogeny to neogenesis. Nat Immunol. 2006;7:344–53.

157. Mills KHG. Induction, function and regulation of IL-17-producing T cells. Eur J Immunol. 2008;38:2636–49.

158. Mosmann TR, Coffman RL. TH1 and TH2 cells: different patterns of lymphokine secretion lead to different functional properties. Annu Rev Immunol. 1989;7:145–73.

159. Abbas AK, Murphy KM, Sher A. Functional diversity of helper T lymphcytes. Nature. 1996;383:787–93.

160. Murphy KM, Reiner SL. The lineage decisions of helper T cells. Nat Rev Immunol. 2002;2:933–44.

161. Gor DO, Rose NR, Greenspan NS. TH1-TH2: a procrustean paradigm. Nat Immunol. 2003;4:503–5.

162. Nakayamada S, Takahashi H, Kanno Y, O'Shea JJ. Helper T cell diversity and plasticity. Curr Opin Immunol. Elsevier Ltd; 2012;24:297–302.

163. Infante-Duarte C, Horton HF, Byrne MC, Kamradt T. Microbial lipopeptides induce the production of IL-17 in Th cells. J Immunol. 2000;165:6107–15.

164. Kanno Y, Vahedi G, Hirahara K, Singleton K, O'Shea JJ. Transcriptional and epigenetic control of T helper cell specification: molecular mechanisms underlying commitment and plasticity. Annu Rev Immunol. 2012;30:707–31.

165. Jadidi-Niaragh F, Mirshafiey a. Th17 cell, the new player of neuroinflammatory process in multiple sclerosis. Scand J Immunol. 2011;74:1–13.

166. Jäger a, Kuchroo VK. Effector and regulatory T-cell subsets in autoimmunity and tissue inflammation. Scand J Immunol. 2010;72:173–84.

167. Codarri L, Gyülvészi G, Tosevski V, Hesske L, Fontana A, Magnenat L, et al. RORγt drives production of the cytokine GM-CSF in helper T cells, which is essential for the effector phase of autoimmune neuroinflammation. Nat Immunol. Nature Publishing Group; 2011;12:560–7.

168. El-Behi M, Ciric B, Dai H, Yan Y, Cullimore M, Safavi F, et al. The encephalitogenicity of T(H)17 cells is dependent on IL-1- and IL-23-induced production of the cytokine GM-CSF. Nat Immunol. Nature Publishing Group; 2011;12:568–75.

169. Bettelli E, Korn T, Kuchroo VK. Th17: the third member of the effector T cell trilogy. Curr Opin Immunol. 2007;19:652–7.

170. Wilson NJ, Boniface K, Chan JR, McKenzie BS, Blumenschein WM, Mattson JD, et al. Development, cytokine profile and function of human interleukin 17-producing helper T cells. Nat Immunol. 2007;8:950–7.

171. Luckheeram RV, Zhou R, Verma AD, Xia B. CD4+T cells: Differentiation and Functions. Clin Dev Immunol. 2012;2012:925135.

172. Merrill JE, Kono DH, Clayton J, Ando DG, Hinton DR, Hofman FM. Inflammatory leukocytes and cytokines in the peptide-induced disease of experimental allergic encephalomyelitis in SJL and B10.PL mice. Proc Natl Acad Sci U S A. 1992;89:574–8.

173. Mix E, Olsson T, Correale J, Kostulas V, Link H. CD4+, CD8+, and CD4- CD8- T cells in CSF and blood of patients with multiple sclerosis and tension headache. Scand J Immunol. 1990;31:493–501.

174. Olsson T, Zhi WW, Hojeberg B, Kostulas V, Yu-Ping J, Anderson G, et al. Autoreactive T lymphocytes in Multiple Sclerosis Determined by Antigen-induced Secretion of Interferon-gamma. J Clin Invest. 1990;86:981–5.

175. Zhang G-X, Yu S, Gran B, Li J, Siglienti I, Chen X, et al. Role of IL-12 receptor beta 1 in regulation of T cell response by APC in experimental autoimmune encephalomyelitis. J Immunol. 2003;171:4485–92.

176. Mondal S, Roy A, Pahan K. Functional blocking monoclonal antibodies against IL-12p40 homodimer inhibit adoptive transfer of experimental allergic encephalomyelitis. J Immunol. 2009;182:5013–23.

177. Gran B, Zhang G-X, Yu S, Li J, Chen X-H, Ventura ES, et al. IL-12p35-deficient mice are susceptible to experimental autoimmune encephalomyelitis: evidence for redundancy in the IL-12 system in the induction of central nervous system autoimmune demyelination. J Immunol. 2002;169:7104–10.

178. Ferber IA, Brocke S, Taylor-edwards C, Ridgway W, Dinisco C, Steinman L, et al. Mice with a disrupted IFN-gamma gene are susceptible to the induction of experimental autoimmune encephalomyelitis (EAE). J Immunol. 1995;156:5–7.

179. Cua DJ, Sherlock J, Chen Y, Murphy C a, Joyce B, Seymour B, et al. Interleukin-23 rather than interleukin-12 is the critical cytokine for autoimmune inflammation of the brain. Nature. 2003;421:744–8.

180. Langrish CL, Chen Y, Blumenschein WM, Mattson J, Basham B, Sedgwick JD, et al. IL-23 drives a pathogenic T cell population that induces autoimmune inflammation. J Exp Med. 2005;201:233–40.

181. Ivanov II, McKenzie BS, Zhou L, Tadokoro CE, Lepelley A, Lafaille JJ, et al. The orphan nuclear receptor RORgammat directs the differentiation program of proinflammatory IL-17+ T helper cells. Cell. 2006;126:1121–33.

182. Hofstetter HH, Ibrahim SM, Koczan D, Kruse N, Weishaupt A, Toyka K V, et al. Therapeutic efficacy of IL-17 neutralization in murine experimental autoimmune encephalomyelitis. Cell Immunol. 2005;237:123–30.

183. Park H, Li Z, Yang XO, Chang SH, Nurieva R, Wang Y-H, et al. A distinct lineage of CD4 T cells regulates tissue inflammation by producing interleukin 17. Nat Immunol. 2005;6:1133–41.

184. Komiyama Y, Nakae S, Matsuki T, Nambu A, Ishigame H, Kakuta S, et al. IL-17 plays an important role in the development of experimental autoimmune encephalomyelitis. J Immunol. 2006;177:566–73.

185. Huppert J, Closhen D, Croxford A, White R, Kulig P, Pietrowski E, et al. Cellular mechanisms of IL-17-induced blood-brain barrier disruption. FASEB J. 2010;24:1023–34.

186. Thakker P, Leach MW, Kuang W, Benoit SE, Leonard JP, Marusic S. IL-23 Is Critical in the Induction but Not in the Effector Phase of Experimental Autoimmune Encephalomyelitis. J Immunol. 2007;178:2589–98.

187. Chen Y, Langrish CL, Mckenzie B, Joyce-Shaikh B, Stumhofer JS, Mcclanahan T, et al. Anti-IL-23 therapy inhibits multiple inflammatory pathways and ameliorates autoimmune encephalomyelitis. J Clin Invest. 2006;116:1317–26.

188. Zhou L, Chong MMW, Littman DR. Plasticity of CD4+ T cell lineage differentiation. Immunity. Elsevier Inc.; 2009;30:646–55.

189. Hirota K, Duarte JH, Veldhoen M, Hornsby E, Li Y, Cua DJ, et al. Fate mapping of IL-17-producing T cells in inflammatory responses. Nat Immunol. Nature Publishing Group; 2011;12:255–63.

190. Ghoreschi K, Laurence A, Yang X-P, Tato CM, McGeachy MJ, Konkel JE, et al. Generation of pathogenic T(H)17 cells in the absence of TGF-β signalling. Nature. 2010;467:967–71.

191. Yeh W-I, McWilliams IL, Harrington LE. Autoreactive Tbet-positive CD4 T cells develop independent of classic Th1 cytokine signaling during experimental autoimmune encephalomyelitis. J Immunol. 2011;187:4998–5006.

192. Lee YK, Turner H, Maynard CL, Oliver JR, Elson CO, Weaver CT. Late Developmental Plasticity in the T Helper 17 Lineage. Immunity. 2009;30:92–107.

193. Lexberg MH, Taubner A, Förster A, Albrecht I, Richter A, Kamradt T, et al. Th memory for interleukin-17 expression is stable in vivo. Eur J Immunol. 2008;38:2654–64.

194. Bending D, Peña HD La, Veldhoen M, Phillips JM, Uyttenhove C, Stockinger B, et al. Highly purified Th17 cells from BDC2 .5NOD mice convert into Th1-like cells in NOD / SCID recipient mice. J Clin Invest. 2009;119:565–72.

195. Shi G, Cox C a, Vistica BP, Tan C, Wawrousek EF, Gery I. Phenotype switching by inflammation-inducing polarized Th17 cells, but not by Th1 cells. J Immunol. 2008;181:7205–13.

196. Yang Y, Weiner J, Liu Y, Smith AJ, Huss DJ, Winger R, et al. T-bet is essential for encephalitogenicity of both Th1 and Th17 cells. J Exp Med. 2009;206:1549–64.

197. Gocke AR, Cravens PD, Ben L-H, Hussain RZ, Northrop SC, Racke MK, et al. T-bet regulates the fate of Th1 and Th17 lymphocytes in autoimmunity. J Immunol. 2007;178:1341–8.

198. Bettelli E, Carrier Y, Gao W, Korn T, Strom TB, Oukka M, et al. Reciprocal developmental pathways for the generation of pathogenic effector TH17 and regulatory T cells. Nature. 2006;441:235–8.

199. Chen W, Jin W, Hardegen N, Lei K-J, Li L, Marinos N, et al. Conversion of peripheral CD4+CD25- naive T cells to CD4+CD25+ regulatory T cells by TGF-beta induction of transcription factor Foxp3. J Exp Med. 2003;198:1875–86.

200. Voo KS, Wang Y-H, Santori FR, Boggiano C, Wang Y-H, Arima K, et al. Identification of IL-17-producing FOXP3+ regulatory T cells in humans. Proc Natl Acad Sci U S A. 2009;106:4793–8.

201. O'Shea JJ, Paul WE. Mechanisms underlying lineage commitment and plasticity of helper CD4+ T cells. Science. 2010;327:1098–102.

202. Zhou L, Lopes JE, Chong MMW, Ivanov II, Min R, Victora GD, et al. TGF-beta-induced Foxp3 inhibits T(H)17 cell differentiation by antagonizing RORgammat function. Nature. 2008;453:236–40.

203. Mukasa R, Balasubramani A, Lee YK, Whitley SK, Weaver BT, Shibata Y, et al. Epigenetic instability of cytokine and transcription factor gene loci underlies plasticity of the T helper 17 cell lineage. Immunity. Elsevier Ltd; 2010;32:616–27.

204. Shaw JP, Utz PJ, Durand DB, Toole JJ, Emmel E a, Crabtree GR. Identification of a putative regulator of early T cell activation genes. Science. 1988;241:202–5.

205. Serfling E, Avots A, Klein-Hessling S, Rudolf R, Vaeth M, Berberich-Siebelt F. NFATc1/αA: The other Face of NFAT Factors in Lymphocytes. Cell Commun Signal. Cell Communication and Signaling; 2012;10:16.

206. Serfling E, Berberich-Siebelt F, Chuvpilo S, Jankevics E, Klein-Hessling S, Twardzik T, et al. The role of NF-AT transcription factors in T cell activation and differentiation. Biochim Biophys Acta. 2000;1498:1–18.

207. Beals CR, Clipstone N a, Ho SN, Crabtree GR. Nuclear localization of NF-ATc by a calcineurin-dependent, cyclosporin-sensitive intramolecular interaction. Genes Dev. 1997;11:824–34.

208. Hermann-Kleiter N, Baier G. NFAT pulls the strings during CD4+ T helper cell effector functions. Blood. 2010;115:2989–97.

209. Baine I, Abe BT, Macian F. Regulation of T-cell tolerance by calcium/NFAT signaling. Immunol Rev. 2009;231:225–40.

210. Macian F. NFAT proteins: key regulators of T-cell development and function. Nat Rev Immunol. 2005;5:472–84.

211. Avots a, Buttmann M, Chuvpilo S, Escher C, Smola U, Bannister a J, et al. CBP/p300 integrates Raf/Rac-signaling pathways in the transcriptional induction of NF-ATc during T cell activation. Immunity. 1999;10:515–24.

212. Crabtree GR. Generic signals and specific outcomes: signaling through Ca2+, calcineurin, and NF-AT. Cell. 1999;96:611–4.

213. Treisman R. Regulation of transcription by MAP kinase cascades. Curr Opin Cell Biol. 1996;8:205–15.

214. Soto-Nieves N, Puga I, Abe BT, Bandyopadhyay S, Baine I, Rao A, et al. Transcriptional complexes formed by NFAT dimers regulate the induction of T cell tolerance. J Exp Med. 2009;206:867–76.

215. Serfling E, Klein-Hessling S, Palmetshofer A, Bopp T, Stassen M, Schmitt E. NFAT transcription factors in control of peripheral T cell tolerance. Eur J Immunol. 2006;36:2837–43.

216. Shen F, Hu Z, Goswami J, Gaffen SL. Identification of common transcriptional regulatory elements in interleukin-17 target genes. J Biol Chem. 2006;281:24138–48.

217. Kaufman DB, Shapiro R, Lucey MR, Cherikh WS, T Bustami R, Dyke DB. Immunosuppression: practice and trends. Am J Transplant. 2004;4 Suppl 9:38–53.

218. Kiani A, Rao A, Aramburu J. Manipulating Immune Responses with Immunosuppressive Agents that Target NFAT. Immunity. 2000;12:359–72.

219. Brabletz T, Pietrowski I, Serfling E. The immunosuppressives FK 506 and cyclosporin A inhibit the generation of protein factors binding to the two purine boxes of the interleukin 2 enhancer. Nucleic Acids Res. 1991;19:61–7.

220. Emmel E a, Verweij CL, Durand DB, Higgins KM, Lacy E, Crabtree GR. Cyclosporin A specifically inhibits function of nuclear proteins involved in T cell activation. Science. 1989;246:1617–20.

221. Macián F, García-Rodríguez C, Rao a. Gene expression elicited by NFAT in the presence or absence of cooperative recruitment of Fos and Jun. EMBO J. 2000;19:4783–95.

222. Satoh E, Mabuchi T, Satoh H, Asahara T, Nukui H, Naganuma H. Reduced expression of the transporter associated with antigen processing 1 molecule in malignant glioma cells, and its restoration by interferon-gamma and -beta. J Neurosurg. 2006/03/03 ed. 2006;104:264–71.

223. Xu Q, Liu G, Yuan X, Xu M, Wang H, Ji J, et al. Antigen-specific T-cell response from dendritic cell vaccination using cancer stem-like cell-associated antigens. Stem Cells. 2009/06/19 ed. 2009;27:1734–40.

224. Pellegatta S, Poliani PL, Corno D, Menghi F, Ghielmetti F, Suarez-Merino B, et al. Neurospheres enriched in cancer stem-like cells are highly effective in eliciting a dendritic cell-mediated immune response against malignant gliomas. Cancer Res. 2006;66:10247–52.

225. Wei J, Barr J, Kong LY, Wang Y, Wu A, Sharma AK, et al. Glioma-associated cancer-initiating cells induce immunosuppression. Clin Cancer Res. 2010/01/14 ed. 2010;16:461–73.

226. Santin AD, Hermonat PL, Hiserodt JC, Chiriva-Internati M, Woodliff J, Theus JW, et al. Effects of irradiation on the expression of major histocompatibility complex class I antigen and adhesion costimulation mulecules ICAM-1 in human cervical cancer. Int J Radiat Oncol Biol Phys. 1997;39:737–42.

227. Muranski P, Borman Z a, Kerkar SP, Klebanoff C a, Ji Y, Sanchez-Perez L, et al. Th17 cells are long lived and retain a stem cell-like molecular signature. Immunity. Elsevier Inc.; 2011;35:972–85.

228. Raddatz BBR, Hansmann F, Spitzbarth I, Kalkuhl A, Deschl U, Baumgärtner W, et al. Transcriptomic meta-analysis of multiple sclerosis and its experimental models. PLoS One. 2014;9:e86643.

229. Reits EA, Hodge JW, Herberts CA, Groothuis TA, Chakraborty M, Wansley EK, et al. Radiation modulates the peptide repertoire, enhances MHC class I expression, and induces successful antitumor immunotherapy. J Exp Med. 2006;203:1259–71.

230. Joo KM, Jin J, Kim E, Ho Kim K, Kim Y, Gu Kang B, et al. MET signaling regulates glioblastoma stem cells. Cancer Res. 2012;72:3828–38.

231. Wang J, Wakeman TP, Lathia JD, Hjelmeland AB, Wang X-F, White RR, et al. Notch promotes radioresistance of glioma stem cells. Stem Cells. 2010;28:17–28.

232. Hemler ME. Tetraspanin proteins promote multiple cancer stages. Nat Rev Cancer. Nature Publishing Group; 2013;14:49–60.

233. Sehgal A, Boynton AL, Young RF, Vermeulen SS, Yonemura KS, Kohler EP, et al. Cell adhesion molecule Nr-CAM is over-expressed in human brain tumors. Int J cancer. 1998;76:451–8.

234. Curtsinger JM, Agarwal P, Lins DC, Mescher MF. Autocrine IFN-γ promotes naive CD8 T cell differentiation and synergizes with IFN-α to stimulate strong function. J Immunol. 2012;189:659–68.

235. Dunn GP, Dunn IF, Curry WT. Focus on TILs: Prognostic significance of tumor infiltrating lymphocytes in human glioma. Cancer Immun. 2007;7:12.

236. Kimchi A. Cytokine triggered molecular pathways that control cell cycle arrest. J Cell Biochem. 1992;50:1–9.

237. Brem R, Oraszlan-Szovik K, Foser S, Bohrmann B, Certa U. Inhibition of proliferation by 1-8U in interferon-alpha-responsive and non-responsive cell lines. Cell Mol Life Sci. 2003;60:1235–48.

238. Weng L, Dai H, Zhan Y, He Y, Stepaniants SB, Bassett DE. Rosetta error model for gene expression analysis. Bioinformatics. 2006;22:1111–21.

239. Yoshida H, Nishina H, Takimoto H, Marengère LE, Wakeham a C, Bouchard D, et al. The transcription factor NF-ATc1 regulates lymphocyte proliferation and Th2 cytokine production. Immunity. 1998;8:115–24.

240. Hock M, Vaeth M, Rudolf R, Patra AK, Pham DAT, Muhammad K, et al. NFATc1 induction in peripheral T and B lymphocytes. J Immunol. 2013;190:2345–53.

241. Quintana FJ, Basso AS, Iglesias AH, Korn T, Farez MF, Bettelli E, et al. Control of T(reg) and T(H)17 cell differentiation by the aryl hydrocarbon receptor. Nature. 2008;453:65–71.

242. Carson MJ, Doose JM, Melchior B, Schmid CD, Ploix CC. CNS immune privilege: hiding in plain sight. Immunol Rev. 2006;213:48–65.

243. Sharma A, Bode B, Wenger RH, Lehmann K, Sartori A a, Moch H, et al. γ-Radiation promotes immunological recognition of cancer cells through increased expression of cancer-testis antigens in vitro and in vivo. PLoS One. 2011;6:e28217.

244. Alapati K, Gopinath S, Malla RR, Dasari VR, Rao JS. uPAR and cathepsin B knockdown inhibits radiation-induced PKC integrated integrin signaling to the cytoskeleton of glioma-initiating cells. Int J Oncol. 2012;41:599–610.

245. De Rosa A, Pellegatta S, Rossi M, Tunici P, Magnoni L, Speranza MC, et al. A radial glia gene marker, fatty acid binding protein 7 (FABP7), is involved in proliferation and invasion of glioblastoma cells. PLoS One. 2012;7:e52113.

246. Santana P, Peña L a, Haimovitz-Friedman a, Martin S, Green D, McLoughlin M, et al. Acid sphingomyelinase-deficient human lymphoblasts and mice are defective in radiation-induced apoptosis. Cell. 1996;86:189–99.

247. Hemler ME. Tetraspanin functions and associated microdomains. Nat Rev Mol Cell Biol. 2005;6:801–11.

248. Inui S, Higashiyama S, Hashimoto K, Higashiyama M, Yoshikawa K, Taniguchi N. Possible Role of Coexpression of CD9 With EGF-Like Growth Factor and Amphiregulin in Cultured Human Keratinocyte Growth. J Cell Physiol. 1997;171:291–8.

249. Carloni V, Mazzocca A, Ravichandran KS. Tetraspanin CD81 is linked to ERK/MAPKinase signaling by Shc in liver tumor cells. Oncogene. 2004;23:1566–74.

250. Oren R, Takahashi S, Doss C, Levy R, Levy S. TAPA-1, the target of an antiproliferative antibody, defines a new family of transmembrane proteins. Mol Cell Biol. 1990;10:4007–15.

251. Rajasekhar VK, Studer L, Gerald W, Socci ND, Scher HI. Tumour-initiating stem-like cells in human prostate cancer exhibit increased NF-κB signalling. Nat Commun. Nature Publishing Group; 2011;2:162.

252. Li Q, Yang XH, Xu F, Sharma C, Wang H-X, Knoblich K, et al. Tetraspanin CD151 plays a key role in skin squamous cell carcinoma. Oncogene. 2013;32:1772–83.

253. Seliger B, Harders C, Lohmann S, Momburg F, Urlinger S, Tampé R, et al. Down-regulation of the MHC class I antigen-processing machinery after oncogenic transformation of murine fibroblasts. Eur J Immunol. 1998;28:122–33.

254. Bicknell DC, Kaklamanis L, Hampson R, Bodmer WF, Karran P. Selection for beta 2-microglobulin mutation in mismatch repair-defective colorectal carcinomas. Curr Biol. 1996;6:1695–7.

255. Challa-Malladi M, Lieu YK, Califano O, Holmes AB, Bhagat G, Murty V V, et al. Combined genetic inactivation of β2-Microglobulin and CD58 reveals frequent escape from immune recognition in diffuse large B cell lymphoma. Cancer Cell. Elsevier Inc.; 2011;20:728–40.

256. Newcomb EW, Demaria S, Lukyanov Y, Shao Y, Schnee T, Kawashima N, et al. The combination of ionizing radiation and peripheral vaccination produces long-term survival of mice bearing established invasive GL261 gliomas. Clin cancer Res. 2006;12:4730–7.

257. Fadul CE, Fisher JL, Gui J, Hampton TH, Côté Anik L, Ernstoff MS. Immune modulation effects of concomitant temozolomide and radiation therapy on patients with glioblastoma multiforme. Neuro Oncol. 2011;13:393–400.

258. Miller CHT, Maher SG, Young H a. Clinical Use of Interferon-gamma. Ann N Y Acad Sci. 2009;1182:69–79.

259. Fujita M, Scheurer ME, Decker S a, McDonald H a, Kohanbash G, Kastenhuber ER, et al. Role of type 1 IFNs in antiglioma immunosurveillance--using mouse studies to guide examination of novel prognostic markers in humans. Clin Cancer Res. 2010;16:3409–19.

260. Shankaran V, Ikeda H, Bruce a T, White JM, Swanson PE, Old LJ, et al. IFNgamma and lymphocytes prevent primary tumour development and shape tumour immunogenicity. Nature. 2001;410:1107–11.

261. Rich JN. Cancer stem cells in radiation resistance. Cancer Res. 2007;67:8980–4.

262. Xu Y, Yang G, Hu G. Binding of IFITM1 enhances the inhibiting effect of caveolin-1 on ERK activation. Acta Biochim Biophys Sin. 2009;41:488–94.

263. Meilinger D, Fellinger K, Bultmann S, Rothbauer U, Bonapace IM, Klinkert WEF, et al. Np95 interacts with de novo DNA methyltransferases, Dnmt3a and Dnmt3b, and mediates epigenetic silencing of the viral CMV promoter in embryonic stem cells. EMBO Rep. Nature Publishing Group; 2009;10:1259–64.

264. Xia X, Zhang Y, Zieth CR, Zhang S-C. Transgenes delivered by lentiviral vector are suppressed in human embryonic stem cells in a promotor-dependent manner. Stem Cells Dev. 2007;16:167–76.

265. Evans SS, Collea RP, Appenheimer MM, Gollnick SO. Interferon-alpha induces the expression of the L-selectin homing receptor in human B lymphoid cells. J Cell Biol. 1993;123:1889–98.

266. Saitou M, Barton SC, Surani MA. A molecular programme for the specification of germ cell fate in mice. Nature. 2002;418:293–300.

267. Panitch HS, Hirsch RL, Haley AS, Johnson KP. EXACERBATIONS OF MULTIPLE SCLEROSIS IN PATIENTS TREATED WITH GAMMA INTERFERON. Lancet. 1987;893–4.

268. Muñoz-Culla M, Irizar H, Otaegui D. The genetics of multiple sclerosis: review of current and emerging candidates. Appl Clin Genet. 2013;6:63–73.

269. Lexberg MH, Taubner A, Albrecht I, Lepenies I, Richter A, Kamradt T, et al. IFN-γ and IL-12 synergize to convert in vivo generated Th17 into Th1/Th17 cells. Eur J Immunol. 2010;40:3017–27.

270. Peck A, Mellins ED. Plasticity of T-cell phenotype and function: the T helper type 17 example. Immunology. 2010;129:147–53.

271. Duhen R, Glatigny S, Arbelaez CA, Blair TC, Oukka M, Bettelli E. Cutting edge: the pathogenicity of IFN-γ-producing Th17 cells is independent of T-bet. J Immunol. 2013;190:4478–82.

272. Gelman AE, Zhang J, Choi Y, Turka L a. Toll-like receptor ligands directly promote activated CD4+ T cell survival. J Immunol. 2004;172:6065–73.

273. Komai-Koma M, Jones L, Ogg GS, Xu D, Liew FY. TLR2 is expressed on activated T cells as a costimulatory receptor. Proc Natl Acad Sci U S A. 2004;101:3029–34.

274. Mansson A, Adner M, Cardell LO. Toll-like receptors in cellular subsets of human tonsil T cells: altered expression during recurrent tonsillitis. Respir Res. 2006;7:36.

275. Crellin NK, Garcia R V, Hadisfar O, Allan SE, Steiner TS, Levings MK. Human CD4+ T cells express TLR5 and its ligand flagellin enhances the suppressive capacity and expression of FOXP3 in CD4+CD25+ T regulatory cells. J Immunol. 2005;175:8051–9.

276. Zastepa E, Fitz-Gerald L, Hallett M, Antel J, Bar-Or A, Baranzini S, et al. Naive CD4 T-cell activation identifies MS patients having rapid transition to progressive MS. Neurology. 2014;

277. Yang K, Chi H. Metabolic Control of Th17 Cell Generation and CNS Inflammation. J Neurol Neurophysiol. 2014;S12.

278. Giorelli M, Livrea P, Minervini MG, Trojano M. Immunomodulatory properties of increased levels of liver X receptor beta in peripheral blood mononuclear cells from multiple sclerosis patients. Exp Neurol. 2007;204:759–66.

279. Weinstock-Guttman B, Zivadinov R, Mahfooz N, Carl E, Drake A, Schneider J, et al. Serum lipid profiles are associated with disability and MRI outcomes in multiple sclerosis. J Neuroinflammation. BioMed Central Ltd; 2011;8:127.

280. Izsepi E, Himer L, Szilagyi O, Hajdu P, Panyi G, Laszlo G, et al. Membrane microdomain organization, calcium signal, and NFAT activation as an important axis in polarized Th cell function. Cytometry A. 2013;83:185–96.

281. Surls J, Nazarov-Stoica C, Kehl M, Olsen C, Casares S, Brumeanu T-D. Increased membrane cholesterol in lymphocytes diverts T-cells toward an inflammatory response. PLoS One. 2012;7:e38733.

282. Tontonoz P, Mangelsdorf DJ. Liver X receptor signaling pathways in cardiovascular disease. Mol Endocrinol. 2003;17:985–93.

283. Bensinger SJ, Bradley MN, Joseph SB, Zelcer N, Janssen EM, Hausner MA, et al. LXR signaling couples sterol metabolism to proliferation in the acquired immune response. Cell. 2008;134:97–111.

284. Cui G, Qin X, Wu L, Zhang Y, Sheng X, Yu Q, et al. Liver X receptor (LXR) mediates negative regulation of mouse and human Th17 differentiation. J Clin Invest. 2011;121:658–70.

285. Xu J, Wagoner G, Douglas JC, Drew PD. Liver X receptor agonist regulation of Th17 lymphocyte function in autoimmunity. J Leukoc Biol. 2009;86:401–9.

286. Castrillo A, Joseph SB, Vaidya S a, Haberland M, Fogelman AM, Cheng G, et al. Crosstalk between LXR and toll-like receptor signaling mediates bacterial and viral antagonism of cholesterol metabolism. Mol Cell. 2003;12:805–16.

287. Chang H-C, Zhang S, Thieu VT, Slee RB, Bruns H a, Laribee RN, et al. PU.1 expression delineates heterogeneity in primary Th2 cells. Immunity. 2005;22:693–703.

288. Hegazy AN, Peine M, Helmstetter C, Panse I, Fröhlich A, Bergthaler A, et al. Interferons direct Th2 cell reprogramming to generate a stable GATA-3(+)T-bet(+) cell subset with combined Th2 and Th1 cell functions. Immunity. 2010;32:116–28.

289. Zhu J, Paul WE. Heterogeneity and plasticity of T helper cells. Cell Res. Nature Publishing Group; 2010;20:4–12.

290. Wen X, Liu H, Xiao G, Liu X. Downregulation of the transcription factor KLF4 is required for the lineage commitment of T cells. Cell Res. Nature Publishing Group; 2011;21:1701–10.

291. Rothenberg E V, Dionne CJ. Lineage plasticity and commitment in T-cell development. Immunol Rev. 2002;187:96–115.

292. Patra AK, Avots A, Zahedi RP, Schüler T, Sickmann A, Bommhardt U, et al. An alternative NFAT-activation pathway mediated by IL-7 is critical for early thymocyte development. Nat Immunol. 2013;14:127–35.

293. Nunomura S, Sato T, Habu S. Molecular basis for functional maturation of thymocytes: increase in c-fos translation with positive selection. J Immunol. 2000;164:5590–5.

294. Yamada T, Park CS, Mamonkin M, Lacorazza HD. Transcription factor ELF4 controls the proliferation and homing of CD8+ T cells via the Krüppel-like factors KLF4 and KLF2. Nat Immunol. 2009;10:618–26.

295. Takahashi K, Yamanaka S. Induction of pluripotent stem cells from mouse embryonic and adult fibroblast cultures by defined factors. Cell. 2006;126:663–76.

296. An J, Golech S, Klaewsongkram J, Zhang Y, Subedi K, Huston GE, et al. Krüppel-like factor 4 (KLF4) directly regulates proliferation in thymocyte development and IL-17 expression during Th17 differentiation. FASEB J. 2011;25:3634–45.

297. Carotta S, Wu L, Nutt SL. Surprising new roles for PU.1 in the adaptive immune response. Immunol Rev. 2010;238:63–75.

298. Soroosh P, Doherty T a. Th9 and allergic disease. Immunology. 2009;127:450–8.

299. Roger T, David J, Glauser MP, Calandra T. MIF regulates innate immune responses through modulation of Toll-like receptor 4. Nature. 2001;414:920–4.

300. Lin M, Rikihisa Y. Ehrlichia chaffeensis downregulates surface Toll-like receptors 2/4, CD14 and transcription factors PU.1 and inhibits lipopolysaccharide activation of NF-κB, ERK 1/2 and p38 MAPK in host monocytes. Cell Microbiol. 2004;6:175–86.

301. Serfling E, Chuvpilo S, Liu J, Höfer T, Palmetshofer A. NFATc1 autoregulation: a crucial step for cell-fate determination. Trends Immunol. 2006;27:461–9.

302. Chuvpilo S, Jankevics E, Tyrsin D, Akimzhanov A, Moroz D, Jha MK, et al. Autoregulation of NFATc1/A expression facilitates effector T cells to escape from rapid apoptosis. Immunity. 2002;16:881–95.

303. Asagiri M, Sato K, Usami T, Ochi S, Nishina H, Yoshida H, et al. Autoamplification of NFATc1 expression determines its essential role in bone homeostasis. J Exp Med. 2005;202:1261–9.

304. Tsukumo S, Unno M, Muto A, Takeuchi A, Kometani K, Kurosaki T, et al. Bach2 maintains T cells in a naive state by suppressing effector memory-related genes. Proc Natl Acad Sci U S A. 2013;110:10735–40.

305. Ehrchen JM, Sunderkötter C, Foell D, Vogl T, Roth J. The endogenous Toll-like receptor 4 agonist S100A8/S100A9 (calprotectin) as innate amplifier of infection, autoimmunity, and cancer. J Leukoc Biol. 2009;86:557–66.

306. Glasmacher E, Agrawal S, Chang AB, Murphy TL, Zeng W, Vander Lugt B, et al. A genomic regulatory element that directs assembly and function of immune-specific AP-1-IRF complexes. Science. 2012;338:975–80.

307. Ouyang X, Zhang R, Yang J, Li Q, Qin L, Zhu C, et al. Transcription factor IRF8 directs a silencing programme for TH17 cell differentiation. Nat Commun. Nature Publishing Group; 2011;2:314.

308. Gibbons DL, Abeler-Dörner L, Raine T, Hwang I-Y, Jandke A, Wencker M, et al. Cutting Edge: Regulator of G protein signaling-1 selectively regulates gut T cell trafficking and colitic potential. J Immunol. 2011;187:2067–71.

309. Agenès F, Bosco N, Mascarell L, Fritah S, Ceredig R. Differential expression of regulator of G-protein signalling transcripts and in vivo migration of CD4+ naïve and regulatory T cells. Immunology. 2005;115:179–88.

310. Weinger JG, Omari KM, Marsden K, Raine CS, Shafit-Zagardo B. Up-regulation of soluble Axl and Mer receptor tyrosine kinases negatively correlates with Gas6 in established multiple sclerosis lesions. Am J Pathol. American Society for Investigative Pathology; 2009;175:283–93.

311. Li Q, Lu Q, Lu H, Tian S, Lu Q. Systemic autoimmunity in TAM triple knockout mice causes inflammatory brain damage and cell death. PLoS One. 2013;8:e64812.

312. Lian L, Wang Y, Flick M, Choi J, Scott EW, Degen J, et al. Loss of pleckstrin defines a novel pathway for PKC-mediated exocytosis. Blood. 2009;113:3577–84.

313. Ding Y, Kantarci A, Badwey J a, Hasturk H, Malabanan A, Van Dyke TE. Phosphorylation of pleckstrin increases proinflammatory cytokine secretion by mononuclear phagocytes in diabetes mellitus. J Immunol. 2007;179:647–54.

314. Lowe CE, Cooper JD, Brusko T, Walker NM, Smyth DJ, Bailey R, et al. Large-scale genetic fine mapping and genotype-phenotype associations implicate polymorphism in the IL2RA region in type 1 diabetes. Nat Genet. 2007;39:1074–82.

315. Brand OJ, Lowe CE, Heward JM, Franklyn J a, Cooper JD, Todd J a, et al. Association of the interleukin-2 receptor alpha (IL-2Ralpha)/CD25 gene region with Graves' disease using a multilocus test and tag SNPs. Clin Endocrinol (Oxf). 2007;66:508–12.

316. Maier LM, Anderson DE, Severson CA, Baecher-Allan C, Healy B, Liu D V, et al. Soluble IL-2RA Levels in Multiple Sclerosis Subjects and the Effect of Soluble IL-2RA on Immune Responses. J Immunol. 2009;182:1541–7.

317. Russell SE, Moore AC, Fallon PG, Walsh PT. Soluble IL-2Rα (sCD25) exacerbates autoimmunity and enhances the development of Th17 responses in mice. PLoS One. 2012;7:e47748.

318. Liao W, Lin J-X, Leonard WJ. Interleukin-2 at the crossroads of effector responses, tolerance, and immunotherapy. Immunity. Elsevier Inc.; 2013;38:13–25.

319. Malek TR, Castro I. Interleukin-2 receptor signaling: at the interface between tolerance and immunity. Immunity. Elsevier Inc.; 2010;33:153–65.

320. Willerford DM, Chen J, Ferry JA, Davidson L, Ma A, Alt FW. Interleukin-2 Receptor alpha chain regulates the size and content of peripheral lymphoid compartment. Immunity. 1995;3:521–30.

321. Sadlack B, Merz H, Schorle H, Schimpl A, Feller AC, Horak I. Ulcerative Colitis-like Disease in Mice with a Disrupted Interleukin-2 Gene. Cell. 1993;75:253–61.

322. Petersen C, Aumüller G, Bahrami M, Hoyer-Fender S. Molecular cloning of Odf3 encoding a novel coiled-coil protein of sperm tail outer dense fibers. Mol Reprod Dev. 2002;61:102–12.

323. Kirschke CP, Huang L. ZnT7, a novel mammalian zinc transporter, accumulates zinc in the Golgi apparatus. J Biol Chem. 2003;278:4096–102.

324. Kambe T. An Overview of a Wide Range of Functions of ZnT and Zip Zinc Transporters in the Secretory Pathway. Biosci Biotechnol Biochem. 2011;75:1036–43.

325. Drieschner N, Kerschling S, Soller JT, Rippe V, Belge G, Bullerdiek J, et al. A domain of the thyroid adenoma associated gene (THADA) conserved in vertebrates becomes destroyed by chromosomal rearrangements observed in thyroid adenomas. Gene. 2007;403:110–7.

326. Bhattacharyya S, Deb J, Patra AK, Thuy Pham DA, Chen W, Vaeth M, et al. NFATc1 affects mouse splenic B cell function by controlling the calcineurin--NFAT signaling network. J Exp Med. 2011;208:823–39.

327. Peng SL, Gerth a J, Ranger a M, Glimcher LH. NFATc1 and NFATc2 together control both T and B cell activation and differentiation. Immunity. 2001;14:13–20.

328. Thomas AA, Ernstoff MS, Fadul CE. Immunotherapy for the Treatment of Glioblastoma. Cancer J. 2013;18:59–68.

329. Mohme M, Neidert MC, Regli L, Weller M, Martin R. Immunological challenges for peptide-based immunotherapy in glioblastoma. Cancer Treat Rev. Elsevier Ltd; 2014;40:248–58.

330. Damal K, Stoker E, Foley JF. Optimizing therapeutics in the management of patients with multiple sclerosis: a review of drug efficacy, dosing, and mechanisms of action. Biologics. 2013;7:247–58.

331. Minagar A. Current and future therapies for multiple sclerosis. Scientifica (Cairo). 2013;2013:249101.

332. Howlader N, Noone AM, Krapcho M, Garshell J, Neyman N, Altekruse SF, Kosary CL, Yu M, Ruhl J, Tatalovich Z, Cho H, Mariotto A, Lewis DR, Chen HS, Feuer EJ, Cronin KA (eds). SEER Cancer Statistics Review, 1975-2010, National Cancer Institute. Bethesda, MD, http://seer.cancer.gov/csr/1975_2010/

Publications

Hoppmann, N, Graetz, C, Poisa-Beiro, L, Paterka, M, Lill, CM, Zipp, F, and Siffrin, V. New candidates for CD4 T cell pathogenicity in experimental neuroinflammation and multiple sclerosis. *Submitted.*

Acknowledgements

For data protection reasons the acknowledgements are not included in the online version.

Curriculum Vitae

For data protection reasons the curriculum vitae is not included in the online version.